

MODELING THE ROLE OF DIFFERENT CELL TYPES IN DEVELOPMENT
AND ENCODING OF VISUAL STATISTICS IN THE PRIMARY VISUAL
CORTEX

PHILIPP JOHN FREDERIC RUDIGER



Doctor of Philosophy
School of Informatics
University of Edinburgh

2015

Philipp John Frederic Rudiger:

Modeling the role of different cell types in development and encoding of visual statistics in the primary visual cortex

Doctor of Philosophy, 2015

SUPERVISORS:

Dr. James Bednar

Dr. Alexander Thiele

LAY SUMMARY

The field of neuroscience has made tremendous progress of the last century and has reached a point where we have collected an overwhelming amount of data describing the brain from the smallest to the largest level, ranging from interactions between individual genes, proteins and cells to the communication between different brain regions. At the same time we still understand very little about how the brain functions, learning about its environment to solve complex sensory and cognitive tasks. In particular the major difficult is in bridging the gap between low-level descriptions of what goes on in the brain and the high-level descriptions of brain function. In this thesis we present a model of visual cortex that is constrained by our knowledge about the interactions of different cell types and their connections, and makes a number of concrete predictions about their role in phenomena ranging from development and learning to the computations they perform.

Computational models have a key role to play in this regard allowing hypothesis about brain function to be tested and generating new predictions, which experimental neuroscientists can confirm or reject. Even so, too many models shy away from trying to integrate information across different levels of description, to begin explaining high-level behaviors based on low level interactions, instead explaining specific phenomena without considering the greater context. In contrast, the model presented here incorporates a wide range of known low-level properties of the brain, demonstrating how they contribute to robust self-organization, learning and eventually function. Further we explore how the model does not only replicate a wide range of phenomena related to visual perception but also makes specific predictions about the role of the dense and long-range connectivity within the primary visual cortex. The model demonstrates how these connections can store statistical information about the visual environment and organism is raised in and use that information to optimize learning and perception.

This work is of tremendous interest not only to fundamental neuroscience but also clinical neuroscience as many developmental, and neurological diseases have been associated with various defects in the development and wiring of the specific cell types studied here. Finally this work demonstrates for the first time how specific connections in the cortex can store statistics about the visual world and use those statistics to optimize computations in the brain.

ABSTRACT

How does the brain make use of information encoded in its circuits through development and learning? The sensory cortex has been known to extract low level features of its visual environment through developmental and activity-dependent processes. Various computational and theoretical models exist describing a wide range of phenomena observed in the primary visual cortex (V1) ranging from the development of orientation tuning, anatomical organization of its circuits, surround modulation and higher level effects like attention. However so far no model has been able to bridge these levels of description.

In this thesis we integrate the information gleaned about cortical development, circuit and cell-type specific interactions, anatomical measurements as well as behavioural and electrophysiological measurements to develop a computational model of V1 that is better constrained and can make predictions about each of these levels of evidence. Through a series of models, which incorporate increasing levels of biophysical detail, becoming increasingly better constrained, we make detailed predictions on the types of interactions required for robust development of cortical maps, anatomical organization and computations performed by the primary visual cortex.

Initial models will demonstrate how anatomical and electrophysiological knowledge can be combined to give a unified account of spatial tuning of the primary visual cortex. As a second step we will investigate the known interactions between different excitatory and inhibitory cell classes in V1 and what role each cell type may play during development. Finally, we demonstrate how various cell classes can interact to give rise to not only robust development but also the development of realistic lateral connectivity patterns, reflecting the statistics of the visual environment the model was trained on. This allows us to explore how the model is able to capture higher-order information about the environment and use that information to optimize neural coding and aid the processing of even complex visual tasks.

The final model represents a comprehensive and well constrained model of the primary visual cortex, which will for the first time be able to relate the physiological properties of individual cell classes to their role in development, learning and function. Additionally this work has implications in clinical neuroscience as the cell types studied here have been implicated in neurological disorders as wide ranging as autism, schizophrenia and Parkinsons.

ACKNOWLEDGEMENTS

First of all I would like to thank my supervisor Jim Bednar for his thoughtful advice and support throughout the course of this project. Secondly I want to thank my partner and friend Josephine for being patient when I worked day and night to finish this project.

DECLARATION

I declare that this thesis was composed by myself, that the work contained herein is my own except where explicitly stated otherwise in the text, and that this work has not been submitted for any other degree or professional qualification except as specified.

Edinburgh, 2015

Philip John Frederic

Rudiger, January 15, 2016

CONTENTS

Abbreviations	ix
1 INTRODUCTION	1
1.1 Organisation of the Thesis	2
2 LITERATURE REVIEW	4
2.1 Early Visual System: Areas and layers	4
2.1.1 Primary Visual Cortex: Topographic Maps, Simple and Complex Cells	6
2.1.2 Development of Topographic Maps in V ₁	8
2.2 Developmental models of the Primary Visual Cortex	10
2.2.1 Functional and Anatomical Properties of Neural Receptive Fields	13
2.3 The Internal Circuitry of Striate Cortex	24
2.3.1 The Mexican Hat	25
2.3.2 Surround Suppression: Feedforward or Feedback?	28
2.3.3 Distinct Inhibitory Populations	30
2.4 GABAergic regulation of plasticity and column structure	37
2.5 Functional Roles of Intracortical Connectivity	39
2.6 Contextual Modulation and Attention	40
2.6.1 Contextual and Attentional Phenomena in V ₁	41
2.7 Natural Image Statistics, Sparsity and Horizontal Connections	42
3 REPRODUCIBLE SCIENCE AND VISUALIZATION	44
3.1 HoloViews: Building Complex Visualizations Easily for Reproducible Science	44
3.2 A unified workflow for the analysis of complex computational models .	53
4 SPATIALLY CALIBRATING MODELS OF PRIMARY VISUAL CORTEX	54
4.1 SCAL-LGN model	55
4.2 Spatially calibrating LGN receptive fields	56
4.2.1 Method	56
4.2.2 Results	57
4.3 The V ₁ model	59
4.4 Spatially calibrating V ₁ receptive fields	63
4.4.1 Methods	63
4.4.2 Feedforward	64
4.4.3 Intracortical connectivity	66
4.4.4 Inhibitory connectivity	69

4.5	Conclusions	69
5	EXPLORING THE ROLE OF INHIBITION IN CORTICAL DEVELOPMENT	71
5.1	The role of inhibition in development	71
5.1.1	The SEPI Model	72
5.1.2	Results	72
5.2	The role of inhibition in surround modulation	72
5.2.1	The LESPI model	72
6	MODELLING THE EFFECTS OF VISUAL STATISTICS ON LONG-RANGE LAT- ERAL CONNECTIVITY IN VISUAL CORTEX	75
7	MODELING THE EFFECT OF VISUAL INPUT STATISTICS ON SURROUND MODULATION IN V1	79
8	GENERAL DISCUSSION	80
8.0.1	Simple and complex cells	80
8.0.2	Inhibitory subtypes	80
8.0.3	Neuromodulation of visuo-cortical information processing	80
	List of Figures	81
	BIBLIOGRAPHY	87

ABBREVIATIONS

e.g. for example

INTRODUCTION

In introducing the topic of neuroscience it is often customary to point out the incredibly complexity of the mammalian nervous system and highlight its incredible ability to adapt to whatever environment it develops in. While this serves to highlight just how interesting a topic it is to begin revealing the computations performed by this structure, it also implicitly highlights the difficulty of the problem. Particularly when trying to develop computational models of the nervous system it is often tempting to abstract away the complexities of biophysical reality and focus on developing toy models that describe particular phenomena very well but lack the ability to provide more general predictions.

This is precisely what David Marr highlighted when stating that the brain and the visual system in particular should be analyzed at three distinct but complementary levels of analysis, later expanded to include a fourth level by Tomaso Poggio. According to Marr and Poggio models of cognitive systems such as the mammalian visual system should describe the system at one or more of the following levels of analysis:

- Learning: How does the system learn to perform the necessary computations?
- Computational: What does the system actually do? What computations does it perform?
- Algorithmic/Representational: How does the system represent the problem and solve it?
- Implementational/Physical: How is the system physically implemented?

Each of these levels of evidence when viewed in isolation can contribute to the overall understanding about the system, however to gain real insights, models should begin abstracting across these levels of analysis to find out where and how evidence from various sources fit together or more interestingly, highlight potential discrepancies.

Visual neuroscience in particular has enjoyed a huge amount of attention with a wide range of descriptive and mechanistic models describing individual phenomena very well. There is however still a serious lack of models that attempt to bridge between our computational understanding of what the visual cortex is doing and

how it self-organizes with the lower level details of how the physical substrate could actually perform those computations.

The aim of this thesis is to begin unifying across various phenomenological models integrating them with existing mechanistic models and come up with better constrained models of visuo-cortical development reaching across all four levels of description. Starting with developmental models of receptive field and orientation map development, the models will work backwards from the lowest level incorporating increasing levels of physical/anatomical detail, hypothesizing about different algorithmic and computational roles for different cell classes and analysing how they contribute both to the self-organization and learning in the developing cortex but also their potential role in the computations performed by the adult cortex. In doing so we will also describe an incredibly flexible yet reproducible workflow developed as part of this thesis to support the analysis of complex, non-linear dynamic systems.

1.1 ORGANISATION OF THE THESIS

Based on the overarching goals laid out above it is crucial to begin by integrating information across Marr's levels of description. The entire first chapter will therefore be devoted towards providing an overview of our current knowledge about the visual system, broadly categorized into the four levels of analysis.

Having established the current state of knowledge about the visual system we then explore how providing a unified account of the spatial scales in anatomical, electrophysiological and behavioural experiments allows us, for the first time to bridge across all three levels and begin highlighting where these very different experiments make similar predictions and where there are seeming discrepancies and highlight where these differences could arise from.

In the second results chapter we extend this analysis to models of cortical development and function that takes into account the anatomical and physiological properties of different cell classes and begin elucidating their role in experimentally observed phenomena ranging from self-organization to particular computations performed by the fully developed cortex, including surround modulation, divisive gain control and sparse coding.

In the final results chapter we demonstrate how a model that respects the known properties of different cell classes and their interactions can develop realistic connectivity patterns that not only allow for the resulting circuit to robustly respond to highly variable input but also encode the statistics of the input to aid in the various complex computations performed by the cortex.

By the end of the thesis we will have presented a unifying account on how different cell classes in the visual cortex self-organize into a robust circuit that can encode the natural image statistics of its rearing environment and meaningfully contribute to incredibly complex computations and inferences performed by “most complex known structure in the universe”.

LITERATURE REVIEW

2.1 EARLY VISUAL SYSTEM: AREAS AND LAYERS

The early stages of mammalian visual system (pictured in figure 2.1) consist of the retina, where rod and cone photoreceptors convert incident photons into electrical and chemical signals. These signals are then further converted from analogue voltages into spike trains by retinal bipolar and ganglion cells and sent down the optic nerve to the lateral geniculate nucleus (LGN). Connections from the two eyes cross over at the optic chiasm to form projections of the right and left visual field contralaterally. The connections from the retina map retinotopically onto the LGN, which ensures that nearby areas of LGN respond to nearby portions of the visual field. After the initial processing in the retina and LGN the visual stream is projected onto the primary visual cortex (V1).

In the retina, summation of various photoreceptor types gives rise to so called center-surround receptive fields. These ON- and OFF-center receptive fields can arise in bipolar cells but are more commonly associated with retinal ganglion cells (RGCs). This receptive field type responds most strongly to spots of light/dark moving through the visual field (as shown in figure 2.2) but can be characterized as simple edge detectors.

In addition to the macro-organization of the visual system into distinct areas the LGN and its downstream structures are further broken down into individual layers and cell classes. The separation of LGN cells into layers also corresponds to functional separations, as layers 1, 4 and 6 usually receive contra-lateral input, while layers 2, 3 and 5 receive ipsi-lateral inputs from the retina. Furthermore, different layers consist of different cell types, with ventral layers 1 and 2 containing larger so called magno-cellular (M) neurons and dorsal layers 3, 4, 5 and 6 containing smaller parvo-cellular (P) neurons with intra-laminar neurons being referred to as konio-cellular (K). Since these three cell types are also present in the retina and make connections mainly with their own cell type it is theorized that each carries its own parallel information stream. Functionally, P-cells have displayed greater sensitivity to chromatic contrast and higher spatial frequencies, linking them to the processing of detail and color, while M-cells have been shown to have greater sensitivity for high temporal frequencies associating them with motion processing.

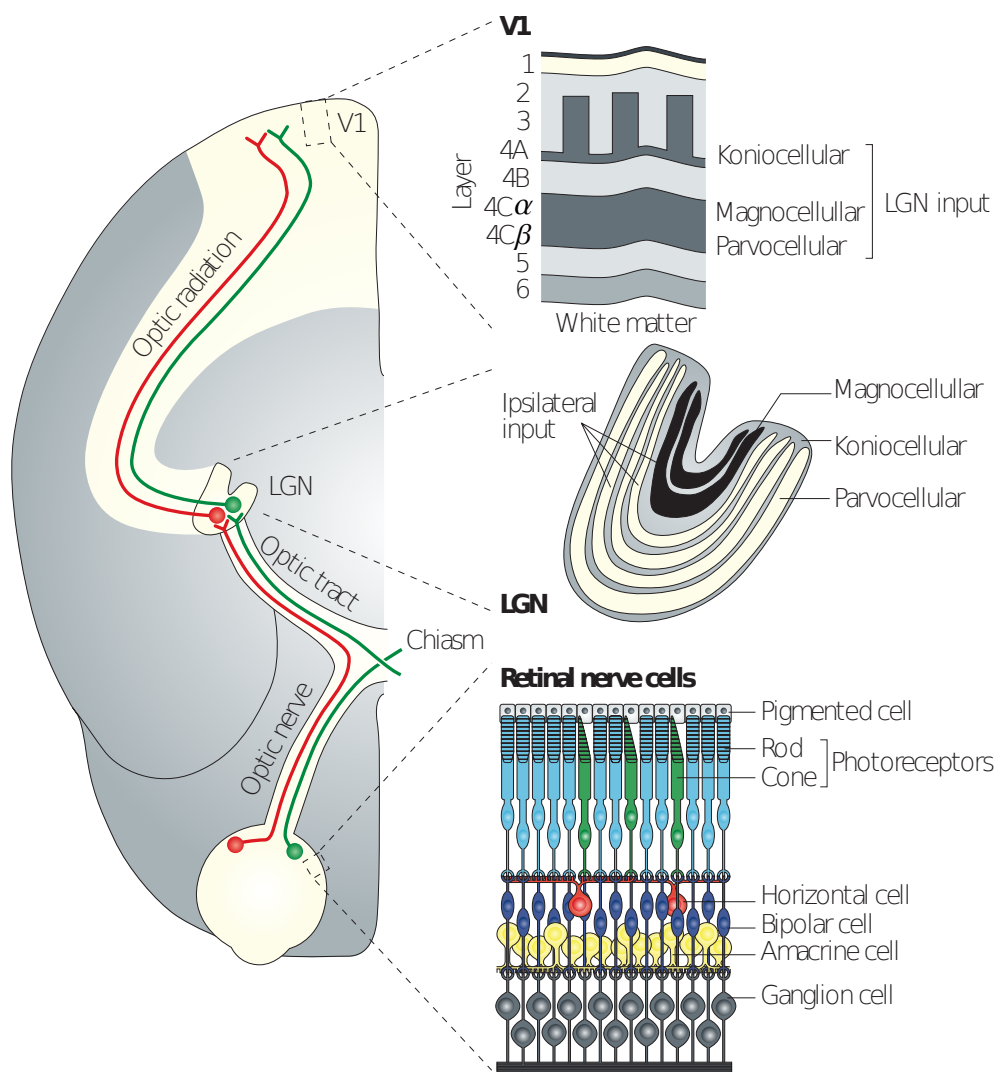


Figure 2.1: The early visual pathway in primates (at least superficially the same for most other mammals) from the retina to the primary visual cortex (V1) via the lateral geniculate nucleus (LGN) of the thalamus. The left panel shows the pathway, while the right panels highlight noteworthy sections including the structure of the retina, the LGN and V1 broken down into their different layers and showing different cell types. Reprinted from Solomon and Lennie (2007).

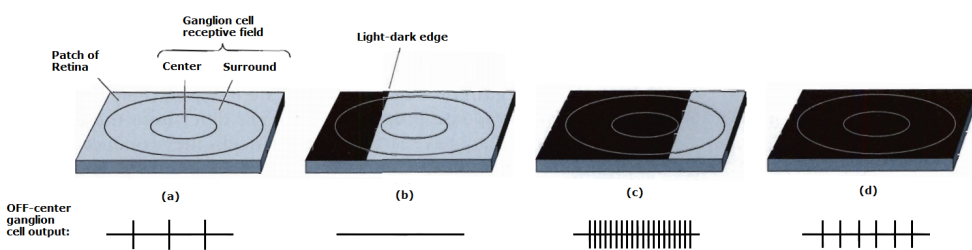


Figure 2.2: The centre-surround receptive field structure of some retinal ganglion cells and LGN neurons, illustrating how a contrast edge activates different portions of the field and thereby results in different activation patterns. From left to right one can see that as the light-dark edge moves into the ON surround field spontaneous activity is suppressed and as it moves further over the OFF center field is deactivated causing activity to sharply spike. Adapted from Bear et al. (2006).

2.1.1 Primary Visual Cortex: Topographic Maps, Simple and Complex Cells

The primary visual cortex (V1) or striate cortex provides the first cortical stage of processing of visual information. The cortex was classically divided into six layers but since many subdivisions have been added after functional sub-groups were discovered. Feedforward input from the LGN is received in layer 4C α and 4C β , which receive input most of their input from M- and P-cells respectively. The neurons in layer 4 then send projections up to layers 2/3, which has a diverse intralaminar network of connections but also sends intracortical projections to a number of higher visual areas, while layers 5 and 6 provide feedback to the LGN.

Neurons in the primary visual cortex (V1) are tuned to respond to a variety of different features or complex combinations of such features, including orientation, spatial and temporal frequency, motion direction, colour or ocular origin. In many mammal species especially primates and carnivores, these feature preferences map smoothly and topographically onto the cortical surface. This mapping extends vertically through the layers of the cortex, giving rise to the notion of distinct cortical columns. Retinotopy arises due to the mapping of visual information straight from the retina to the LGN and then to the cortex. Other response preferences such as orientation and direction selectivity rarely arise in the LGN and are usually thought of as an emergent phenomenon in the cortex.

The receptive fields of V1 neurons are different in that often are no longer simple ON- or OFF-centre surround fields, forming more complex spatiotemporal patterns. They are commonly modeled using Gabor filters as shown in Figure 2.4, which have elongated ON and OFF regions or lobes, generated by localizing a full-field sine grating with a Gaussian envelope. Orientation selectivity and spatial frequency preference are determined by the orientation and spacing of ON- and OFF-regions

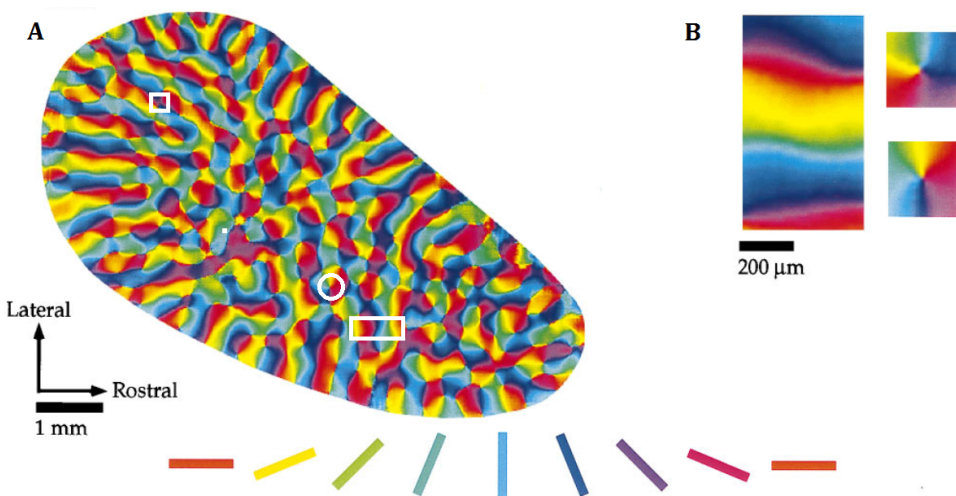


Figure 2.3: A) Orientation preference map in a ferret generated by overlaying the activity maps for different orientations and artificially colouring each area according to the orientation preference laid out in the legend below. The image also highlights three recurrent features of orientation maps in white. The square highlights a saddle point, where a patch of cortex selective for a particular direction is almost bisected by a patch selective to another direction. The circle highlights a pinwheel arrangement, where different orientations preference patches are arranged in a circular shape. Finally the rectangular shape highlights a linear zone in which orientation preference change continuously. B) Magnifications of a linear zone and two pinwheel arrangements. Adapted from [Bosking et al. \(1997\)](#).

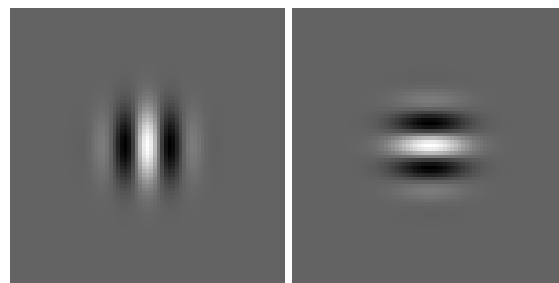


Figure 2.4: Gabor Patches at 0 degree and 90/180 degree orientations with clearly visible ON (white) and OFF (black) regions.

respectively. It is also possible for V1 cells to filter temporal patterns by employing spatio-temporal shifts in their ON and OFF lobes, giving rise to direction selectivity.

Orientation selective neurons can generally be classed as simple or complex cells, depending on whether they display some form of spatial/phase invariance. In reality this classification is less clear with cells being somewhere on a gradient from pure simple cells to a complex cell with the degree of phase invariance being the determining factor. Apart from phase invariance the neurons may also exhibit contrast invariance, such that even at very low contrast they will respond more strongly to their preferred orientation than to the orthogonal orientation.

In context of this project topographic feature maps and RF interactions play a fundamental role as they provide the basis around which the neural circuit organize. The functional organization of V1 arises during the development of the animal and are thought to be mediated largely by activity dependent processes as the next section will show.

2.1.2 *Development of Topographic Maps in V1*

The development and maturation of cortical topographic feature representations in the form of maps is closely linked to function and can reveal a lot about how the cortex is capable of capturing and encoding statistics of the natural world. Developmental studies involve imaging the same area of the cortex over a number of days and investigating what drives development of orientation maps and other topographic arrangements. Early developmental studies found, using relatively limited optical imaging techniques on ferrets shortly after eye opening, that the iso-orientation domains in the V1 develop very early in development and subsequently show very little change ([Chapman et al., 1996](#)) (pictured in figure 2.5). These and other experiments (?) showed that orientation preference develops even in absence of visual input although the maps do not fully mature. This seems to suggest that orientation maps and other topographic organizations develop initially even in absence of external vi-

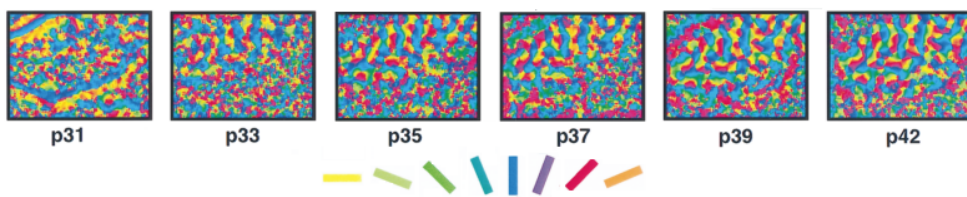


Figure 2.5: Development of orientation map in ferret visual cortex from postnatal day 31 to 42 revealed using chronic optical imaging of intrinsic signals. Adapted from (Chapman et al., 1996).

sual input through internally generated visual activity such as retinal waves but then require external stimulation to fully mature.

In the initial stages of development various preprogrammed guidance cues set up the basic connectivity between the LGN and the cortical processing areas. Some successful models of development have focused on the afferent connections between the LGN ON and OFF cells and their targets in the visual cortex as the driving force behind the development of orientation columns (Jin et al., 2011). This is likely to tell only part of the story as even during prenatal development, retinal waves, consisting of periodic activity in retinal ganglion cells (RGCs), spread across the retina driving neighboring RGCs to fire in a correlated fashion, which allows the primary visual cortex to develop topographic feature maps (Firth et al., 2005). The most prominent proposals in theory and in models have been focused the termination pattern of both the geniculocortical afferents in layer 4 (Katz et al., 2000; Ringach, 2007) and adjustments in feedforward and lateral connectivity through activity dependent, competitive processes (Bednar and Miikkulainen, 2003).

It is now generally accepted that the development of topographic maps is driven activity dependent weight modification in form of Hebbian learning or some variant thereof (?). The LISSOM and GCAL models, which provide the basis of the modeling work proposed in this project have shown that robust map development can be achieved with a small number of relatively simple mechanisms including homeostatic plasticity, lateral gain control in LGN and lateral connectivity in V1 (Stevens et al., 2013) and will be considered in more detail at a later stage. These models can account for the development of orientation preference maps through both intrinsic activity such as retinal waves (Bednar and Miikkulainen, 2003) and visually induced retinal activity. Experiments show that at the very least these processes are required to achieve the finely tuned precision, which can now be observed at single cell resolution (Ohki et al., 2005; ?).

Lateral intra-areal connections in particular have been implicated in map development as their functional connectivity seems to be closely related to map structure (Gilbert and Wiesel, 1983). Experiments in layer 2/3 of the tree shrew involving orient-

tation preference mapping and subsequent axonal staining have shown that although short range connections show no preference in their terminations, long range connections longer than 500 μm , preferentially link neurons with co-oriented and co-axially aligned receptive fields (Bosking et al., 1997). In iso-orientation regions cells therefore make short-range connections largely with cells that prefer the same direction as them, while the connectivity at pinwheels short-range connections are made with cells with a wide range of orientation preferences (?). However, it is known that the patchy lateral connectivity in V1 does not arise until after the orientation map has emerged (Ruthazer and Stryker, 1996), indicating that they may be involved in some higher-order processing not required during initial development.

The development of the early visual pathway is probably driven by a number of mechanisms complementing each other at various stages starting with guidance cues setting up coarse predetermined connectivity patterns, which are then refined through Hebbian processes driven by in- and extrinsically stimulated activity. Although the structure of a neurons receptive field is constantly changing and varies widely from cell to cell, a lot of work has gone into measuring the exact structure and functional properties of neural receptive fields and their underlying anatomical correlates, the neurite arbors.

2.2 DEVELOPMENTAL MODELS OF THE PRIMARY VISUAL CORTEX

As it is thought that the cortex captures statistics about the sensory streams to construct internal models of the world, it is clear that function, structure and development are closely linked. Recognizing this close association, Dr. Bednar began developing models of the sensory cortex (Bednar and Miikkulainen, 2003) based on self-organizing maps (SOMs). Since then these models have been refined substantially but still implement the retina, LGN and V1 as a set of neuronal sheets with feedforward and lateral connectivity self-organizing into the complex topographic maps as seen in carnivore and primate species. It can explain the development of robust yet adaptive topographic maps using only a small set of mechanism including contrast-gain control, an adaptive single-neuron threshold, and lateral connectivity giving rise to GCAL (Law et al., 2011). Extensions of this model explaining the development of complex cells and of contrast dependent size tuning (Antolík and Bednar, 2011) as well as a continuous time model incorporating LGN/V1 onsets using hysteresis functions are in development (Stevens, 2011).

The GCAL model is based on several core observations about information-processing in V1 and the cortex in general. As previous sections have shown, the primary visual cortex of primates responds strongly to specific low-level features in its visual input

including orientation, color and direction. Selectivity to these features are conserved across a wide range of contrasts and neurons form topographic feature maps across the surface of V1 by virtue of self-organization. While these experimentally confirmed findings are specific to vision, the concept of equipotentiality proposes that different areas in the cerebral cortex are cytoarchitectonically highly similar, becoming differentiated based largely on the statistical patterns in their inputs during development and are thus capable of capturing any sensory modality. While details surrounding this hypothesis are still controversial, experiments such as those by Sur et al. (1990) have at least partly validated this view. In this particular study, experimentalists rewired optic nerve axons to interface with neurons in the medial geniculate nucleus (MGN), part of the pre-cortical auditory pathway, and subsequently showed that neurons in the primary auditory cortex (A1) would become receptive to features usually associated with V1. This is behind much of what has made V1 such a popular model area for neuroscience and suggests that many of the insights that can be gleaned from the study of V1 could be applied to the cortex as a whole.

The architecture of the GCAL model in its simplest form and as it will initially be used in this project relies on only four sheets, a retinal sheet for the presentation of stimuli, two RGC/LGN sheets and a V1 sheet. These sheets are connected with different intra- and inter-areal connection fields. This simple model can only be used to demonstrate retinotopy, orientation preference and the emergence of simple cell-like RFs but more complex models have been shown to additionally account for complex cells, ocular dominance, motion direction, spatial frequency, temporal frequency, disparity and color. All these models are trained by presenting it with a visual input on the retina, allowing the response to propagate through the different sheets and then adjusting the connections weights to V1 neurons based on a local learning rule. The response of a given neuron j at time $t + \delta t$ can be calculated as the thresholded dot product between the activations of every input neurons i at time t , or $\eta_i(t)$, and their associated weights stored in the connection field:

$$\eta_j(t + \delta t) = \sigma \left(\sum_p \gamma_p \sum_{i \in F_{jp}} \eta_i(t) \omega_{ij} \right) \quad (2.1)$$

where η_i is the activation of all units i in connection field F_{jp} , which contains all neurons unit j receives its inputs from. ω_{ij} is the connection weight from i to j . σ is a half-wave rectifying function with a variable threshold point (θ) dependent on the average activity of the unit, effectively acting as a homeostatic mechanism, pulling the activity of neuron back to a desired level. γ_p is an arbitrary multiplier for the overall strength of all connections i in projection p and thus a free parameter.

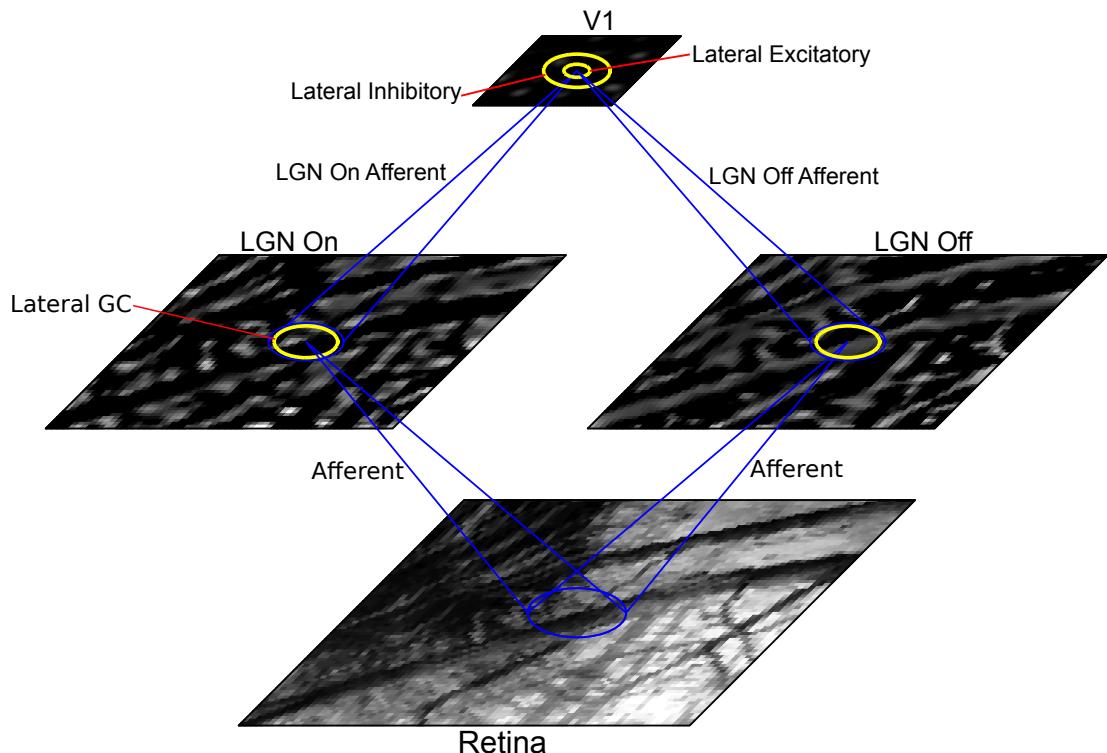


Figure 2.6: Schematic of simplest GCAL model for development of simple cells with surround modulation, retinotopic organization and orientation preference maps. It consists of a retinal sheet, two RGC/LGN for ON and OFF cell responses and one V1 sheet, connected with intra- and inter-areal projections. The sheets are drawn to scale, with larger sheets for the RGC/LGN and retinal layers to avoid edge effects. Projections are illustrated with blue (feedforward connections) and yellow (lateral connections) ovals with cones converging on their target, all drawn to scale to show their spatial extents. RGC/LGN sheets consist of units with hardwired Difference of Gaussian RFs with ON and OFF center-surround regions. LGN Afferent projections to V1 are initially unspecific but develop Gabor-like RF structures through Hebbian learning as they are observed experimentally.

The connection weights ω_{ij} are adjusted after each iteration using a simple Hebbian learning rule, capturing correlations between pre- and post-synaptic activities. The Hebbian connection weight update for unit j is expressed as a function of the presynaptic activity η_i , the post-synaptic response η_j and the Hebbian learning rate α , taking the form:

$$\omega_{ij}(t+1) = \frac{\omega_{ij}(t) + \alpha\eta_j\eta_i}{\sum_{k \in F_{j,p}} (\omega_{kj}(t) + \alpha\eta_j\eta_k)} \quad (2.2)$$

This function also constrains runaway changes in weights by employing divisive post-synaptic weight normalization and thus eliminates the instability associated with classical Hebbian learning.

This limited number of mechanisms already gives rise to an incredibly robust model of development of topographic map development and generates different experimentally observed RF profiles. To add further robustness to the model and to allow it to respond across a wide range of contrasts, contrast-gain control was introduced in the LGN sheets (marked as Lateral GC). This mechanism was closely modeled on the divisive normalization model introduced and validated by Bonin et al. (2005). Finally, the lateral excitatory and inhibitory fields in the V1 sheet give rise not only to the topographic map structure but also to some surround modulation effects. In particular, it can explain the size tuning properties of V1 neurons as the excitatory field will boost the response to a growing centered disk up to a certain peak, after which point the lateral inhibitory field dominates and reduces the response to the stimulus as it grows further. It may also explain effects such as iso-orientation suppression but this has as of yet not been explored in detail.

Overall, due to the simplicity of its mechanisms and its explanatory strength, GCAL provides an ideal starting point to explore the contribution of feedforward, lateral and feedback components to V1, how bottom-up attention can arise and how top-down attention can modulate the processing architecture.

2.2.1 *Functional and Anatomical Properties of Neural Receptive Fields*

The spatial properties of RFs in the LGN and V1 are of particular interest in the context of this PhD project as they provide the basis of a realistic model of the parafoveal regions of the primary visual cortex in macaques, allowing direct comparisons between model in experiment in a system where the spatial scales are of great importance. Before attempting to model the effects of higher- and extra-cortical influences on information processing in V1, the spatial properties of each set of afferent con-

nections entering V1 need to be thoroughly understood and incorporated into the model.

The extents and structure of neural receptive fields are defined by the axonal and dendritic arborization of afferent, horizontal and feedback connections, whether that is in the LGN, the V1 or higher up in the cortical architecture. While these extents can theoretically be measured physically by tracing the neurites of a number of cells, this has only systematically been possible for corticogeniculocortical neurite complex as tracing studies along the retinal-geniculate pathway are generally infeasible. Therefore spatial properties of LGN RFs have been estimated through stimulus driven protocols. The following sections will outline the methods employed in characterizing geniculate RFs and detail the relative contribution of afferent, lateral and feedback connections to para-foveal RFs in the LGN and V1 of macaques.

2.2.1.1 *Receptive Fields in the Lateral Geniculate Nucleus*

The spatiotemporal structure of receptive field becomes increasingly more complex when moving up in the visual processing hierarchy. As described earlier, receptive fields in the LGN are primarily made up of antagonistic center-surround regions although Gabor-like lobes are also sometimes observed. Even at this early stage of processing, lateral and feedback connections can modulate neural responses and have been found to exert a suppressive effect (Hubel and Wiesel, 1961). More recent studies have concluded that this suppressive effect is mediated primarily by lateral connections and acts as a form of contrast-gain control allowing for the encoding of a high dynamic range of luminance values Bonin et al. (2005). As pointed out previously the LGN receives a large proportion of its inputs from feedback cells originating in layer 6 of V1 (Sherman and Guillery, 2002). It is unclear how these feedback connections contribute to the RF properties of LGN neurons but most evidence suggests they are mainly involved in higher level modulatory processes especially in regard to the processing of motion and thus do not directly contribute to the RF structure (Sillito et al., 2006).

Estimating the relative contribution and effect of the various LGN afferents on its neural receptive fields has been attempted using a variety of protocols. Unfortunately little to no data is available from tracing studies, primarily because the LGN is embedded deep in the brain making it incredibly difficult to trace individual neurites from and to their origin. Therefore a number of protocols were developed by which the parameters of the center-surround fields could be estimated. After measuring the response of retinal ganglion cells (RGCs) to moving bar stimuli cats (Rodieck, 1965; Rodieck and Stone, 1965a), Rodieck and Stone (1965b) found that by fitting a Difference of Gaussian (DoG) model (see 2.3) to the data it was possible to estimate the

relative strength and size of the central and surround portions of the receptive field. It wasn't until later that systematic recordings of this kind were carried out in the LGN of macaques at which point the moving bar stimuli were replaced with sine gratings of varying spatial frequency.

$$R = k_c e^{-\frac{f}{f_c}^2} - k_s e^{-\frac{f}{f_s}^2} \quad (2.3)$$

As not all papers can be considered, the data from three different studies making use of protocols with increasing complexity will be considered. [Derrington and Lennie \(1984\)](#) was the first of such studies, attempting to characterize the spatial and temporal properties of parvocellular LGN neurons in *Macaca mulatta* by fitting DoG models to the responses. The analysis and confidence intervals of this first study were rather limited so the first study that will be considered here is [Spear et al. \(1994\)](#), which also considered the effect of aging on receptive field properties. They found that the receptive field center radius only increased very weakly with eccentricity, the smallest RF center radii were confined to parvocellular neurons and that the RF surround was significantly smaller in parvocellular layers. This provides a first estimate for the mean sizes of the central and surround portions of the classical RFs in macaque but the clear problem with this approach is that it completely ignores the influence of the non-classical surround and therefore may underestimate the extents of the central field, while overestimating the strength of the classical RF surround.

The next detailed study of LGN neural RFs was carried out by Levitt et al. [Levitt et al. \(2001\)](#), investigating the effects of visual deprivation on their visual response properties. The study additionally set out to determine the trans-species correspondence of so called X, Y and W pathways, which were identified in the cat. As in the [Spear et al. \(1994\)](#) study they found little difference in RF center radii between parvo- and magnocellular neurons. They also found that magnocellular neurons had greater nonlinearity indices but could find no compelling evidence that magnocellular neurons can be classified into distinct linear (X) and nonlinear (Y) types. There was a tendency for parvocellular neurons to exhibit greater spatial resolution and the highest temporal resolution to be magnocellular. This seems to support the general conclusion reached by [Derrington and Lennie \(1984\)](#), which had additionally concluded that magno- and parvocellular neurons can be further identified by their chromatic properties. Finally, their analysis extended to earlier data from different species of macaque, which showed that there is some variation in the distribution of ON and OFF cells between *M. mulatta* and *M. fascicularis*. Overall their results on spatial tuning match those found by previous studies quite closely, which is unsurprising as the measuring and fitting protocols were highly similar.

In an attempt to calculate the relative contributions of different neural connections, determine differences between the K-, M- and P-cellular pathways and measure contrast dependent tuning, a number of more recent studies have introduced more complex measurement and fitting protocols. In particular, these experiments for the first time attempted to separate out the influence of the non-classical or extra-classical surround (ECRF or nCRF), which is thought to be mediated by lateral and feedback connections. Therefore, a new measurement and fitting protocol, introduced by Sceniak et al. (1999) in form of the integrated DoG (iDoG) model to describe spatial summation in the visual cortex, was used. Instead of measuring the response to varying spatial frequency, this protocol involves the presentation of drifting sine grating disks with varying apertures at the neurons optimum spatial frequency. The rationale behind this new protocol was that the optimal spatial frequency would maximally drive the CRF excitatory center, while minimizing the influence of the CRF surround. Therefore the resulting area summation tuning curve would represent only the response from the CRF excitatory center and the ECRF surround. Additionally the spatial frequency response measurement protocol was modified by confining the drifting sine gratings to a circular aperture, reducing influences from beyond the CRF. While these assumptions do not necessarily hold for reasons that will be discussed later, they provide a first systematic attempt at separating the contributions from the CRF and ECRF.

Sceniak et al. (2006) were the first to study spatial RF properties of LGN neurons of macaques by measuring both spatial frequency and area summation response functions and fitting the results with DoG and iDoG models respectively to estimate the spatial parameters of the probed neurons. These results represent the best estimates of the spatial properties of LGN receptive fields. The first thing to note is the clear discrepancy between the estimates of CRF excitatory center radius estimates in this paper compared to previous estimates. This may be explained by the more homogeneous distribution of cells as the sample population was taken exclusively from layer 4. Additionally the older protocol failed to confine the drifting sine grating to a disk, which may have resulted systematic underestimation of the excitatory component due to suppressive effects. While excitatory extents vary hugely across the various studies the suppressive surround estimates are fairly consistent. Furthermore, the spatial extent of the excitatory CRF centers were found to be contrast invariant, while both the ECRF and CRF suppressive surround extents were found to increase at lower contrast levels. In summary, looking back at all the studies considered here excitatory CRF extents are generally distributed between $0.05\text{--}0.5^\circ$ in radius, while inhibitory CRF and suppressive ECRF radii are distributed anywhere between $0.6\text{--}1.5^\circ$ and the suppression index is quite high ($SI > 0.8$) for 80% cells.

While these results provide the best estimates that are currently available the protocols used rely on a number of flawed assumptions. The DoG model fitted to the spatial frequency tuning curve relies on the assumption that no other components are contributing to the response. Although the limited size of the sine grating disk drive should reduce long range influences on the response and the ECRF surround is frequency invariant over a broader spectrum than the CRF, further contributing mechanisms cannot be excluded and may therefore affect the estimates. Similarly the iDoG model fitted to area summation tuning curves may be affected by a number of unaccounted mechanisms. Additionally the iDoG model (see 4.4) actually corresponds to an even luminance disk of variable size rather than the sine grating disks that were used by Sceniak et al. (2006). The decision to use technically incorrect stimuli was made to minimize the influence of the inhibitory CRF surround, which may itself still have some influence on the response. While all these limitations should be held in mind, it is still the best attempt at controlling unaccounted contributions and thus provides the best data on the spatial properties of macaque LGN RFs until detailed histological studies become feasible.

2.2.1.2 *Receptive Fields in the Primary Visual Cortex*

The receptive field properties of neurons in V1, in contrast to LGN neurons, have been characterized to a far greater extent with a number of studies publishing direct anatomical data on neurite arborization in addition to studies involving stimulus protocols such as those employed to characterize LGN RFs. A number of reviews have been published in the past decade to classify different portions of the receptive field and link them to their physiological substrate in the form of feedforward (FF), lateral and feedback (FB) connections. In order to attain a proper understanding of the spatial distribution of afferent neurites, populations of V1 neurons are targeted by, this section will summarize the results.

Recent analyses have established a more complex model for the classification of the spatial properties of neural RFs in V1 than the simpler classical and extra-classical RF structure utilized in earlier work. The structure of a V1 receptive field has been visualized by Angelucci and Sainsbury (2006) and can be seen in Figure 2.7. It is broken down into the minimum response field (mRF), the summation response field (sRF), which itself is broken down into the high contrast and low contrast summation RF (hsRF and lsRF) and the far surround. In particular, a distinction has been made between the near surround, which extends as far as the lsRF and a suppressive far surround that extends beyond the lsRF. The distinction between the hsRF and lsRF has been introduced to account for the contrast dependence of size tuning. Problematically not all studies nor even all the latest studies use this means of defining

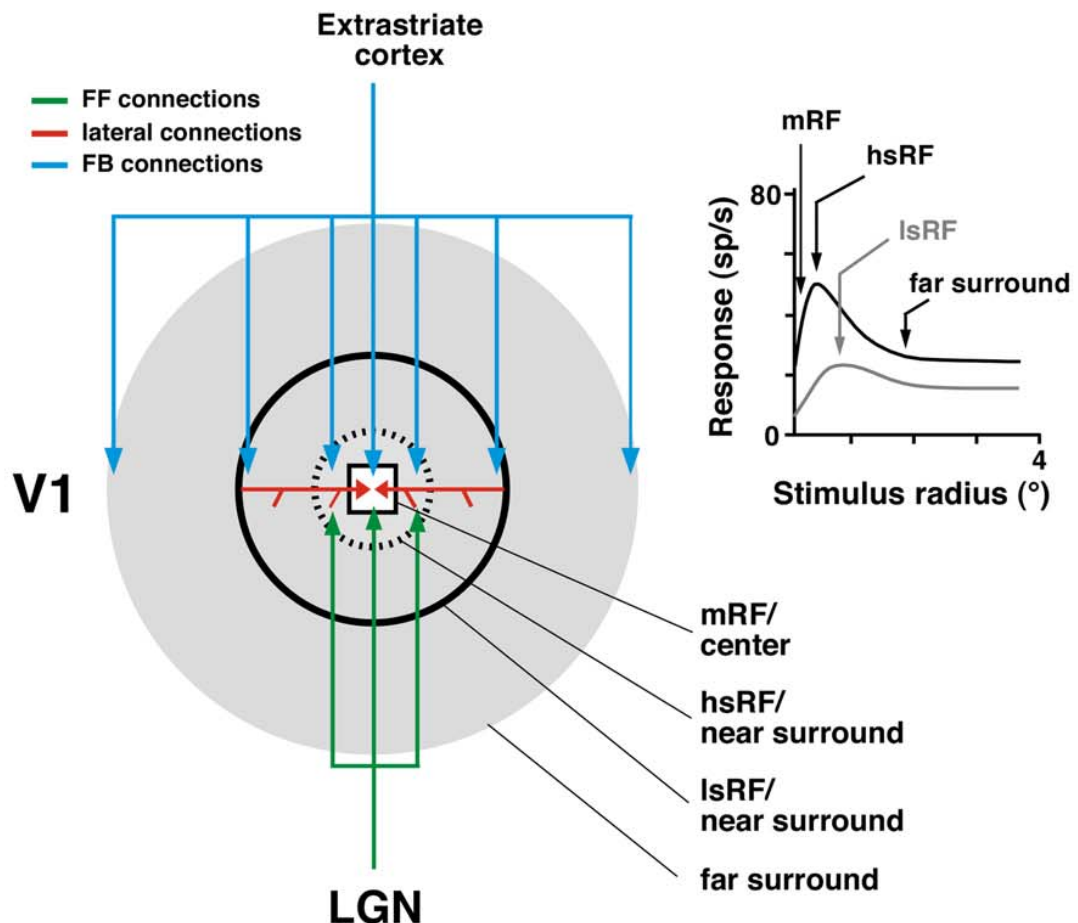


Figure 2.7: The receptive field structure of V1 neurons showing the minimum receptive field (mRF), high contrast summation RF (hsRF) and low contrast summation RF (lsRF). Taken from [Angelucci and Bressloff \(2006\)](#).

different portions of the RF, which may have led to discrepancies of how the sizes of different RF areas are reported. The following sections will attempt to integrate the results from studies employing different means of classifying RFs.

The studies reviewed in [Angelucci and Sainsbury \(2006\)](#) seem to indicate that geniculocortical FF projections integrate signals in the hsRF, while lateral connection underly the lsRF and may thus account for the contrast dependence of spatial summation as well as modulatory effects in the near surround. Classification through measurement of spatial dimensions and onset latencies indicate that inter-areal FB connections seem to be responsible for modulatory influences from the far surround. The influence and spatial properties of each of these projections will be detailed in the following sections.

Geniculocortical Afferents and the Minimum and High Contrast Summation RF The primary visual cortex receives most of its driving inputs through the three previously detailed M-, P- and K-cellular geniculocortical pathways. The M-pathway principally terminates in layers 4C α and 6, the Parvocellular afferents terminate in layers 4A, 4 β and 6, while K-cells primarily target layer 1 and some regions of layer 3. By combining anatomical-tract tracing with physiological recording the spatial extents of feed-forward connections have been measured in detail and linked back to the different RF regions.

The minimum response field as defined above is commensurate to the classical RF and is usually mapped using drifting gratings masked to a small disk of optimal parameters for that particular neuron. It is surrounded by the high contrast summation RF, which is measured by increasing the size of a drifting grating disk at high contrast until the neuron reaches its peak response. Using a combination of tracing and electrophysiological recording (Angelucci and Sainsbury, 2006) found that the visuotopic extent of LGN afferents matches the hsRF size of the target V1 neuron. The diagram and bar chart in Figure 2.8 show how closely the estimates from tracing studies match the results from physiological classifications of RF areas for magno- and parvo-cellular pathways. The close match between these different experiments suggests geniculocortical afferents may underly the extent of a V1 neuron's mRF. Recent evidence has also shown that the an LGN neurons hsRF is roughly commensurate with a V1 cell's mRF. This seems to suggest that the mRF of V1 cells is a product the summation of LGN cells at their peak spatial summation, while the hsRF region of V1 neurons is defined by the integration of excitatory inputs from partially suppressed LGN cells. Beyond that it seems likely FF components partially contribute to surround suppression in V1, however the spatial scales of surround modulation as well as its orientation specificity seem to rule out LGN afferents as the major contributor to the modulatory surround (Angelucci et al., 2002b; Angelucci and Sainsbury, 2006).

Having established the contribution of geniculate afferents to the RF of V1 neurons its time to look at their spatial distribution. In their extensive studies and culminating review paper, Angelucci et al. Angelucci and Bressloff (2006) first fitted the iDOG to the spatial summation response curve of a number of V1 neurons, injected the recording sites with tracers and then measured the labeled connections and cell bodies. The linear extents of the labeled connections were converted to visual field coordinates using magnification factor (MF) estimates by Van Essen et al. (1984). Additionally the anatomic extent of the label was measured in LGN and again converted to visual space coordinates using MFs measured by Connolly and Van Essen (1984) and LGN

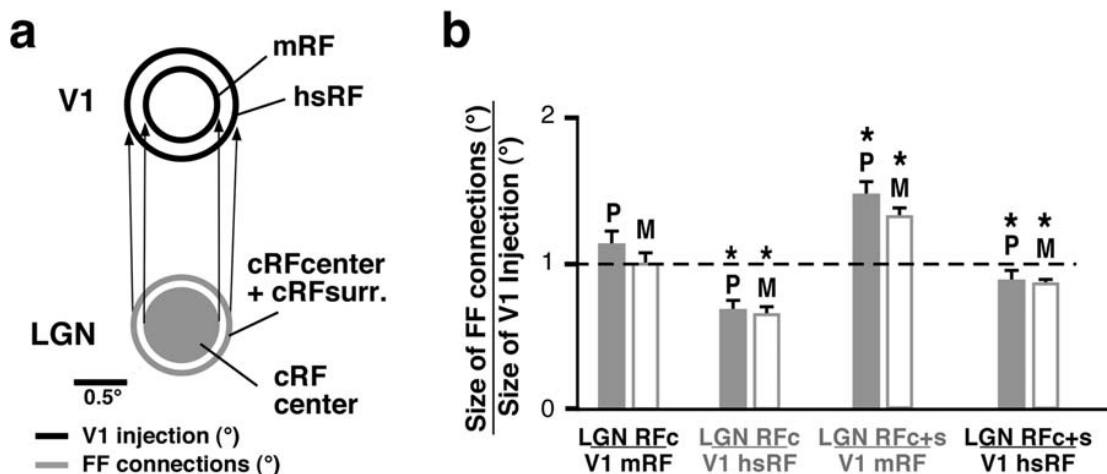


Figure 2.8: Comparisons between electrophysiological characterisation of RF structure and the spatial structure of geniculocortical projections to V1 in (a) diagrammatic and (b) chart form. Both demonstrate that the mRF and hsRF are coextensive with the spatial extents of geniculocortical afferents to V1. Taken from Angelucci and Bressloff (2006).

RF size estimates by Derrington and Lennie (1984). These calculations were used to arrive at the aggregate receptive field (ARF) size, which takes the form:

$$\text{ARF}_{\text{deg}} = D^{\circ} + \text{RF}_{\text{mean}} \quad (2.4)$$

where RF_{mean} is the mean RF size of cells recorded at the edge of the injection site, which could reflect the mRF, hsRF or lsRF, and D° is defined as:

$$D^{\circ} = D_{\text{mm}} / M F_{\text{mm/deg}} + S_{\text{deg}} \quad (2.5)$$

where D_{mm} is the diameter, $M F_{\text{mm/deg}}$ is the magnification factor and S_{deg} is the RF scatter at the injection site. The results show a close match between mRF and hsRF sizes as estimated in V1 and sizes of the RF center and RF center + surround as measured in LGN, once again reaffirming the idea that the mRF and hsRF are primarily driven by geniculocortical afferents. The latest review (Angelucci and Bressloff, 2006) has measured the size of the hsRF in V1 neurons of macaques at 2.8° eccentricity as having mean of about $1^{\circ} \pm 0.1$, which is roughly 2.2x larger than the mRF of the same cell based on results from Angelucci et al. (2002b) and Levitt and Lund (2002). Estimates from the latest anatomical study summarized in table ?? provides slightly higher estimates with means of 1.09° and 1.41° in layer 4C α and 4A/C β respectively.

In addition to the spatial extents of V1 RFs, Angelucci and Sainsbury (2006) also estimated the number of LGN afferents that would contact an individual V1 neuron. According to their estimates a single neuron in layer 4C α can be expected to receive roughly 11 projections from LGN M-cells. Although they were not able to put their

own estimates to the Parvocellular pathway, based on anatomical data from cats they determined that on average 10 geniculate cells converge on a V1 layer 4 cell having observed only a maximum of 30. They conclude that the geniculocortical pathway in macaques exhibits an even lower level of convergence than in cats.

In summary, evidence from anatomical and electrophysiological data seems to suggest that the hsRF of V1 neurons and by proxy the geniculocortical afferents are on average between $1.0\text{--}1.5^\circ$ in size, exhibiting highly limited convergence with only about 10 cells targeting a single layer 4 V1 cell.

Lateral Connections and the Low Contrast Summation RF Horizontal, lateral or intra-areal connections have been proposed as the mechanism for a number of observed phenomena, including the contrast dependence of size tuning, which is why it is thought they underly the extent of the lsRF. Classically it has been assumed that lateral connectivity manifests itself through short-range excitatory and long-range inhibitory connections (von der Malsburg, 1973; Obermayer et al., 1990). More recent studies have indicated that intra-laminar projections usually originate in excitatory pyramidal neurons in layers 2/3, 4B, upper 4C α and 5/6 and at least in layers 2/3 have been shown to target 80% excitatory and 20% inhibitory neurons. The spatial scale of these connections has led several studies to conclude that they may mediate modulation of RF center properties in the near surround (Angelucci et al., 2002b). Lateral connection could therefore provide a simultaneous mechanism for a number of observed effects including the expansion of the summation RF at low stimulus contrast (Sceniak et al., 1999), colinear facilitation (Mizobe et al., 2001) as well as suppression from the near surround outside the hsRF but within the lsRF (Sceniak and Hawken, 2001; Levitt and Lund, 2002). The previous section showed that such phenomena could not be adequately accounted for by geniculocortical afferents, measurement of spatial extents and response latencies of horizontal connections reaffirm this view and have shown that the lsRF and lateral connections are coextensive (Angelucci et al., 2002b).

Apart from the exact spatial dimensions of horizontal connections, it is important several other functionally important properties. While layer 2/3 neurons display patchy connectivity, linking regions with similar functional properties such as orientation preference or ocular dominance, this has been shown not to be the case in macaque layer 4B, upper 4C α (Angelucci et al., 2002b). In addition, it was found that horizontal connections in macaque V1 are isotropic in visual space unlike the anisotropy along the axis of preferred orientation observed in tree shrews (Bosking et al., 1997) and several other species. This may also indicate that contour completion in macaques is mediated by feedback connections. Horizontal connections have been

shown to illicit only subthreshold responses (Hirsch and Gilbert, 1991) and are thus limited to modulatory influence. However, as the surround modulation extends far beyond the monosynaptic spread of lateral connections it is unlikely they account for modulation from the far surround. Polysynaptic chains of lateral connections are also an unlikely substrate for the far surround due to the slow conduction velocity of their axons. In particular, Bair et al. (2003) showed that onset latencies of suppression from the far surround were almost equal to the delays from the near surround. This makes it likely that far surround modulation is mediated primarily by inter-areal feedback connections, which we will look at in detail at a later stage.

Having established that spatial profile of lateral connections is commensurate to that of the lsRF and vice versa the data from both sources will be laid out and analyzed. Anatomic data suggests that the spatial spread of lateral connections can be anywhere between 3-10 mm (on average 6-7 mm) in total length (Angelucci et al., 2002b), which is broken down by layer in table ???. Along its principal axis the visuotopic monosynaptic spread of V1 horizontal connections has a mean of $2.47^\circ \pm 0.3^\circ$. This falls well within the range of estimates for the lsRF as published in a number of studies (Shushruth et al., 2009; Sceniak et al., 1999; Sceniak and Hawken, 2001), which were fit with the same integrated DoG model and stimulus protocol as used in the Sceniak et al. (2006) paper on the spatial properties of LGN neurons, reviewed previously.

In summary, there is strong evidence that lateral connections underly the extent of the lsRF and mediate a number of effects in the near surround, including contrast dependent size tuning, colinear facilitation and low contrast suppression. Unlike in other species horizontal connections are isotropic but do exhibit patchy connectivity in layer 2/3. The extents of horizontal connections range between 3-10 mm, which averages to around 2.5° in visual space.

Feedback from Higher Cortical Areas and the Far Surround As the previous two sections have shown, modulatory influences to V1 RFs extend well beyond the spatial spread of both geniculocortical afferents and horizontal connections. This extended modulatory field is known as the far surround and is thought to be mediated by feedback from higher cortical areas. The far surround has generally been characterized as suppressive, especially for iso-oriented gratings in the center and far surround. More detailed analysis has shown that the far surround can also exhibit response facilitation under some stimulus conditions. This section will characterize the function, termination patterns and spatial extents of feedback connections from higher cortical areas to V1.

The notion of a hierarchical organization of cortical visual areas has been around for quite some time and more recent analysis of feedforward and feedback connections has affirmed this view. At the bottom of this hierarchy is V₁, sending partially segregated FF projection to areas V₂, V₃, V₄ and visual area middle temporal (MT), which all send FB projections back to V₁ (Felleman and Van Essen, 1991). Feedforward projection from V₁ to V₂ arise mainly from layer 4B and to a lesser degree from layer 2/3 and 6. Feedback connections on the other hand arise from layers 2/3A and 5/6 and terminate in the same layers from which FF connections are sent, which means the cells projecting up the hierarchy often overlap with the termination regions of FB projections being sent back down (Angelucci et al., 2002b).

Just like lateral connections FB connections do not drive their target cells, exhibiting only modulatory influence on the RF center (Bullier et al., 2001). Inactivation of areas V₂ and MT has been shown to reduce the firing rate of V₁ neurons to stimuli in their RF center (Hupé et al., 1998), suggesting FB inputs are summed with FF inputs to increase activity. The exact balance between excitation and inhibition of FB connections is so far not very well explored in macaques but evidence from rats suggest that they almost exclusively target excitatory cells. However Angelucci and Bressloff (2006) and Schwabe et al. (2006) have proposed a regimen where FB connections in the far surround target pyramidal neurons, which in turn send monosynaptic horizontal connections to excitatory and inhibitory neurons in the RF center and can thus mediate both suppressive and facilitatory effects depending on stimulus properties.

Feedback connections have been thought to underly a number of top-down effects in V₁, including attention (Treue, 2003), the reverse hierarchy theory of visual learning (Ahissar and Hochstein, 2004) but more recent studies have suggested they contribute directly to the response of V₁ neurons to simple visual patterns (Angelucci et al., 2002b; Angelucci and Bullier, 2003; Schwabe et al., 2006). Notably Schwabe et al. (2006) and Ichida et al. (2007) seem to have resolved the conflicting evidence about the far surrounds suppressive and facilitatory role. Using both experimental and theoretical work they found that while the far surround is suppressive under high contrast conditions, the response of a neuron to a low contrast stimulus in the RF center is facilitated by a small annular stimulus in the far surround. This indicates that excitatory and inhibitory surround mechanisms have similar extents and that the sign of their contribution depends on changes in local excitation/inhibition balance brought about by surround stimulation.

The spatial and functional organization of the FB pathway is thought to differ significantly from FF connections. They seem to exhibit less precise retinotopic organization and terminate in a more diffuse fashion than FF connections. However, more recent evidence suggests that at least a subset of FB connections exhibit patchy and

functionally specific termination patterns (Angelucci and Bressloff, 2006). Evidence from new world primates has also shown that V2 FB axons to V1 link regions of similar orientation preference and that their terminal fields are anisotropic along the axis of the preferred orientation of the originating cell in V2 (Shmuel et al., 2005). The discrepancy between different studies in finding diffuse and patchy FB termination patterns may be attributable to different labeling methods and given that CTB labeling is the more mature and tested procedure it seems likely that FB connections do exhibit patchy terminations in layers 1B, 2/3, 4B and 5/6 and diffuse terminals in layer 1A. The observation of patchy connectivity is also consistent with their proposed functional role in mediating feature-specific influences from the far surround.

The anatomical spatial extents of FB connections from higher cortical areas have been measured in a number of tracing studies. Angelucci et al. (2002b) provides a measurements broken down by area, measuring the extents of FB connections from V2, V3 and MT to V1 (see table ??). Once converted into degrees of visual space the results are the following: Feedback from V2 has a mean size of 3.4° in layer 2/3 and 3.8° in layers 5/6, FB from V3 a mean size of 5.6° in layers 2/3 and 6.7° and FB from MT a mean size of 15.3° and 26.6° in the upper and lower layers respectively. The largest far surround field measured was 28° in diameter and the measurement was still limited by the maximal presented stimulus size (Ichida et al., 2007). These results clearly indicate that cortical feedback to V1 increases in its spatial extents and becomes less spatially and retinotopically specific when moving up in the cortical hierarchy to the point where it covers huge portions of the visual field.

Feedback projection from higher cortical areas to V1 mediate a number of important contextual effects and has been implicated in the early stages of visual attention but also seem to be closely involved in the processing of simple visual stimuli. This section has summarized current knowledge on the spatial termination patterns of FB connections to V1, indicating how they could give rise to functional properties of V1 information processing. While this information will aid the development of a strongly constrained model, without an understanding of the information content being fed back to V1 from higher cortical areas understanding of their true function will be limited.

2.3 THE INTERNAL CIRCUITRY OF STRIATE CORTEX

The previous section outlined the overall structure of the early visual system, breaking down the contribution of inputs from various sources on the receptive field (RF) of neurons in primary visual cortex (V1). While this provides general anatomical constraints and sheds some light on the functional circuitry underlying many of the

contextual effects that have been observed in the primary visual cortex, it does not address many of the fundamental questions about the functional significance of recurrent cortical processing. In particular, it does not address the delicate balance in both strength and spatial extent between excitation and inhibition that is required to halt runaway excitation, sparsify the inputs and thereby allow for the formation of concentrated activity bubbles around which self-organization can take place. This section will cover how the understanding of intra-cortical connectivity has evolved and how this has been reflected in various developmental and non-developmental models.

2.3.1 *The Mexican Hat*

Before complex tracing and circuit reconstruction techniques became available, considerations about the connectivity profiles in the cortex were largely theoretical or based on data from other anatomical structures, which were at the time more amenable to study. Anatomical data and electrophysiological studies in the retina had shown that there is a strong lateral inhibitory component involved in decorrelating photoreceptor activities, thereby enabling more efficient coding of the input (Atick and Redlich, 1992). Lateral inhibition was taken to be a general principle of sensory systems and, among others, Blakemore et al. (1970) suggested repulsive interactions between neighboring contours could account for psychophysical data. Further evidence of lateral inhibition as a general feature of sensory systems was provided by a variety of theoretical models of self-organization, highlighting the necessity of effective local excitatory and long range inhibitory interactions for the formation of local activity bubbles, which in turn provided the basis for orderly map organization (von der Malsburg, 1973; Miller et al., 1989).

The connectivity profile employed in the various self-organizing map models became known as the Mexican hat profile due to its strong resemblance to a sombrero. A simulated Mexican hat profile is shown in 2.9 generated through a simple difference of Gaussian (DoG), whereby a small positive Gaussian kernel is combined with a larger inhibitory kernel. A large variety of cortical models have successfully employed this connection profile to explain a variety of effects ranging from topographic map organization, orientation tuning and contextual effects. Problematically, it is unclear how biologically realistic the assumption of strong local excitation and broadly tuned or untuned inhibition is.

Since then a number of lines of evidence have come together to show that this spatial connectivity profile does indeed seem to exist, at least when considering the aggregate circuit under certain stimulus conditions. Electrophysiological and optical

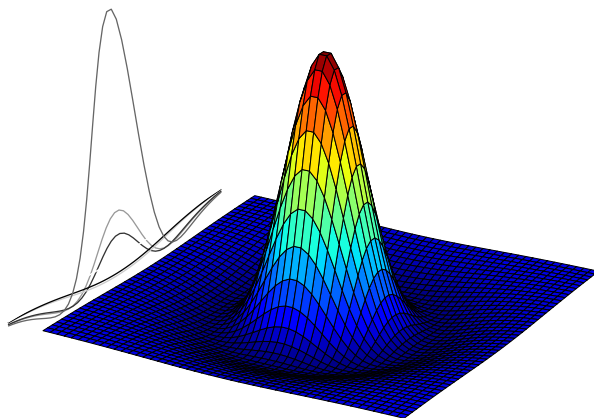


Figure 2.9: 3D plot of Mexican Hat connectivity.

imaging have both confirmed that strongly driven cortical neurons receive strong local excitation and long-range lateral inhibition (Grinvald et al., 1994; Sceniak and Hawken, 2001). At high contrasts Grinvald et al. (1994) showed that a neuron responding to a small, central grating stimulus in isolation exhibits far greater levels of activity than when presented with a co-linear surround stimulus alongside the central stimulus. This highlights an interaction between the center and surround RF that is not only dependent on the orientation statistics but also on the contrast levels in the input. In particular Hirsch and Gilbert (1991) and Weliky et al. (1995) showed that lateral connections impinging onto a neuron would exert a small excitatory effect, when embedded in a low contrast surround, while high contrast would flip the sign of these contextual influences and suppress the central neurons activity. Additionally, Hirsch and Gilbert (1991) found that laterally evoked EPSPs, presumably underlying facilitatory effects, experienced strong voltage-dependent enhancement, speculating that this would allow stimuli in the surround to modulate cRF responses without driving the response on its own. This provides functional evidence that the aggregate circuit can produce a Mexican hat profile under the right stimulus conditions but also suggests that the underlying circuitry is more complex.

Precisely how these two input-dependent modes of contextual integration emerge is unclear. However, as anatomical tracing techniques have become more sophisticated and biomarkers for different cell types were discovered, attempts have been made at teasing apart the cortical circuit. These anatomical surveys showed that long-range connections extending beyond a single orientation column were almost exclusively excitatory and 80% of these excitatory synapses target other excitatory

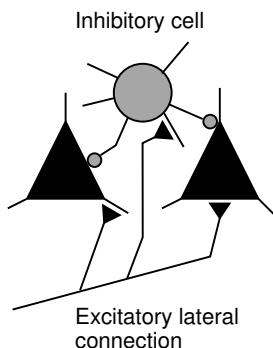


Figure 2.10: Local microcircuit for long-range suppression through di- or poly-synaptic circuit in V1. Reproduced from [Miikkulainen et al. \(2005\)](#) as adapted from [Weliky et al. \(1995\)](#).

pyramidal neurons ([Hirsch and Gilbert, 1991](#); [Kisvárday et al., 1997](#)). The remainder of these connections were shown to target inhibitory interneurons, which would in turn contact pyramidal neurons, suggesting a di- or poly-synaptic mechanism for long range suppression. On the basis of some of this work [Douglas and Martin \(1991\)](#) developed what has become known as the canonical microcircuit for the neocortex. This circuit includes separate inhibitory and excitatory neurons, which are driven by thalamic afferents and recurrent connections. Further work has fleshed out the spatial profiles of these connections, which ultimately gave rise to the simplified circuit described in Figure 2.10. This goes some way toward reconciling anatomy with the experimentally measured functional connectivity profile at high contrast levels.

More recent attempts at reconciling anatomy with function have been able to further resolve some of the problem. In particular, there is clear evidence showing that excitatory synapses onto excitatory and inhibitory neurons differentially target their recipient neurons. Excitatory connection onto inhibitory interneurons seem to preferentially synapse perisomatically, in contrast with recurrent long-range excitatory connections which have been shown to target their recipient neurons dendritically ([Gilbert and Wiesel, 1990](#); [McGuire et al., 1991](#)). Additionally, at least a subset of inhibitory interneurons seem to preferentially target the soma of pyramidal and stellate cells they inhibit ([Markram et al., 2004](#)). On that basis it is reasonable to assume that inhibitory connections are, in general, stronger and may act divisively.

Although these divergent properties of excitatory and inhibitory neurons were only discovered recently it had long been proposed that inhibitory interneurons are inherently more effective at suppressing activity than recurrent excitatory connections are at exciting the network, but due to a high threshold or some other related mechanism the inhibitory neurons are not strongly recruited unless there is strong afferent input ([Sillito, 1979](#)), as would be the case under high contrast conditions. Although it is now clear that network effects allow for strong long-range inhibition through di-

or poly-synaptic connections under the right stimulus conditions, the mechanisms by which contrast dependent behaviors emerge from the cortical circuit are still only vaguely characterized.

A number of models have been developed to explain contrast dependence of contextual effects on the basis of the general principle of asymmetry between the response properties of excitatory and inhibitory neurons. One of the first to publish such a model were Stemmler et al. (1995), who suggested inhibitory neurons require higher external input rates before activating because they receive significantly less spontaneous background input as compared to excitatory neurons, an effect known as stochastic resonance. Although this mechanism has at least been theoretically reaffirmed (Bezrukov and Vodyanoy, 1997), there is no experimental data establishing it as a functionally significant mechanism in V1. Other models, hoping to account for a wider array of RF effects implement such a mechanism directly by setting a higher threshold in the inhibitory population and introducing very strong lateral excitation of inhibitory neurons (Schwabe et al., 2006). Another suggestion was made by Somers et al. (1998), who in addition to a simple threshold asymmetry, also point to the claim by Thomson and Deuchars (1994) and others (Abbott et al., 1997; Tsodyks and Markram, 1997), that synaptic depression causes recurrent excitation to quickly decline in efficacy during high frequency stimulation, while facilitation of excitatory synapses onto inhibitory interneurons increases transmission efficacy as presynaptic firing rates increase (Thomson et al., 1995). The suggestion that inhibitory neurons have a higher contrast threshold has become very popular in the theoretical literature of the past 20 years, however as of yet there is only limited evidence to support this core assumption and there are a number of alternative or concurrent mechanisms that may explain all or at least some of the contrast dependent effects.

As the last paragraphs have shown, inhibition and in particular surround inhibition are at the core of the major discussions on contrast dependent effects and surround modulation and a more thorough understanding of the spatial, temporal and functional dynamics of surround inhibition is required.

2.3.2 Surround Suppression: Feedforward or Feedback?

The last section highlighted how little we still know about the origin of surround suppression and inhibition. There is still significant controversy whether surround suppression originates in feedforward or feedback pathways or whether both contribute over different spatial scales. This includes suggestions that surround suppression in the classical RF are mediated through synaptic depression in the thalamo-cortical afferents (Carandini et al., 2002), broadly tuned inhibition by thalamo-cortical recip-

ients, long-range excitation of local inhibitory interneurons or even through various feedback mechanisms. This section will detail the evidence for each of these proposals, the possibly anatomical origin of each of these mechanisms and tease apart the circuit by looking at interactions between surround suppression, stimulus size and contrast.

Since the circuitry of the cortex is so complex, the task of segregating feedforward and feedback contributions to surround suppression is difficult. Although only a starting point, one way of starting to tease these two possible contributions apart is to look at the time course of suppression. In the literature early and late components to surround suppression have been identified. The early component is characterized as being driven by lower CRF contrasts with spatio-temporally broad band tuning and little adaptation (Levitt and Lund, 1997; Cavanaugh et al., 2002a). The late component on the other hand is driven more strongly by high contrast stimuli in the CRF, has sharp spatio-temporal tuning and can be strongly affected by adaption (Levitt and Lund, 1997). Evidence suggests that the early, broadly tuned component originates in the LGN and the thalamocortical recipient layer of visual cortex (Blasdel and Fitzpatrick, 1984; Hawken et al., 2009). In monkey cortex in particular, this broadly tuned suppressive effect is only weakly evident in the LGN and is thought to arise much more strongly in layer 4 of striate cortex (Webb et al., 2005), which may have some correspondence to the broadly tuned inhibitory population identified by Hirsch et al. (2003). Carandini et al. (2002) on the other hand suggest that there is a synaptic explanation for surround suppression, primarily due to the speed with which the suppression arrives, its immunity to cortical adaptation and the fact that it is restricted to the CRF. However, they concede that synaptic depression doesn't account for gain control and the abolishment of cross-orientation suppression by GABA^A blockade, so a mechanism that can account for all these phenomena may still be preferable. In that vein, Webb et al. (2005) propose two inhibitory mechanism one of which sums local activity in a neurons CRF and divides the response of the CRF and the later component that receives inputs from a much larger area but provides narrowly tuned suppression. The broadly tuned component in particular has a strong relationship with contrast gain control, which has been firmly established to act divisively. Independent work by Xing et al. (2005) supports the suggestion of two inhibitory components and further expand on the size dependence of these two components. Specifically, they conclude that the tuned component is recruited far more strongly for larger stimuli, which seems to confirm a contribution from beyond the CRF.

This recent work has identified two clear and distinct inhibitory components but have not yet fully described which mechanisms and circuits they are mediated by, the next section will attempt to address this shortcoming.

2.3.3 *Distinct Inhibitory Populations*

In order to begin teasing apart the origin of intracortical surround suppression mediated by local inhibitory circuits it is necessary to consider the different candidate cell classes. While there are a long list of different inhibitory cell types based on their morphology and spiking behavior, recent techniques have divided inhibitory into several broad, functionally distinct classes based on their immunoreactivity. The two cell types considered here are parvalbumin (Pv-ir) and somatostatin (Sst-ir) immunoreactive neurons, which are primarily differentiated by the cellular locus of their synaptic targets. While Pv-ir neurons seem to target pyramidal cells perisomatically, Sst-ir neurons target their recipients dendritically. The following subsections will detail the anatomical, physiological and functional differences between these cell classes.

2.3.3.1 *Parvalbumin Immunoreactive cells*

The two main cell types, which exhibit parvalbumin immunoreactivity are the chandelier and basket cells (Binzegger et al., 2004). While chandelier cells make up only a small fraction of GABAergic neurons in the cortex and are primarily found in layer 2/3, the fast-spiking (FS) basket cells are the predominant interneuron subtype in the mammalian cortex across all lamina, accounting for 42% in layer 2/3 and layer 5 and 78% in layer 4 of the cat (Hogan et al., 1992; Huxlin and Pasternak, 2001) and up to 74% across cortical layers in macaque (Van Brederode et al., 1990). The abundance in the thalamocortical recipient layers and the fact that they preferentially target the soma and proximal dendrites of spiny neurons with multiple strong synapses, exhibiting high probability of GABA release (Freund and Katona, 2007; Markram et al., 2004), ensures basket cells are of tremendous interest. On that basis it has been suggested that the perisomatic connectivity profile of basket cells gives them the ability to provide shunting inhibition to layer 4 spiny neurons, acting divisively to control their response gain (Wilson et al., 2012).

Basket cells can be further subdivided, primarily based on their size, into clutch and large basket cells. However all basket cells can make multiple connections onto a target pyramidal neuron (Somogyi et al., 1983) and have a considerable spatial extent (Kisvárday et al., 2002). In particular, studies in cat area 17 and macaque V1 have identified basket cells 1-2 mm in extent (Somogyi et al., 1983; Lund, 1987; Lund and Yoshioka, 1991; Martin et al., 1983) and single cell tracing studies have even identified large basket cells, which give off a roughly uniform number of boutons across a large diameter spanning up to two hypercolumns (Buzás et al., 2001). A schematic representation of the basket cell connectivity profile is summarized and compared against both the orientation column structure and the excitatory connection profile

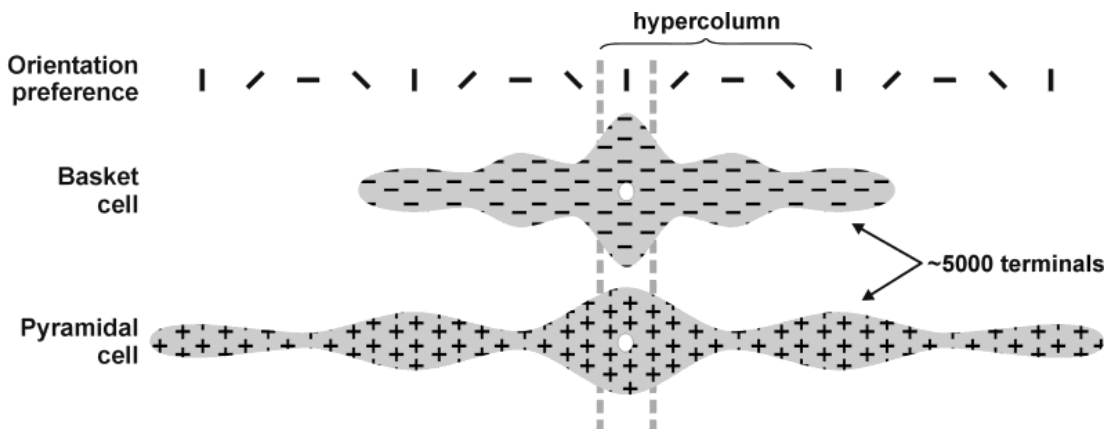


Figure 2.11: Summary schematic comparing relationship between long-range basket cell and excitatory connectivity with the underlying orientation preference structure. Upper legend represents different orientation domains in the cortical topographic map. Grey dotted lines indicate the orientation column within which soma of the simplified basket cell and excitatory neuron are found. The grey field with minus signs indicates the extent of inhibition provided by the basket cell connections considered in the current study. The grey region with plus signs indicates the excitatory field of a stereotypical pyramidal cell based on previous data by [Bosking et al. \(1997\)](#); [Kisvárday et al. \(1997\)](#) and others. The height of the grey plus/minus regions indicates the number of axon terminals provided in that column. While basket cell terminals show local maxima every half hypercolumn distance, pyramidal cell terminals are maximal at every full hypercolumn distance. Reproduced from [Buzás et al. \(2001\)](#).

in Figure 2.11. Functionally such a connectivity profile may indicate that basket cells can suppress neurons with widely varying orientation, which may implicate basket cells as an important mechanism to sharpen orientation preference.

In terms of their spiking behavior Pv-ir cells are characterized as being fast fast-spiking (FS) neurons, often firing in bursts with a very short response latency. Further, evidence from somatosensory cortex in rodent and lagomorph species suggests they receive strong input from thalamocortical afferents arriving in layer 4 and very effectively suppress sustained firing from spiny neurons receiving inputs from the thalamus ([Swadlow, 2003](#)), implicating them in feedforward inhibition. This feedforward inhibition circuit is shown in Figure 2.12. Their effectiveness in suppressing feedforward activity can be explained by the large number of thalamocortical axons they receive, which exhibit faster kinetics than those targeting spiny neurons ([Cruikshank et al., 2007](#); [Gabernet et al., 2005](#)), and the fact that they evoke large inhibitory responses in spiny cells ([Cruikshank et al., 2007](#); [Gabernet et al., 2005](#)).

It is also important to note that the thalamocortical synapses onto the Pv-ir population have been shown to be depressed by repetitive activation, resulting in weaker feedforward inhibition at high stimulation frequencies ([Gabernet et al., 2005](#)), a prop-

erty which may indicate lower activation of the PV population at high contrasts. The Pv-ir population may also play an important role in network homeostasis as activity blockade has been shown to decrease the efficacy of Pv-ir inhibition (Bartley et al., 2008), thereby indirectly up-regulating activity in excitatory cells. Further, selectively up-regulating Pv-ir cells using optogenetic stimulation was shown to have a similar effect as lowering the contrast, which is to increase preferred size and weakening surround suppression (Nienborg et al., 2013). This is compatible with the idea that Pv-ir neurons provide strong feedforward inhibition such that the input drive in the cortex is decreased, as would be observed under low contrast conditions. Overall then, Pv-ir neurons show strong interaction with stimulus contrast and may be involved in regulating the gain of the network with complex implications for the contrast response of the network.

There is still considerable debate on the extent to which this subpopulation is tuned to a particular orientation. Most visuo-cortical models employ broad, non-specific GABAergic inhibition (Somers et al., 1998; Troyer et al., 1998). This seems to be supported by anatomical evidence, which has long shown that inhibitory projections are generally diffuse and display low specificity for specific stimulus features (Albus and Wahle, 1994; Kisvárdy et al., 1997). Further, electrophysiological data paints a similar picture, revealing suppression that is broadly tuned for stimulus attributes, providing orientation unspecific suppression from a visual region that is coextensive with the classical RF (DeAngelis and Robson, 1992). Recent attempts at studying the Pv-ir neurons at the single neuron level have revealed a mixed picture. While the cells as a whole were broadly tuned to various stimulus features, individual branches often displayed very high specificity, which may underlie subfield antagonism and contribute to a push-pull configuration (Kisvárdy et al., 2002). Studies in mouse visual cortex seem to confirm such a dual purpose of Pv-ir neurons, although they also find higher heterogeneity in the Pv-ir population (Runyan et al., 2010). This may indicate a laminar differentiation in function as studies of Pv-ir neurons in the thalamocortical recipient layer 4 have characterized them to exhibit very broad tuning, due to their low spiking threshold and more convergent inputs (Ma et al., 2011). However, even in layer 2/3 most Pv-ir cells displayed broad orientation tuning (Hofer et al., 2011). Further studies in cat area 17 find very similar results identifying a class of inhibitory complex cells in layer 4 exhibiting weak orientation tuning (Hirsch et al., 2003), which can primarily be accounted for by the tuning of synaptic responses and a lower spike threshold (Nowak et al., 2008). A more recent study in auditory cortex seems to affirm these conclusions, hypothesizing that ‘while PV neurons may provide broadly tuned feedforward inhibition for a rapid control of ascending inputs to excitatory neurons, the delayed and more selective inhibition from SOM neurons

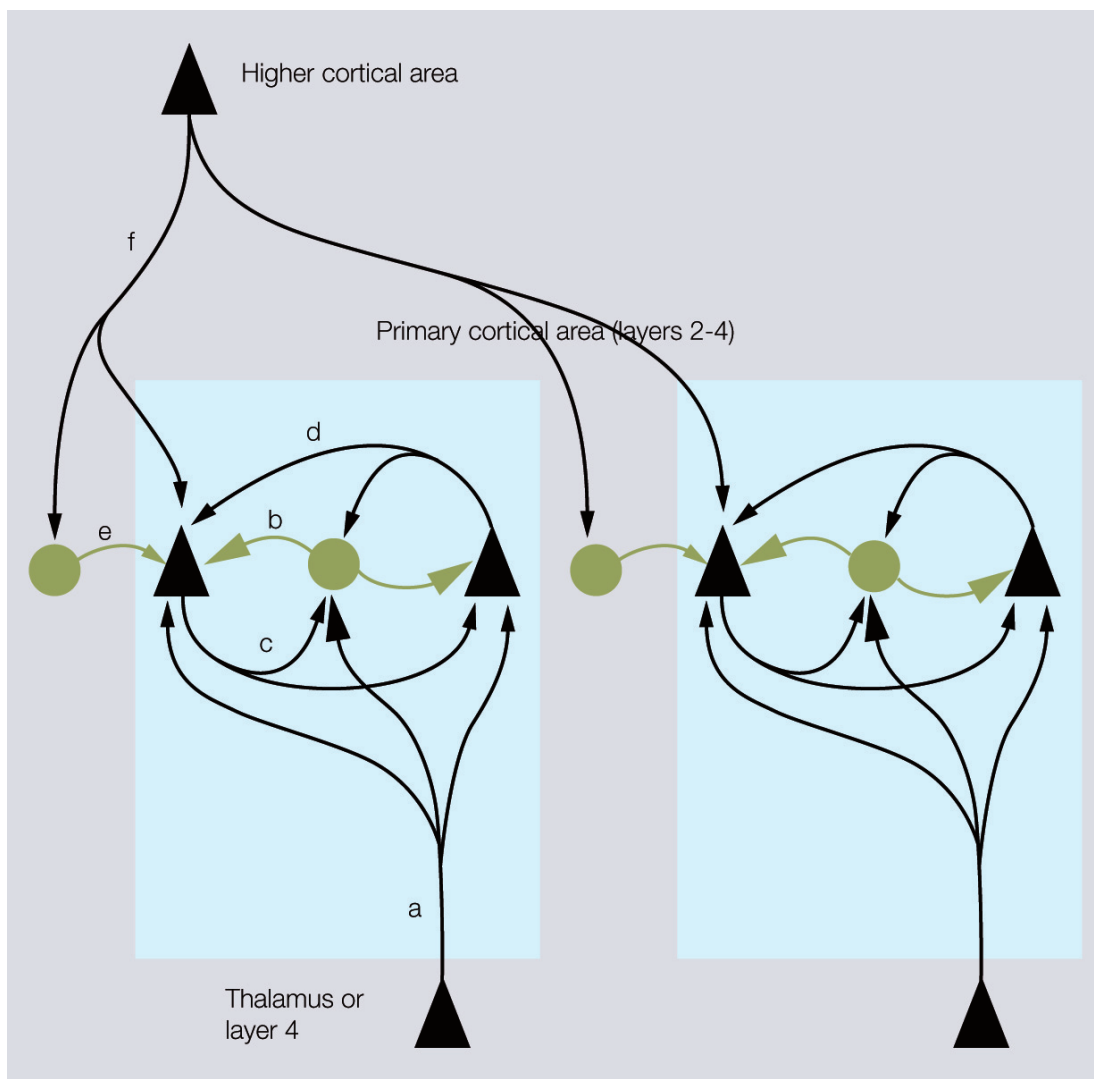


Figure 2.12: Inhibitory networks involving fast-spiking parvalbumin-immunoreactive neurons in thalamocortical, interlaminar and interareal cortical circuits. Feedforward excitatory thalamocortical inputs to pyramidal cells, spiny stellate neurons (\blacktriangle) and fast spiking interneurons (\bullet) in layers 2-4 (a). Inputs to interneurons are stronger (large arrowheads) than inputs to spiny cells. PV neurons provide strong (large rectangular endings) feedforward inhibition (b) to spiny cells. Feedback inhibition (c) results from PV neurons that are excited by the same spiny neurons that they inhibit. These reciprocally connected spiny neuron/PV neuron pairs share common inputs (e.g., cells in layer 4 from thalamus or cells in layer 2/3 from layer 4) creating recurrent excitatory (d) and inhibitory subnetworks (contained within blue shaded boxes). ‘Lateral’ inhibition (e) of these subnetworks results from PV neurons that are driven by excitatory feedback connections (f) from outside the subnetworks (e.g., by layer 5 to layer 2/3 connections or feedback from higher cortical areas). Notice that ‘lateral’ inhibition is weaker (small rectangular endings) than feedforward and feedback inhibition and impinges on multiple subnetworks. Reproduced from Burkhalter (2008).

may provide a specific modulation of feedback inputs on their distal dendrites' (Li et al., 2014). Further study will be needed to confirm whether these results extend to the primate, however it is clear that basket cells generally display weaker tuning than spiny neurons in V1.

Based on our current knowledge of Pv-ir cell population and more specifically the basket cells, it is clear that they provide a good candidate mechanism to account for a number of phenomena. Their fast response profile, large spatial extent and the relative weakness in their orientation tuning may allow them to carry out fast, adaptive gain control, broadly tuned suppression and thereby sharpen the orientation preference of the PNs in their vicinity. So while synaptic depression may still provide an alternative explanation for many of these phenomena, it is likely that the Pv-ir population carries out at least some of these functions.

2.3.3.2 Somatostatin Immunoreactive cells

The Sst-ir population has been characterized to a lesser extent, but a general consensus is beginning to emerge around their function and electrophysiological properties. The Sst-ir cells account for around half of the non-PV-expressing neurons (Gonchar et al., 2007; Xu et al., 2010) and preferentially synapse onto distal dendrites and dendritic tufts of pyramidal neurons (Di Cristo et al., 2004; Silberberg and Markram, 2007), on the basis of which it has been suggested that Sst-ir neurons act subtractively (Wilson et al., 2012).

In trying to characterize the excitatory inputs to Sst-ir cells in layer 2/3 of the mouse, Xu and Callaway (2009) determined that unlike Pv-irs, the main source of excitation of Sst-irs were horizontal axons within layer 2/3 not the ascending layer 4 axons. This property also contributed to the size dependent responses of the Sst-irs, which were shown to be recruited progressively more strongly when they were exposed to optogenetic photostimulation of increasing diameter. Importantly, the Sst-ir response grew larger even when photostimulation reached beyond its maximal dendritic extent, demonstrating that the recruitment of increasingly more distant pyramidal cells provided their main excitatory drive. This putative circuit is shown in Figure 2.13, exhibiting their pooling of tuned, excitatory input from pyramidal cells across a large area, providing only very local inhibition. Additionally it seems that Sst-ir interneurons are capable of disinhibiting the thalamocortical recipient layer 4 by targeting Pv-ir cells (Xu et al., 2013).

In terms of their response properties the Sst-ir neurons have been shown to exhibit much lower levels of spontaneous and evoked activity, stronger orientation and direction selectivity and longer response latencies than Pv-ir neurons in mouse visual cortex (Ma et al., 2011). These properties are consistent across both layer 2/3 and

4 and may point to a role in gating later arriving intracortical excitatory inputs. In terms of their tuning properties Sst-ir neurons display smaller On/Off subfields with less overlap than nearby spiny neurons and orientation tuning on par with pyramidal neurons. While most data on their tuning properties comes from rodent visual cortex, which does not exhibit a topographic organization of orientation tuning, it seems the stronger orientation selectivity of Sst-ir cells can be accounted for by their preferential connectivity to neurons with similar orientation preference as well as a higher spiking threshold and weaker excitatory inputs (Bartley et al., 2008). Another interesting feature of Sst-ir response properties is the fact that although their excitatory inputs are weak, they are facilitating resulting in delayed but strong activation under high frequency stimulation (Beierlein et al., 2003; Bartley et al., 2008; Tan et al., 2008). Based on these properties, Sst-ir neurons would only be recruited to provide significant inhibition if the stimulus contrast or size reaches a certain level (Adesnik et al., 2012). Thus they could provide a direct mechanism for contrast dependent size tuning and surround modulation effects, being only weakly recruited when contrast or stimulus size is low but becoming strongly activated at higher contrast levels and for larger stimulus sizes.

Another suggested role for Sst-ir neurons is the gating of feedback signals on the distal dendrites of principal neurons. The Martinotti cells, which provide strong axonal projections to layer 1 of the cortex, make up a large proportion of Sst-ir neurons in layer 2/3 of the cortex and are therefore well placed to suppress feedback signals arriving in the superficial layers of the cortex (Fanselow et al., 2008; Gentet et al., 2012). In the rodent somatosensory cortex, Gentet et al. (2012) showed that Sst-irs in layer 2/3 become spontaneously active during passive wakefulness but are strongly suppressed during active whisking behavior, presumably by the vasoactive intestinal peptide (Vip)-ir population. The Sst-ir cells may therefore be involved in mediating top-down control of sensory processing, effectively gating context-dependent processing in a state dependent manner.

In summary, Sst-ir neurons seem to provide delayed and feature-selective feedback inhibition, which puts them in a good position to effectively gate late arriving intracortical excitatory inputs arriving from either lateral or feedback connections but may also be implicated in suppressing feedforward inhibition by inactivating layer 4 Pv-ir cells.

2.3.3.3 *Vasointestinal peptide expressing interneurons*

The previous review focused primarily on the two most common types of inhibitory interneurons, the Parvalbumin (PV) and Somatostatin-expressing (Sst) cells, since then a number of studies have focused on the role of 5HT_{3ar}-expressing interneurons

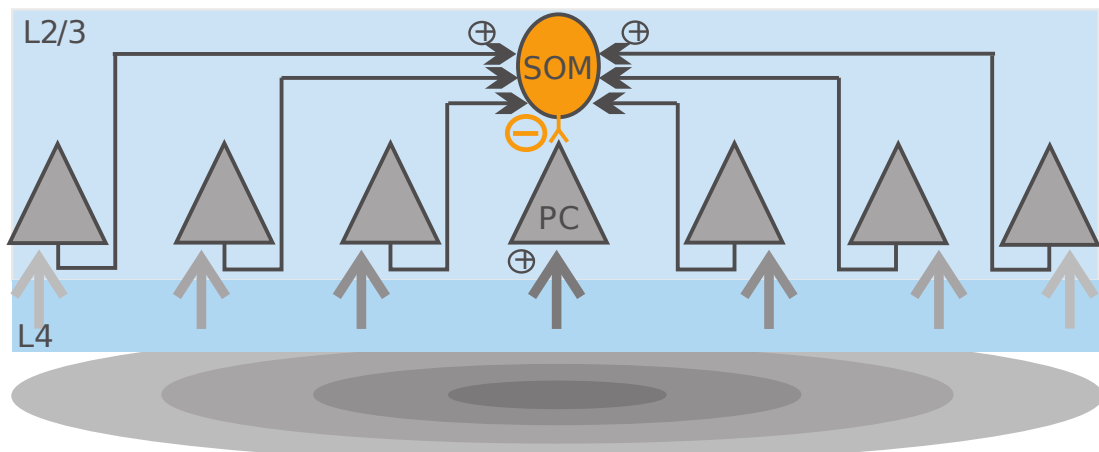


Figure 2.13: Schematic illustration of the cortical circuit in layer 2/3 contributing to surround suppression. As a visual stimulus expands (larger stimuli are shown in lighter grey), recruitment of adjacent PCs increases Sst-ir excitation through horizontal axons (horizontal arrows). Reproduced from Adesnik et al. (2012).

and particularly the vasointestinal peptide (Vip)-expressing subgroup (Fu et al., 2014; Higley, 2014; Kepcs and Fishell, 2014; Lee et al., 2013).

The Vip subgroup is particularly concentrated in upper, associative layers and feedback layers of the cortex, as shown in figure 2.14 by Rudy et al. (2011). The most striking finding was their central role in state dependent modulation during active whisking tasks. Lee et al. (2013) found that S1-projecting vM1 pyramidal neurons strongly recruited Vip-expressing interneurons in superficial layers of somatosensory barrel cortex, which in turn inhibited somatostatin-expressing interneurons causing effective disinhibition of cortical pyramidal cells. These results were then affirmed through optogenetic stimulation of Vip neurons in mouse V1, artificially mimicking the effects of locomotion (Fu et al., 2014). When considered in conjunction with previous studies that established strong cholinergic and nicotinic inputs to Vip neurons from the basal forebrain (Wickersham et al., 2007), this suggests a strong involvement of Vip neurons in a cortical circuit responsible for the enhancement of activity in sensory cortex by behavioural state.

2.3.3.4 Connectivity between different cell types

In order to gain an understanding of the circuits the different interneuron cell types are involved in, it is important to consider their interconnectivity. Several studies have sought to determine the connectivity between Pv-ir, Sst-ir and other interneuron types. The core findings of these studies determined that Pv-ir cells preferentially inhibit one another, Sst-expressing cells avoid one another and inhibit all other types of interneurons particularly the Pv-ir cells (Xu et al., 2013), while a third type, the Vip-

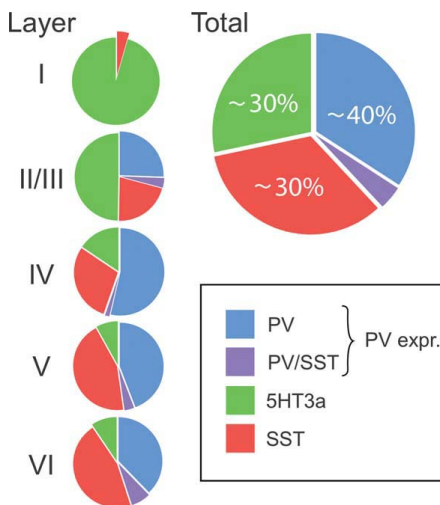


Figure 2.14: Distribution of GABAergic interneurons in S1 cortex by immunohistological marker. Reproduced from [Rudy et al. \(2011\)](#).

ir cells preferentially inhibit Sst-ir cells ([Pfeffer et al., 2013](#)). This connectivity profile is schematically represented in Figure 2.15. In mouse cortex the Pv-ir, Sst-ir and Vip-ir cells accounted for about 40%, 18% and 8% of the GABAergic population, respectively ([Xu et al., 2010](#)), and although these percentages vary considerably across species Pv-ir and Sst-ir are always the two most commonly expressed GABAergic populations.

Recent tracing techniques have also been able to establish that excitatory cells provide orientation specific inputs to the inhibitory population. Using viral tracing techniques [Liu et al. \(2013\)](#) are able to trace inputs to inhibitory and excitatory neurons in the cat visual cortex.

2.4 GABAERGIC REGULATION OF PLASTICITY AND COLUMN STRUCTURE

Experience dependent plasticity has been shown to shape the organization of the sensory cortex during the critical period and beyond. Dark rearing ([Fregnac and Imbert, 1978](#)) and monocular deprivation (MD) experiments ([Shatz et al., 1978](#)) in particular have confirmed the fundamental importance of sensory experience in shaping the development of the cortex. The mechanisms controlling the onset of the critical period and regulation of plasticity thereafter have also been studied extensively and a large body of evidence points to the important role of the inhibitory neurotransmitter γ -aminobutyric acid (GABA) in regulating synaptic plasticity. However as the above paragraphs have shown the population of GABAergic neurons is highly heterogeneous with hugely divergent anatomical and functional profiles. Using specific pharmacological and genetic populations it has been possible to narrow down the

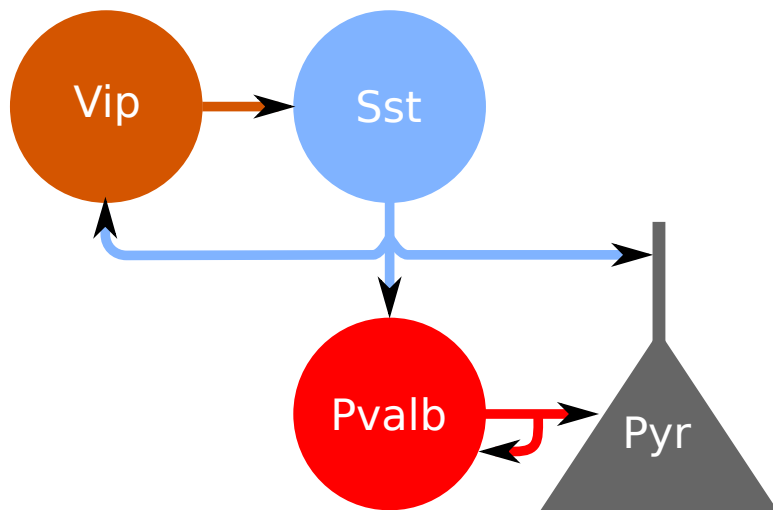


Figure 2.15: Connectivity between somatostatin (Sst), parvalbumin (Pv), vasoactive intestinal peptide (Vip) expressing and pyramidal (Pyr) cell types. Adapted from [Pfeffer et al. \(2013\)](#).

involvement of certain interneuron subtypes in shaping critical period plasticity and column structure in the cortex.

One of the first indications that GABAergic circuits are involved in shaping plasticity came when it was shown that a gene-targeted disruption of the GABA synthetic enzyme glutamic acid decarboxylase 65 (GAD65) could delay critical period onset indefinitely ([Fagiolini and Hensch, 2000](#)). In order to further narrow down the specific GABA circuits underlying visual cortical plasticity, more specific pharmacological manipulations were required. On that basis [Fagiolini et al. \(2004\)](#) used benzodiazepine infusions, known to selectively enhance GABA type A (GABA_A) receptor-mediated currents through the $\alpha 1$ subunit ([Rudolph et al., 1999](#)), in conjunction with MD to prematurely trigger ocular dominance plasticity in mice. These GABA_A receptor- $\alpha 1$ subunits are preferentially enriched at somatic synapses receiving input from Pv-ir large basket cell terminals ([Klausberger et al., 2002](#)), strongly implicating large basket cells in visual cortical plasticity.

Beyond controlling the timing of critical period plasticity further experiments using benzodiazepines have shown strong effects on the columnar organization of the cortex. The experiment by [Hensch and Stryker \(2004\)](#) locally infused regions of cat area 17 with the GABA_A agonist diazepam and an inverse agonist (DMCM) and studied the effects on the ocular dominance columns. Chronic treatment with diazepam had little effect in the functional properties of mature cortical neurons *in vivo* apart from enhancing inhibitory postsynaptic currents. However, the treated hemisphere exhibited reduced binocularity of single unit responses and wider OD columns near the infusion site. Infusion with the benzodiazepine inverse agonist DMCM had the

inverse effect, resulting in less discrete and narrower columns near the infusion site. These results suggest that the diazepam mediated enhancement in competition reduces binocularity of single-unit responses, as well as sharpening and widening the anatomical segregation of monocular regions near the infusion site. This once again suggests that GABA_A inhibitory currents, primarily originating from Pv-ir neurons in the cortex, are fundamentally important to shaping the plasticity and organization of the cortex.

In order to establish how ocular dominance plasticity emerges during monocular deprivation, Kuhlman et al. (2013) developed even more precisely targeted pharmacological manipulations. By selectively expressing specific receptors on Pv-ir cells they were able to selectively up- and down-regulate their activity. Their results indicate that a rapid, but transient reduction in Pv-ir cell firing restores pyramidal cell firing to pre-deprivation levels allowing competitive plasticity to occur. Pv-ir neurons therefore seem to play a permissive role in visual cortical plasticity. Interestingly adult sensory plasticity such as reinforced associative learning occurs through a similar mechanism, where cholinergic activation of layer 1 interneurons suppresses Pv-ir neural activity allowing associative fear learning to occur (Letzkus et al., 2011). All this work suggests a crucial role for Pv-ir neurons in controlling cortical plasticity during the critical period and beyond.

2.5 FUNCTIONAL ROLES OF INTRACORTICAL CONNECTIVITY

A major feature of the neural code in the cortex is the elimination of redundancy in order to achieve a sparse representation of the input or if there is insufficient information to fill in the missing information based on remembered statistics of the visual world. Sparse coding in developmental models of the primary visual cortex can be achieved by allowing lateral inhibitory connections to develop non-isotropic connectivity, which allows the network to learn the redundant features of the input and suppress them. If such development is not allowed to take place and isotropic surround suppression is employed, cross-orientation stimuli, belonging to a separate object or contour may be suppressed, thus reducing the information content encoded by the network. Therefore long-range isotropic suppression has to be considered destructive (Miikkulainen et al., 2005). Similarly, strong lateral excitation will activate neural ensembles representing non-existing inputs based solely on previous input statistics. While this is desirable when very little information is available it can disrupt sparse code formation by expanding the activity bubble or causing the false detection of a stimulus. Therefore the sensory cortex has to maintain a fine balance not only between excitation and inhibition but also in combining past information with

the feedforward information stream arriving in the cortex. Identifying and modeling the circuits involved in these processes is a fundamental challenge for neuroscience and will hugely contribute to extending our understanding of cortical information processing.

Over the last decade evidence for multiple separate inhibitory populations, subserving different functions, has been considerably strengthened. Although their precise properties in regard to morphological and electrophysiological heterogeneity are still unclear there are a number of identifiable circuit elements. Afferent input provides strong, low latency excitation to the Pv-ir neurons in the thalamocortical recipient layer 4, which in turn act as both a feedforward inhibition and dynamic gain control mechanism on the broadly activated excitatory cell population. This results in local decorrelation of the neural activity, which allows recurrent excitation to amplify the activity in the local neural ensemble. Meanwhile Sst-ir neurons begin to integrate the local activity through the local and long-range orientation-specific lateral connections. If their inputs are sufficiently strong they will activate allowing this polysynaptic circuit to reduce long range correlation in the input activity, further reducing redundancy. If they are only weakly activated on the other hand, long-range lateral excitatory connections aren't outcompeted and the circuit can fill in weak or missing information based on past statistics. Under such regimen the differential recruitment of the two separate inhibitory populations would be responsible for a shift in cortical state from a mode of redundancy-reduction and feature discrimination to one of visual inference. Additionally, modulatory inputs to the cortex like cholinergic modulation arriving from the nucleus basalis may mediate a number of effects, whether that is a shift in the circuit from a down-state, where information is recurrently processed, to a feedforward heavy up-state, by reducing feedforward inhibition and boosting feedforward excitation, or a mode in which task-relevant information is selectively filtered, is still unclear. The following sections will outline how these possibilities have begun to be explored by constructing a model based on the available experimental evidence and will outline plans to begin testing some of these different hypothesis.

2.6 CONTEXTUAL MODULATION AND ATTENTION

The computational task in vision is to map visual experience to the cortical representation of that particular stimulus or if no such representation exists, to extract lower level features in order to encode them for future reference. Using this statistical model the brain is then able to decide, which visual features carry behavioral importance and which can be safely ignored. As such the neocortex has to combine prior

information with the incoming information stream and quickly and reliably identify the most salient stimuli. It has often been argued that this process is mediated by bottom-up and top-down processes, although it seems likely that there is close coupling between the two. This section will outline high level models of attentional modulation, attempts to understand the neurobiological processes behind them and more basic contextual modulation phenomena may underly many of these higher level effects.

2.6.1 *Contextual and Attentional Phenomena in V1*

A number of phenomena associated with attention and contextual modulation, including iso-orientation suppression or facilitation, boundary detection, contour completion and noise exclusion have been observed in V1. Although these phenomena are generally associated with bottom-up attention they lay the foundation for higher level phenomena such as pop-out and figure-ground segregation and may reveal more about general mechanisms applying also to higher visual areas.

Basic contextual effects such as iso-orientation suppression have already been discussed and models have begun to suggest the functional connectivity mediating implicating both lateral and feedback connections. While, Li (2002) has proposed that pre-attentive bottom-up processes allow V1 to generate a saliency map of the visual input. However, the fact that higher cortical areas have also been associated with saliency signaling and the lack of long range intra-areal connectivity in V1 suggest that while it can encode local saliency, feedback is required to globally integrate saliency across visual space.

Feedback modulation of V1 activity has been implicated in a number of effects, spatial attention being chief among them. Spatial attention is thought to be able to select multiple low and high level objects in the visual space across V1 and higher visual areas (McMains and Somers, 2004). It is thought to underly noise exclusion, observed by Dosher and Lu (2000) and may be explained by effects similar what has been experimentally observed during iontophoretic application of ACh. Other effects that have been commonly been associated with feedback in some form are the signaling of illusory contours, which have been shown to be negatively signaled or deemphasized in V1 (Ramsden et al., 2001) and boundary detection (Poort et al., 2012). In the planning section, concrete proposals will be made suggesting what mechanisms may account for these phenomena and how they can be implemented.

2.7 NATURAL IMAGE STATISTICS, SPARSITY AND HORIZONTAL CONNECTIONS

It has long been hypothesized that connectivity in the cortex captures the statistics of the sensory input in order to perform predictions and maintain sparse representations of novel inputs (Simoncelli and Olshausen, 2001). A wide range of work has explored the role of the distributions of light intensities, color statistics and spatial correlations in natural images. In particular, the power law distribution of spatial frequencies in natural images has been widely discussed in the literature but ultimately this largely seems to reflect the scale invariance within natural images (Ruderman, 1997).

Numerous studies and models have since been devised to address whether the visual system takes advantage of the correlational structure of natural images. These types of normative models were able to show that surround inhibition, whether subtractive or divisive, could cancel out correlations effectively whitening or decorrelating the activity in the visual system (Srinivasan et al., 1982; Atick and Redlich, 1992). In doing so they quickly found that simple decorrelation wasn't sufficient to optimally represent natural images because whitening does not eliminate all structure in a natural image, e.g. edges and lines remain. By introducing an explicit sparsity constraint, Olshausen and Field (1996) were able to develop V1-like simple cell receptive fields with varying orientations, spatial frequencies and sizes. These models indicated that sensory system was optimizing two constraints, sparsity and statistical independence. However, even these approaches cannot achieve complete statistical independence since there are higher order correlations even between non-overlapping receptive fields.

By introducing divisive normalization, Schwartz and Simoncelli (2001) were able to show that these types of dependencies could be further eliminated. Furthermore, the weights used in the computation of the normalization signal could be specifically optimized to maximize the independence of the normalized responses. Additionally, they demonstrated that the optimal weights were at least partly due to the prevalence of extended contours in natural images. Attempting to quantify the co-occurrence statistics of contours in natural images, Geisler et al. (2001) demonstrated that the performance in contour detection tasks could be predicted by a local grouping rule derived from the co-occurrence statistics. The first explicit link to horizontal connectivity was made by Sigman et al. (2001), who noted that the pattern of long-range patchy connectivity in the primary visual cortex, linking iso-orientation columns has a close correspondence with the observation of co-circularity in natural image statistics. Noting the processes of iso-orientation suppression and contour integration, they argue that iso-orientation suppression may serve to further reduce redundancies in neural

coding, thereby achieving greater statistical independence, which would explain why neural responses appear most sparse when presented with natural stimuli. Secondly, observing that visual cortex can also exhibit colinear facilitation under low contrast conditions (Sceniak et al., 1999; Kapadia et al., 1999), they suggest that under low signal-to-noise conditions the cortex may act to enhance repeated statistics to aid the identification of contours and form.

These theoretical studies have hugely advanced our thinking about the computations performed by the early visual cortex, however very little work has been done to look at the actual structure of horizontal connectivity in V1, largely due to the difficulty in obtaining data from more than just a few cells. Even on the question whether horizontal connections are anisotropic along the axis of preferred orientation of the neuron, as would be expected from theoretical studies, there is conflicting evidence. The result has been confirmed in monkey (Sincich and Blasdel, 2001), tree shrew (Bosking et al., 1997) and cat (Schmidt et al., 1997), but conflicting results exist in macaque Angelucci et al. (2002b). By performing analyses on an old tree shrew dataset Hunt et al. (2011) investigated whether horizontal connections captured the co-circularity of natural image statistics. Although they found neurons, which exhibited co-circularity and anti-cocircularity and hypothesize a role for both, given the small number of lateral connections fields and the fact that second order properties are highly sensitive to even small errors in the data, it is unclear how strong this result is. Further research in this area is desperately needed.

REPRODUCIBLE SCIENCE AND VISUALIZATION

Although the subject of this thesis is centered around modeling of the visual cortex a reproducible workflow is crucial to all scientific fields and especially so in the computational sciences. As part of the work presented in this thesis, we describe a new workflow to make the exploration, analysis and publication of complex models easier and more reproducible at every step. In particular this chapter describes how the HoloViews library developed to aid the work as part of the PhD achieves these goals and provides a general solution to data visualization, storage and analysis that is now used in a number of research projects.

Developing such a workflow was essential to allow quick exploration of the highly non-linear models developed as part of this research. This chapter will reproduce a paper on the HoloViews library published in the Proceedings of 14th Python in Science Conference published as joint first author with Jean-Luc Stevens. This paper will detail the principles behind the design of the library and we will summarize how the library fits into an overall workflow reaching from launching complex parameter searches to the exploration of the resulting data and preparation of figures and results for the final published figures.

3.1 HOLOVIEWS: BUILDING COMPLEX VISUALIZATIONS EASILY FOR REPRODUCIBLE SCIENCE

HoloViews: Building Complex Visualizations Easily for Reproducible Science

Jean-Luc R. Stevens^{††*}, Philipp Rudiger^{††}, James A. Bednar[‡]

Abstract—Scientific visualization typically requires large amounts of custom coding that obscures the underlying principles of the work and makes it difficult to reproduce the results. Here we describe how the new HoloViews Python package, when combined with the IPython Notebook and a plotting library, provides a rich, interactive interface for flexible and nearly code-free visualization of your results while storing a full record of the process for later reproduction.

HoloViews provides a set of general-purpose data structures that allow you to pair your data with a small amount of metadata. These data structures are then used by a separate plotting system to render your data interactively, e.g. within the IPython Notebook environment, revealing even complex data in publication-quality form without requiring custom plotting code for each figure.

HoloViews also provides powerful containers that allow you to organize this data for analysis, embedding it whatever multidimensional continuous or discrete space best characterizes it. The resulting workflow allows you to focus on exploring, analyzing, and understanding your data and results, while leading directly to an exportable recipe for reproducible research.

Index Terms—reproducible, interactive, visualization, notebook

Introduction

Scientific research alternates between stretches of speculative, exploratory investigation and periods where crucial findings are distilled and disseminated as publications or reports. The exploratory phase typically involves running many different analyses with interactive plotting tools before the important aspects of the data are determined. The final results are then typically prepared as static figures for dissemination, often putting together many subfigures into a complicated figure that reveals multiple interrelated aspects of the results.

Current software tools provide relatively poor support for this dual exploring/reporting nature of scientific research, severely limiting scientific progress. On the one hand, developing new exploratory visualizations typically requires large amounts of custom software coding, which is slow, error-prone, and distracts from the actual scientific analysis. Moreover, this process typically involves a large amount of trial and error, generating transitory code and analyses that make it difficult to later reproduce the steps that led to any particular

result [Cro13]. Switching to different tools for final, non-interactive, publication-quality figures exacerbates this problem, further disconnecting the reported results from the process by which they were created. This lack of reproducibility is a serious handicap both for progress within a single lab and for the community as a whole, making it nearly impossible for researchers to build on each others' work even for purely computational projects [Cro13].

Here we will describe a new Python software package built to address these problems directly, by providing simple tools for gradually building elaborate visualizations and analyses interactively yet reproducibly. HoloViews supports immediate exploration of data as it is obtained, without requiring custom coding, and then supports incrementally revealing more complex relationships between datasets, culminating in the final publication of fully reproducible scientific results.

In this paper we will focus on the high-level design principles that allow HoloViews to achieve these goals and we encourage the reader to visit holoviews.org for concrete examples. As detailed below, we show how this is achieved by enforcing a strict separation in the declaration of the semantic properties of the data and the specification of plotting options, allowing the user to declaratively specify their intent and let HoloViews handle the visualization.

The interactive interpreter

To understand this approach, we need to consider the history of how we interact with computational data. The idea of an interactive programming session originated with the earliest LISP interpreters in the late 1950s and remains a popular way to interact with dynamic languages such as Python.

However, like most such command prompts, the standard Python prompt is a text-only environment. Commands are entered by the user, parsed, and executed, with results displayed as text. This offers immediate feedback and works well for data that is naturally expressed in a concise textual form. Unfortunately, this approach begins to fail when the data cannot be usefully visualized as text, as is typical for the large datasets now commonplace. In such instances, a separate plotting package offering a rich graphical display would normally be used to present the results outside the environment of the interpreter, via a graphical user interface.

This disjointed approach reflects history: text-only environments, where interactive interpreters were first employed,

[†] These authors contributed equally.

^{*} Corresponding author: jlstevens@ed.ac.uk

[‡] Institute for Adaptive and Neural Computation, University of Edinburgh

Copyright © 2015 Jean-Luc R. Stevens et al. This is an open-access article distributed under the terms of the Creative Commons Attribution License, which permits unrestricted use, distribution, and reproduction in any medium, provided the original author and source are credited.

appeared long before any graphical interfaces. To this day, text-only interpreters are standard due to the relative simplicity of working with text. Proprietary attempts to overcome these limitations, such as the Mathematica Notebook [Wol03], have remained constrained by limited interoperability and a lack of standardized open formats. Other approaches focusing explicitly on reproducibility involve building a recipe for reproducing results only at the end of the scientific project [knitr], when it is often too late to capture the important steps involved. Here we consider how graphical output can be integrated fully into an interactive workflow, addressing both exploration and reproducibility simultaneously.

Fixing the disconnect between data and representation

At the same time as text-based interpreters have failed to overcome the inherent limitations of working with rich data, the web browser has emerged as a ubiquitous means of interactively working with rich media documents. In addition to being universally available, web browsers have the benefit of being based on open standards that remain supported almost indefinitely. Although early versions of the HTML standard only allowed passive page viewing, the widespread adoption of HTML5 has made it possible for anyone to interact with complex, dynamic documents in a bi-directional manner.

The emergence of the web browser as a platform has been exploited by the Python community and the scientific community at large with tools such as the IPython Notebook [Per07] and SAGE MathCloud [Ste05]. These projects offer interactive computation sessions in a notebook format instead of a traditional text prompt. Although similar in design to the traditional text-only interpreters, these notebooks allow embedded graphics or other media (such as video) while maintaining a record of useful commands in a rich document that supports the gradual development of a document with interleaved code, results, and exposition.

Yet despite the greatly improved interactive capabilities of these tools, the spirit of the original interpreter has not yet been restored: there is still an ongoing disconnect between data and its representation. This artificial distinction is a lingering consequence of text-only displays, forcing a strict split between how we conceptualize "simple" and "complex" data. Although the IPython notebook now offers the means to give objects rich media representations, few packages have so far embraced this and none have supported easy composition of related figures. As a result the most common way to visualize complex data remains for the user to specify a detailed list of steps to get subfigures using an external plotting package such as Matplotlib [Hun07], then often combining subfigures using a GUI-based image editor.

Here we introduce HoloViews, a library of simple classes designed to provide an immediately available representation for even complex data in notebooks, analogous to the way simple datatypes are displayed in interactive sessions. HoloViews is not a plotting package; instead, it offers a set of useful data structures paired with rich, customizable visual representations that display effortlessly in the IPython Notebook environment. The result is research that is more interactive, concise, declarative, and reproducible. Figure 1 shows a self-contained

example of building a complex visualization showing the declaration of an `Image` object followed by an example of how to compose HoloViews objects together.

Design principles

The core design principle of HoloViews is to *automatically* and *transparently* return and display declarative data structures to the user for immediate feedback without requiring additional code. Although this concept is familiar and intuitive when interactively working with simple data types, it is worth reviewing explicitly what is going on so that the appropriate graphical extension of these ideas is clear.

When executing an addition operation like `1 + 2.5` at a Python prompt, the expression is parsed, converted into bytecode, and then executed, resulting in the float value `3.5`. This floating-point value is immediately returned to the user in the appropriate displayable representation, giving the user immediate feedback. Of course, this representation is not the float itself, but the string "`3.5`". Such strings are automatically generated by the interpreter, via the displayed object's `__repr__` method.

The Python interpreter also provides such automatic, immediate feedback for more complex data types like large NumPy arrays, but for such data the displayed string has very little utility because it is either incomplete or impractical. In a terminal, this restriction is a result of the `__repr__` method only supporting a text-based display value. Using HoloViews in the IPython Notebook, you can give your array a more useful, interpretable default visual representation as an image, curve, or similar plot according to the following principles:

- It must be easy to assign a useful and understandable default representation to your data. The goal is to keep the initial barrier to productivity as low as possible -- data should simply reveal itself.
- These atomic data objects (elements) should be almost trivially simple wrappers around your data, acting as proxies for the contained arrays along with a small amount of semantic metadata (such as whether the user thinks of some particular set of data as a continuous curve or as a discrete set of points).
- Any metadata included in the element must address issues of *content* and not be concerned with *display* issues -- elements should hold essential information only.
- There are always numerous aesthetic alternatives associated with rich visual representations, but such option settings should be stored and implemented entirely separately from the content elements, so that elements can be generated, archived, and distributed without any dependencies on the visualization code.
- As the principles above force the atomic elements to be simple, they must then be *compositional* in order to build complex data structures that reflect the interrelated plots typical of publication figures.

The outcome of these principles is a set of compositional data structures that contain only the essential information underlying potentially complex, publication-quality figures.

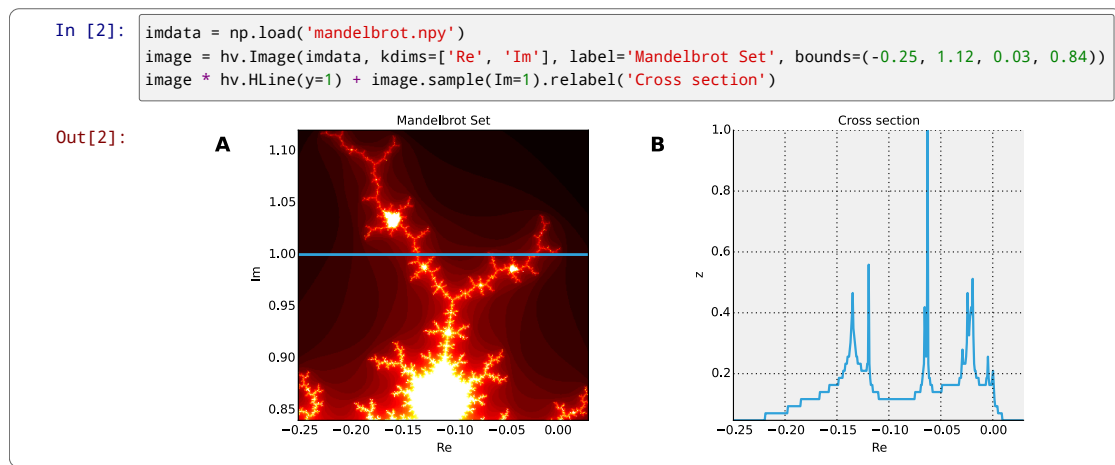


Fig. 1: Example of a composite HoloViews data structure and how it is displayed in an IPython Notebook session. The `imdata` array loaded using Numpy corresponds to the displayed portion of the Mandelbrot set. **A.** The `Image` element displays `imdata` overlaid via the `*` operator with a horizontal line element (`HLine`). **B.** A `Curve` element generated via the `.sample()` method of the `image`, showing a cross-section of the fractal along the indicated blue horizontal line. The curve is concatenated with the `Overlay` in **A** via the `+` operation.

These data structures have an understandable, default visualization that transparently reveals their contents, making them a useful proxy for the data itself, just as the text `3.5` is a proxy for the underlying floating-point value. This default visualization may then be customized declaratively to achieve the desired aesthetics, without complicating the objects themselves.

In the next section we will discuss the data structures that hold the important content. Starting with the simple primitive elements, we examine how they can be composed into complex figures and embedded in high-dimensional spaces for exploration. Along the way we will discover how our implementation realizes the design principles outlined and manages to keep the state of the data separate from its visual representation.

Data Structures

In this section we discuss the data structures that hold the raw data and the essential semantic content of interest. The Elements section introduces each of the primitives, and the Collections section explains how they can be combined. Finally, we will discuss working with Elements embedded in high-dimensional continuous or discrete spaces.

Elements

The atomic classes that wrap raw data are the Element primitives. These classes are named by the natural representation they suggest for the supplied data, with `Image`, `Curve`, and `Scatter` being some simple examples. These elements are easily constructed as they only require the raw data (such as a NumPy array) to display.

In Figure 1, we have some examples of the Element primitives. On the left, in subfigure **A**, we see the `Image` primitive containing a two-dimensional NumPy array. This `Image` is declared by supplying the NumPy array `imdata` along with the optional metadata, including a suitable label and

a declaration of the bounding region in the complex plane. The visual output is automatically generated and shows that the array is a part of the Mandelbrot set. Our object merely holds the supplied NumPy array, which remains easily accessed via the `.data` attribute. In part **B** of Figure 1 we have an example of a `Curve` containing a horizontal cross section of the image, as computed by the `sample` method.

Although the names of the Elements suggest that these objects are about visualization, they are primarily concerned with content and *not* display. The visually meaningful class names offer a convenient way to intuitively understand the dimensionality of the data in terms of an appropriate visual representation. For instance, in Figure 1 **A**, the name `Image` conveys the notion that the contained data is in the form of a two-dimensional NumPy array that can be meaningfully displayed as an image.

The particular `Image` shown in Figure 1 **A** was constructed as a visualization of the Mandelbrot Set, defined in the complex plane. In particular, the `kdims` argument declares that the *x*-axis is along the real axis and that the *y*-axis is along the imaginary axis. This information is then reflected in the visual output by assigning the appropriate axis labels. This semantic information is also passed to the `Curve` object generated by sampling the image using `image.sample(Im=1)`.

This `Curve` object is also able to pass on this semantic information to other Elements with different visual representations so that they faithfully reflect the space in which the Mandelbrot Set is defined. For instance, you can pass the curve directly to the constructor of the `Scatter` or `Histogram` elements and a new visual representation of the resulting object will retain the original semantic dimension labels. This type of operation merely changes the representation associated with the supplied data.

Note that in the declarations of `Image`, the dimensions of the axes are declared as key dimensions (`kdims`). Key dimensions correspond to the independent dimensions used to index or slice the element, with the remaining dimensions

called value dimensions (`vdims`). In the case of this image, there is a single value dimension, for the values in the supplied NumPy array, which are then visualized using the default colormap of the `Image` elements (the 'hot' color map).

As key dimensions are indexable and sliceable, we can slice the `Image` to select a different subregion of the Mandelbrot Set. Continuous values are supported when slicing an `Image` and the result is then a new `Image` containing the portion of the original NumPy array appropriate to the specified slice. The mapping between continuous space and the discrete array samples is specified by the bounds, allowing us to apply the slice `[-0.2:0, 0.85:1.05]` to select the corresponding part of the complex plane. The first component of this slice selects the first key dimension (the real axis '`Re`') from `-0.2` to `0.0` while the second component of the slice selects the second key dimension (the imaginary axis '`Im`') from `0.85` to `1.05`. You can apply a similar slice along the real axis to select a portion of the curve object shown in Figure 1 **B**.

There are many additional element classes, one for each of the common visual representations for data. These elements form an extensible library of primitives that allow the composition of data structures with complex, meaningful visualizations. Within the set of all elements, you can cast your data between representations so long as the number of key and value dimensions is consistent. You can then index and slice your elements along their respective key dimensions to get new elements holding the appropriately sliced data of interest.

Collections

The elements are simple wrappers that hold the supplied data and allow a rich, meaningful default representation. An individual element is therefore a data structure holding the semantic contents corresponding to a simple visual element of the sort you may see in a publication. Although the elements are sufficient to cover simple cases such as individual graphs, raster images, or histogram, they are not sufficient to represent more complex figures.

A typical published figure does not present data using a single representation, but allows comparison between related data items in order to illustrate similarities or differences. In other words, a typical figure is an object composed of many visual representations combined together. HoloViews makes it trivial to compose elements in the two most common ways: concatenating representations into a single figure, or overlaying visual elements within the same set of axes.

These types of composition are so common that both have already been used in Figure 1 as our very first example. The `+` operation implements concatenation, and `*` implements overlaying elements together. When you compose an object using the `+` operator, a default four-column layout is used but you can specify the desired number of columns using the `.cols` method. Layouts are easily specified but also support multiple options for customizing the position and sizing of elements.

When we refer to subfigures 1 **A** and 1 **B**, we are making use of labels generated by HoloViews for representing a composite data structure called a `Layout`. Similarly, subfigure 1 **A** is

itself a composite data structure called an `Overlay` which, in this particular case, consists of an `Image` element overlaid by the `HLine` element.

The overall data structure that corresponds to Figure 1 is therefore a `Layout` which itself contains another composite collection in the form of an `Overlay`. The object in Figure 1 is in fact a highly flexible, compositional tree-based data structure: intermediate nodes correspond either to `Layout` nodes (+) or `Overlay` nodes (*), with element primitives at the leaf nodes. Even in this potentially complex tree, all the raw data corresponding to every visual element is conveniently accessible via key or attribute access by selecting a leaf element using its path through the tree, and then inspecting the `.data` attribute, making it simple to declare which part of a complex dataset you want to work with at a given time.

As any element may be a leaf of such a tree, there needs to be an easy way to select subtrees or leaf elements. This is achieved with a semantic, two-level labeling system using "group" and "label" strings supported throughout HoloViews. We have seen an example of a label string in Figure 1, where it was used to title the image "Mandelbrot Set". The textual representation of the layout in Figure 1 (see Out[6] of Figure 4) shows how the supplied label is used in the attribute-based indexing scheme of the layout. The strings "Image", "Overlay", "HLine" and "Curve" are default group names, but you can supply your own names to define semantic groupings for your data. To illustrate this system, you can access the sampled data (a NumPy array) in Figure 4 using `content.Curve.Cross_Section.data`.

With the ability to overlay or concatenate any element with any other, there is great flexibility to declare complex relationships between elements. Whereas a single element primitive holds semantic information about a particular piece of data, trees encode semantic information between elements. The composition of visual elements into a single visual representation expresses some underlying semantic value in grouping these particular chunks of data together. This is what composite trees capture; they represent the overall *semantic content* of a figure in a highly composable and flexible way that always preserves both the raw data and associated metadata for further interactive analysis and reproduction.

Spaces

A single plot can represent at most a few dimensions before it becomes visually cluttered. Since real-world datasets often have higher dimensionality, we face a tradeoff between representing the full dimensionality of our data, and keeping the visual representation intelligible and therefore effective. In practice we are limited to two or at most three spatial axes, in addition to attributes such as the color, angle, and size of the visual elements. To effectively explore higher dimensional spaces we therefore have to find other solutions.

One way of dealing with this problem is to lay out multiple plots spatially. Plotting packages like ggplot [Wic09] and seaborn [Was14] have shown how this can be done easily using various grid-based layouts. Another solution is to present the data sequentially over time as an animation. A third solution is to provide interactive control, allowing the user to reveal

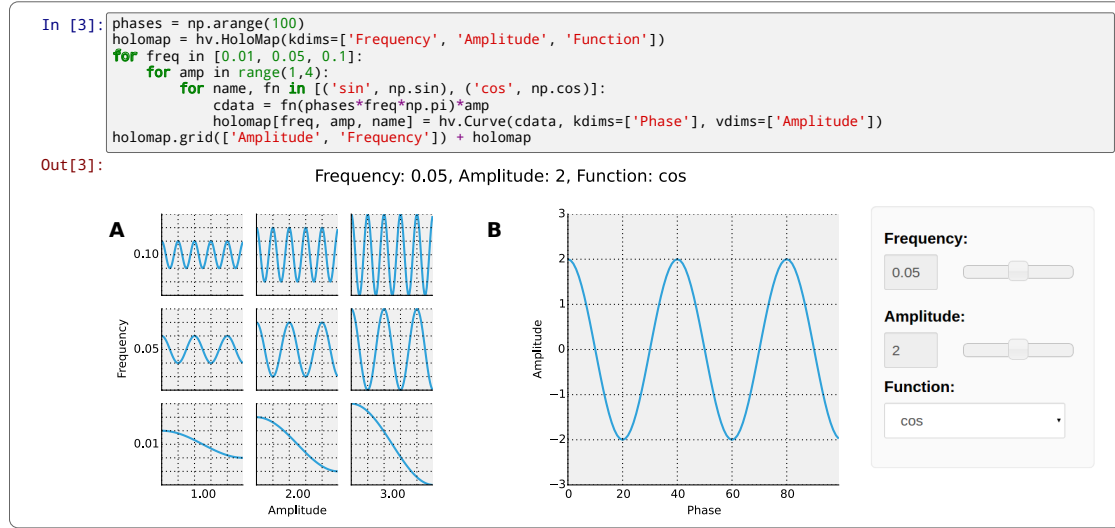


Fig. 2: Example of a `Layout` object containing two different representations of a multi-dimensional space. Both representations contain `Curve` objects embedded in three dimensions (`Frequency`, `Amplitude`, `Function`), but not all of these dimensions can be visualized at once. In **A**, two of the dimensions are mapped onto the rows and columns of a grid, and the remaining `Function` dimension can be selected using the widget at the right. In **B**, only a single curve is shown, with the three sliders at the right together selecting the appropriate curve from the 3D `HoloMap` space. When two `HoloMaps` are joined in a `Layout` like this, it will automatically find the joint set of dimensions the `HoloMaps` can be varied over. In this way `HoloMaps` allow users to explore data naturally and conveniently even when its dimensionality exceeds what can be sensibly displayed on the screen at once.

further dimensionality by interacting with the plots using various widgets.

HoloViews provides support for all three of these approaches, via composable data structures that embed collections of `Element` objects in any arbitrarily dimensioned space. Fundamentally, this set of data structures (subclasses of `NdMapping`) are multi-dimensional dictionaries that allow the user to declare the dimensionality of the space via a list of key dimensions (`kdims`).

The list of supported `NdMapping` classes includes:

- **HoloMaps:** The most flexible high-dimensional data structure in HoloViews, allowing `Element` instances to be embedded in an arbitrarily high-dimensional space, to be rendered either as a video animation or as an interactive plot that allows exploration via a set of widgets.
- **GridSpaces:** A data structure for generating spatial layouts with either a single row (1D) or a two-dimensional grid. Each overall grid axis corresponds to a key dimension.
- **NdLayouts/NdOverlays:** Similar to `Layout` or `Overlay` objects, where the contained objects vary over one or more dimensions.

To explore a high-dimensional space of height as a function of age across different countries and years, you could declare `space=HoloMap(kdims=['Country', 'Year'])`. Now we can treat `space` as a dictionary and insert instances of classes such as `Curve` or `Scatter` with the appropriate (`country`, `year`) keys. For instance, the age and height `Curve` for the USA in 1988 (`usa`) can be inserted using `space['USA', 1988] = usa`. Note that the order of the indexing corresponds to the order of the declared key dimensions.

All of the above classes are simply different ways to package and view a high-dimensional dataset. Just as with `Elements`, it is possible to cast between these different spaces via the constructor. In addition, they can all be tabularized into a HoloViews `Table` element or a pandas `DataFrame` [McK10], a feature that is also supported by the `Element` primitives.

To get a sense of how composing data and generating complex figures works within this framework, we explore some artificial data in Figure 2. Here we vary the frequency and amplitude of sine and cosine waves, demonstrating how we can quickly embed this data into a multi-dimensional space. First, we declare the dimensions of the space we want to explore as the key dimensions (`kdims`) of the `HoloMap`. Next, we populate the space iterating over the frequencies, amplitudes, and the two trigonometric functions, generating each `Curve` element individually and assigning to the `HoloMap` at the correct position in the space.

We can immediately go ahead and display this `HoloMap` either as an animation or using the default widgets, as in Figure 2 **B**. Visualizing individual curves in isolation is not very useful, of course; instead we probably want to see how the curves vary across `Frequency` and `Amplitude` in a single plot. A `GridSpace` provides such a representation and by using the space conversion method `.grid()` we can easily transform our three-dimensional `HoloMap` into a two-dimensional `GridSpace` (which then allows the remaining dimension, the choice of trigonometric function, to be varied via the drop-down menu). Finally, after composing a `Layout` together with the original `HoloMap`, we let the display system handle the plotting and rendering.

If we decide that a different representation of the data would

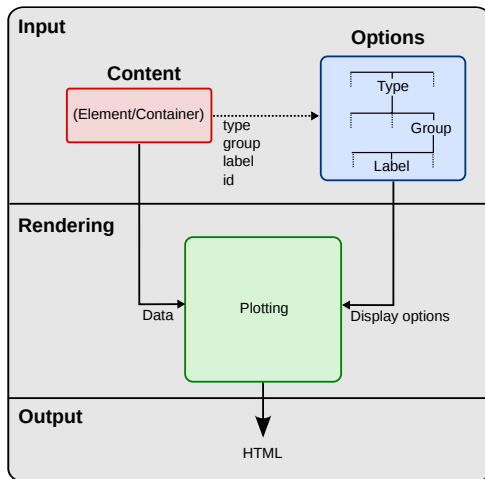


Fig. 3: This view of the HoloViews display and customization systems illustrates the complete separation between the content (data) to be displayed, the display options, and the rendering/plotting system. The display options are stored entirely separately from the content as a tree structure, with the appropriate options being selected with user-controllable levels of specificity: general options for all objects of a given type, more specific options controlled by user-definable group and label strings, or arbitrarily specific options based on the integer id assigned to each content object. Plotting and rendering happens automatically through the use of IPython display formatters. These combine the content with the specified display options, call an external plotting library, which returns an HTML representation that can then be rendered in the notebook.

be more appropriate, it is trivial to rearrange the dimensions without needing to write new plotting code. Even very high-dimensional spaces can be condensed into an individual plot or expressed as an interactive plot or animation, by simply specifying which part of the data we are interested in rather than writing new brittle and error-prone custom plotting code.

Customizing the visual representation

In this section we show how HoloViews achieves a total separation of concerns, keeping the composable data structures introduced above completely separate from both customization options and the plotting code. This design is much like the separation of content and presentation in HTML and CSS, and provides the same benefits of making the content easily maintainable while the presentation is easily controllable.

The only required connection between the above data structures and the custom display options is a single, automatically managed integer. Using this integer attribute we can make the data structures behave as if they were rich, stateful, and individually customizable objects, without actually storing anything to do with visualization on the objects. We will show how this separation is useful and extensible so that the user can quickly and easily customize almost every aspect of their plot. For instance, it is easy to change the font size of text, change the subfigure label format, change the output format (e.g. switch from PNG to SVG) and even alter the plotting backend (currently defaulting to Matplotlib) without changing any part of the underlying object being rendered.

Figure 3 provides an overall summary of how the different components in the display system interact. The declarative data structures define what will be plotted, specifying the arrangements of the plots, via Layouts, Overlays, and spaces. The connection between the data structure and the rendered representation is made according to the object type, the aforementioned integer attribute, and optionally specified group and label strings. By collecting the display options together and associating them with particular objects via these attributes, the visual representation of the content may be easily customized, e.g. to tweak aesthetic details such as tick marks, colors and normalization options. Once the user has specified both content and optionally customized the display the rendering system looks up the appropriate plot type for the object in a global registry, which then processes the object and looks up the specified options in order to display it appropriately. This happens transparently without any input from the user. Once the plotting backend has rendered the plot in the appropriate format, it will be wrapped in HTML for display in the notebook.

The default display options are held on a global tree structure similar in structure to the composite trees described in the previous section, but with nodes holding custom display options in the form of arbitrary keywords. In fact, these option trees also use labels and groups the same way as composite trees except they additionally support type-specific customization. For instance, you may specify colormap options on the Image node of the tree that will then be applied to all Images. If this chosen colormap is not always suitable, you can declare that all Image elements belonging to a group (e.g. `group='Fractal'`) should use a different colormap by overriding it on the `Image.Fractal` node of the tree. This form of inheritance allows you to specify complex yet succinct style specifications, applying to all objects of a particular type or just to specific subsets of them.

To explore how option setting works in practice, Figure 4 shows an example of customizing Figure 1 with some basic display options. Here we use an optional but highly succinct method for setting the options, an IPython cell magic `%%opts`, to specify aspect ratios, line widths, colormaps, and sublabel formats. By printing the string representation of the content (`Out [6]`) and the options (`Out [7]`), we can see immediately that each entry in the options tree matches a corresponding object type. Finally, in the actual rendered output, we can see that all these display options have taken effect, even though the actual data structure differs from the object rendered in Figure 1 only by a single integer attribute.

A major benefit of separating data and customization options in this way is that all the options can be gathered in one place. There is no longer any need to dig deep into the documentation of a particular plotting package for a particular option, as all the options are easily accessible via a tab-completable IPython magic and are documented via the `help` function. This ease of discovery enables a workflow where the visualization details of a plot can be easily and quickly iteratively refined once the user has found data of interest.

The options system is also inherently extendable. New options may be added at any time, and will immediately

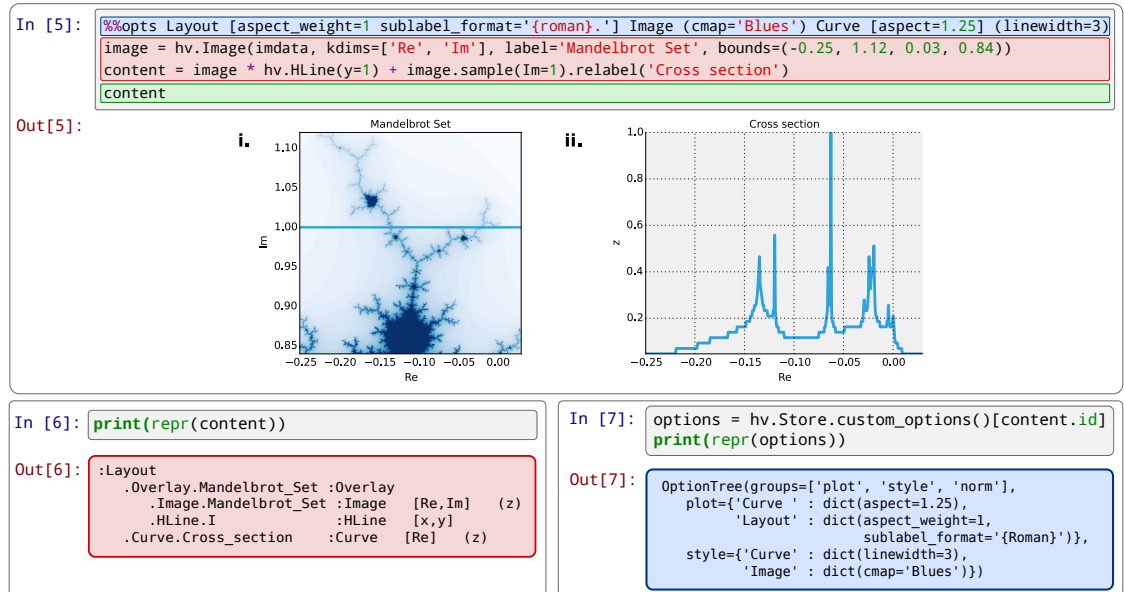


Fig. 4: An example of customizing the display of Figure 1’s data using the default Matplotlib backend. In [5] is color coded according to the components in Figure 3, where red is the content, blue is the display options (using an optional IPython-specific succinct syntax), and green is what triggers the rendering. Out [5] shows how the supplied options have affected the final plots, compared to Figure 1. Finally, Out [6] and Out [7] show the textual representations of the content and the style specification respectively, demonstrating how the two are separate yet linked.

become available for tab-completion. In fact, the plotting code for each element and container type may be switched out completely and independently, and the options system will automatically reflect the changes in the available customization options. This approach lets the user work with a variety of plotting backends at the same time, without even having to worry about the different plotting APIs.

The separation between content, options and plotting explicitly supports the workflows that are common in science, repeatedly switching between phases of exploration and periods of writing up. Interesting data can be collected and curated over time, where each step is instantly and transparently visualizable without any custom code cluttering up the notebook. Visualizations of data that are worth keeping can be customized through an interactive and iterative process, and the final set of plotting options can then be expressed as a single data structure separate from the actual displayed data, ready to be applied to the next batch of data from a subsequent measurement or experiment. Throughout, the scientist curates the data of interest, as revealed in associated visual representations, along with the visualization options and a separate codebase of general-purpose plots (mostly included in HoloViews, but potentially extended locally for specific domains). Each of these three aspects of the process (data, options, and code) can be developed, maintained, archived, and improved independently, providing comprehensive support for the natural process of exploration and dissemination common to all scientific disciplines.

Discussion

This paper demonstrates a succinct, flexible, and interactive approach for data exploration, analysis, and visualization. HoloViews restores the immediate feedback cycle that is characteristic of working with simple data in an interpreter. This is achieved by having declarative objects display themselves with good defaults allowing the user to immediately understand their data. In the majority of cases this eliminates the need to write plotting code and allows the user to keep a concise and reproducible recipe of their work, from exploration to the final publication. HoloViews thus allows scientists to capture the entire workflow involved in a research project.

Without a strictly enforced separation of concerns, workflow stages often end up mixing both data processing and visualization. Although a displayed representation is always necessary for understanding, it has been a dead end for further data processing. Because HoloViews objects represent themselves visually but also contain the raw data, the ability to continue processing is never terminated and exploration can continue. Furthermore, the chosen representation can easily be changed, turning what used to be a highly disjointed workflow into a open-ended process concerned with the semantics of the data. Only once results worth disseminating are attained does it become necessary to consider the details of visualization.

The compositionality of HoloViews is superficially reminiscent of systems such as the Grammar of Graphics [Wil05] for the R language, but the aim of HoloViews is quite different. Instead of expressing all the complexities of graphics, the declarative data structures in HoloViews define a language for the semantics of the actual data. This language focuses on how the researcher conceptualizes it, *independent* of the exact

details of plotting. The need for an automatic and useful visual representation is driven by the need to immediately present the data in a meaningful format.

HoloViews is one of many packages designed for working with large, multidimensional datasets, but it differs from each of these in important ways. For instance, Python’s `seaborn` [Was14] and R’s `ggplot2` [Wic09] library support laying out high-dimensional data into subplots and grids, while Python’s Bokeh library and R’s shiny [shiny] web application framework provide widgets for interactive data exploration. While each of these packages can provide extremely polished interactive graphics, getting them set up for specific sets of data requires significant additional effort and custom code, placing a barrier to their primary use case, the interactive exploration of data. HoloViews instead tries to avoid custom coding altogether as far as possible, with users instead supplying metadata to declare the properties of the data and option settings to control its visual appearance.

Although HoloViews is a general purpose library for working with data at every stage, it actually represents a significant advance over previous approaches focused only on achieving reproducibility of the final result. Simply by keeping specifications for figures succinct, HoloViews allows the entire recipe to be preserved in the notebook, not scattered over separately imported plotting code files. Secondly, because HoloViews can directly express the complex relationships between different bits of data as subfigures, it can capture entire figures within notebooks that would previously have required unreplicable work in external drawing programs. Lastly, HoloViews exports the actual data alongside published figures, allowing it to be tested automatically (as is done for the project web site) without conflating it with arbitrary display choices. HoloViews makes it possible to reproduce results from every step of the project, up to and including the final published figures, in a way that has not previously been practical.

Although HoloViews aims to provide good default behavior, scientific work often requires highly specialized visualizations. For that reason we have made it easy to extend the defaults and integrate new visualizations. Firstly, as many plotting and styling options as possible are exposed in an easily accessible manner, while providing a powerful, inheritance-based system for changing these options when required. Secondly, the options system has been designed to work well with the compositional data structures provided by HoloViews. Thirdly, HoloViews makes it trivial to add completely novel types of Elements with corresponding plots (or to override specific code in existing plots) using custom code when needed, and these custom plots will then combine seamlessly with other objects to make composite figures. Finally, not only is it possibly to implement new plot classes but entire plotting backends may be added and exposed to the user, such as the prototype Bokeh backend, which is well suited to live interaction and large datasets. Thus default plots are simple and straightforward, but even complex figures are easily achievable. Many such examples, ranging from simple to complex, can be found in the Tutorials and Examples sections of holoviews.org.

In this paper, we have focused on how a user can quickly build data structures for their content of interest. An even more

powerful approach is for a developer to integrate HoloViews directly into a library, analysis tool, or simulator. By returning HoloViews objects (which do not depend on any plotting library), any Python package can immediately have access to flexible, compositional data structures that automatically double as a visualization system. This is exactly the approach taken by the ImaGen image generation library and the Topographica neural simulator, two very different projects that both output data wrapped in HoloViews data structures.

Conclusion

Based on the key principles of: (1) making data immediately and transparently visualizable, (2) associating data directly with its semantic description, (3) keeping display option settings separate from the data, (4) keeping display code separate from both data and display options, (5) explicitly expressing the relationships between data elements compositionally, and (6) keeping the original data accessible even in complex visualizations, Holoviews supports the entire life cycle of scientific research, from initial exploration, to dissemination and publication, to eventual reproduction of the work and new extensions. Existing approaches for achieving some of these goals individually have been very limiting and only partially successful, each adding significant new costs along with the benefits they offer. HoloViews instead addresses the underlying problems fundamental to current methods for scientific research, solving seemingly intractable issues like reproducibility almost as a side effect of properly supporting the basic process of doing science.

Acknowledgments

This work was funded in part by grant 1R01-MH66991 to the University of Texas at Austin from the USA National Institute of Mental Health, by grant EP/F500385/1 from the UK EPSRC and MRC research councils, and by the Institute for Adaptive and Neural Computation at the University of Edinburgh.

REFERENCES

- [Cro13] Crook et al., "Learning from the Past: Approaches for Reproducibility in Computational Neuroscience", *20 Years of Computational Neuroscience*, J.M. Bower, ed., Springer, 9:73-102, 2013.
- [Wol03] Stephen Wolfram, *The Mathematica Book*, Fifth Edition, Wolfram Media/Cambridge University Press, 2003.
- [knitr] Foundation for Open Access Statistics, *knitr*, <http://yihui.name/knitr>, 2015.
- [Per07] Fernando Perez and Brian E. Granger, IPython: a System for Interactive Scientific Computing, *Computing in Science and Engineering*, 9:21-19, 2007.
- [Ste05] William Stein and David Joyner. SAGE: System for Algebra and Geometry Experimentation. *ACM SIGSAM Bulletin*, 39:61-64, 2005.
- [Hun07] John D. Hunter. *Matplotlib: A 2D graphics environment*, Computing In Science & Engineering, 9(3):90-95, 2007.
- [Wic09] Hadley Wickham, *ggplot2: elegant graphics for data analysis*, Springer New York, 2009.
- [Was14] Michael Waskom et al.. *seaborn: v0.5.0*, Zenodo. 10.5281/zenodo.12710, November 2014.
- [McK10] Wes McKinney, *Data Structures for Statistical Computing in Python*, Proceedings of the 9th Python in Science Conference, 51-56, 2010.
- [Wil05] Leland Wilkinson, *The Grammar of Graphics*, Springer-Verlag New York, 2005.
- [shiny] RStudio, Inc, *shiny: Easy web applications in R.*, <http://shiny.rstudio.com>, 2014.

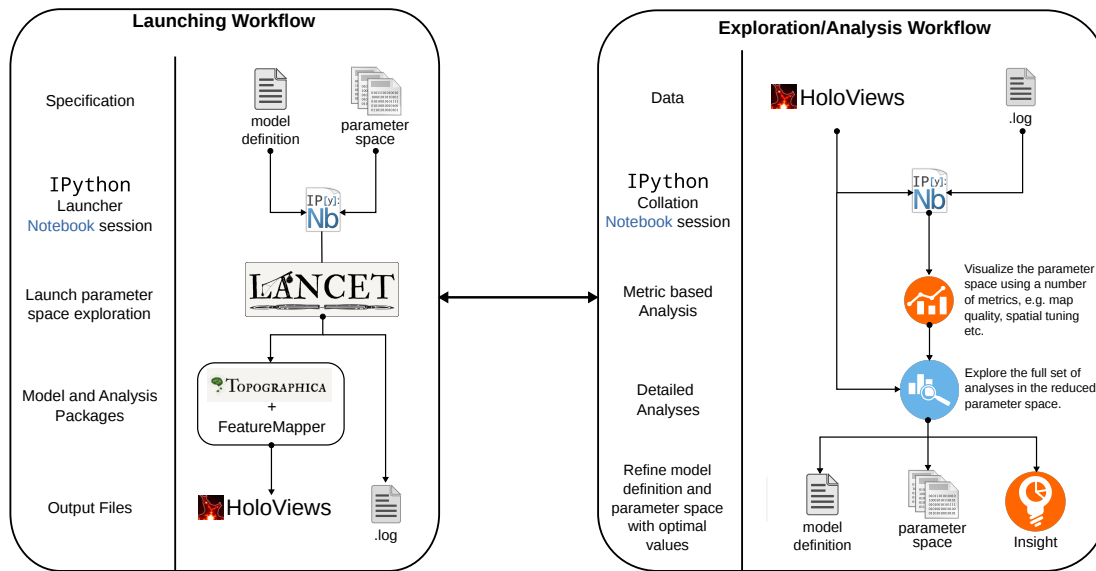


Figure 3.1

3.2 A UNIFIED WORKFLOW FOR THE ANALYSIS OF COMPLEX COMPUTATIONAL MODELS

HoloViews is only a small part of an overall workflow developed as part of this project in collaboration with a colleague. This section will describe the overall workflow:

- IPython notebooks - a reproducible record of your work
- HoloViews - access to data independent of plotting details
- Easy data exploration of even large parameter spaces
- Publication quality figures
- Cite papers published using HoloViews
- Reiterate how central all this is to working with complex models

SPATIALLY CALIBRATING MODELS OF PRIMARY VISUAL CORTEX

One of the major obstacles in modern neuroscience is integrating the vast amount of experimental data that has been generated, highlighting where different sources of evidence is and is not in agreement and offering testable hypothesis to resolve such discrepancies. The primary visual cortex is one of the most well studied areas in the mammalian brain and we have previously seen that it has been extensively explored at varying levels of description, from development, circuits and anatomy to surround modulation, behavioural studies and theoretical models of computation. In order to provide a better account on how all this information fits together in a generalized model describing the organization and computations performed by the cortex, a unified reference frame regarding the various spatial scales and their origins is desperately needed. A careful read of the literature highlights just how dependent various effects are on the spatial scales involved. Here we will present a model that takes these various levels of evidence into account to allow comparing whether using known anatomical properties we can predict the known response properties of the cortex after development. This will allow bridging between known measurements of anatomy and circuitry and electrophysiological or even behavioral experiments performed on visual cortex.

So far only very few attempts have been made at developing models that take into account the various spatial properties that have been described in the literature ranging from anatomy to electrophysiological measurements. In particular to begin making sense of the surround modulation literature, which is highly dependent on the precise choice of stimulation protocol, it is essential to take into the various spatial scales involved. Therefore this chapter will demonstrate how existing models of cortical development, specifically the Gain Control Adapation Lateral model (GCAL) ([Stevens et al., 2013](#)) can be calibrated to match known measurements of spatial extents more closely in a new S-patially CAL-ibrated (SCAL) model.

We will begin by looking at the size of receptive fields in the lateral geniculate nucleus and then progress toward V1, going back and forth between anatomical and electrophysiological measurements both in the literature and in the model. Additionally we will pay attention to the difference in observed connectivity between excitatory and inhibitory neurons. In tuning this model we will mostly rely on results

gleaned from studies in macaque monkeys, where available, supplementing missing data with data from other primates and cats.

4.1 SCAL-LGN MODEL

Before we proceed let us describe the model we have chosen as the starting point of this research. The GCAL model put forth in Stevens et al. (2013) will serve as the starting point. Here we will describe the equations governing the RGC/LGN layers of this model and then discover how it has been adjusted.

All the models introduced in this thesis will build on the LGN model introduced here. All the models operate by presenting a new retinal input at each iteration updating the activation of each unit in each sheet. The neurons in the sheets are firing-rate point neurons, with the main state being a floating point activation value. For all models, the activation level η for a unit at position j in an ON/OFF sheet O at time $t + \delta t$ is defined as:

$$\eta_{j,O}(t + \delta t) = f \left(\frac{\gamma_O \sum_{i \in F_{j,P}} \Psi_i(t) \omega_{ij}}{k + \gamma_S \sum_{i \in F_{j,S}} \eta_{i,O}(t) \omega_{ij,S}} \right) \quad (4.1)$$

The constant $\gamma_O = 14.0$ is an arbitrary multiplier for the overall strength of connections from the photoreceptor sheet to the ON/OFF sheets, chosen to give typical activations in the range 0.0 to 1.0, while γ_S is the strength of the feed-forward contrast-gain control. Ψ_i is the activation of unit i in the two-dimensional array of neurons on the photoreceptor sheet from which ON/OFF unit j receives input (its afferent connection field $F_{j,P}$) and $\eta_{i,O}(t)$ is the activation of other ON/OFF units on the previous time step (received over the suppressive connection field $F_{j,S}$). The activation function f is a half-wave rectifying function that ensures the activation of ON/OFF units is always positive.

The weights ω_{ij} represent the fixed connection weights from photoreceptor i to the ON or OFF unit j defined with a standard difference-of-Gaussians (DoG) kernel. The connection fields for ON units have a positive center and negative surround, and vice versa for OFF units. More precisely, the weight ω_{ij} from an ON-center cell at location $(0,0)$ in the ON sheet and a photoreceptor sheet in location (x,y) on the photoreceptor sheet is given by:

$$\omega_{ij} = \frac{1}{Z_c} \exp \left(-\frac{x^2 + y^2}{2\sigma_c^2} \right) - \frac{1}{Z_s} \exp \left(-\frac{x^2 + y^2}{2\sigma_s^2} \right) \quad (4.2)$$

The kernel sizes of the central Gaussian σ_c and surround mechanism σ_s are what we will be determining here. Unlike simple DoG kernels, the center-surround are

jointly normalized to 1.0 using Z_c and Z_s . The weights for an OFF-center cell are the negative of the ON-center weights (i.e., surround minus center). The center of the connection field of each ON/OFF unit is mapped to the location in the photoreceptor sheet corresponding to the location of that unit in sheet coordinates, making the projection retinotopic.

The weights $\omega_{ij,s}$ in the denominator of equation 4.1 specify the spatial profile of the lateral inhibition received from other ON/OFF units when contrast-gain control is active. The weights of these connections have a fixed, circular Gaussian profile so that for a neuron located at (0,0) in either the ON or OFF sheet:

$$\omega_{ij,s} = \frac{1}{Z_s} \exp\left(-\frac{x^2 + y^2}{2\sigma_s^2}\right) \quad (4.3)$$

where (x, y) is the location of the presynaptic neuron, σ_s determines the width of the Gaussian, and Z_s is a normalizing constant that ensures that the total of all the lateral inhibitory weights ω_{ij} to neuron j sum to 1.0. This gain-control projection is activated once per iteration before activity is sent to the V1 sheet.

4.2 SPATIALLY CALIBRATING LGN RECEPTIVE FIELDS

In spatially calibrating the spatial properties of LGN receptive fields we must take into account how they will contribute to the V1 receptive fields. One major issue in accurately modeling the LGN connectivity is that no detailed anatomical measurements exist describing the extent of LGN neurons and spatial measurements are highly dependent on stimulus parameters.

In 4.2 we summarize population estimates from a number of studies, measured by presenting disk masked sine gratings of varying sizes and fitting the responses with a Difference of Gaussian model. The estimates here vary widely with the results from (Sceniak et al., 2006) being the particular outlier. Another concern is that it is not clear how these values translate into the existing LGN model. To confirm this we will replicate the experimental protocols used to obtain these values.

4.2.1 Method

The area summation curves were measured in the model by presenting the model with disks of sine gratings of increasing size and varying phase and at the optimal spatial frequency of each neuron. The size tuning curves obtained in this way were then fitted with the integrated Difference of Gaussian model described by the following equation:

Connection	Literature	Species	Ecc. (°)	Model	Layer	$R_{c/s}$
LGN Center	Sceniak et al. (2006)	macaque	2-5	parvo	-	median = 0.46° mean = 0.5°
	Levitt et al. (2001)	macaque	0-10	parvo	-	0.069 ± 0.076°
	Spear et al. (1994)	macaque	0-10	parvo	-	0.087 ± 0.046°
	Bonin et al. (2005)	macaque	13.9	parvo	-	0.6 ± 0.4° / 0.4 ± 0.2°
LGN Surround	Sceniak et al. (2006)	macaque	2-5	parvo	-	median = 0.51° (0.15-0.85)
	Levitt et al. (2001)	macaque	0-10	parvo	-	0.33 ± 0.076°
	Spear et al. (1994)	macaque	0-10	parvo	-	0.53 ± 0.39°
	Bonin et al. (2005)	macaque	13.9	parvo	-	2.0 ± 1.1° / 1.8 ± 2.6°

Table 4.1: Estimates of LGN neuron spatial tuning properties fitted using Difference of Gaussian models with either subtractive or divisive suppressive components.

$$R(s) = R_0 + K_e \int \int r e^{-\frac{r^2}{a}} dr d\theta - K_i \int \int r e^{-\frac{r^2}{b}} dr d\theta \quad (4.4)$$

where R_0 is the spontaneous response rate, K_e the excitatory gain, K_i the inhibitory gain, a the excitatory space constant and b the inhibitory space constant. By separating the inhibitory and excitatory components in equation 4.4 and define them as R_e and R_i , we can formulate a subtractive and divisive version of this equation:

$$R = R_0 + R_e - R_i \quad (4.5)$$

$$R = R_0 + \frac{R_e}{1 + R_i} \quad (4.6)$$

4.2.2 Results

A set of area-summation curves measured at varying contrast levels can be seen in Figure 4.1. These curves were then fitted using the iDoG model resulting in the fit shown in Figure 4.2. Through an iterative process we could determine establish a rough correspondence between the kernel sizes used in the model definition and those obtained through the model fitting process. However, in particular the surround size was consistently overestimated using this procedure.

Note that neither of these models captures the mechanisms of the SCAL-LGN model described above, which although it too operates on DoG center-surround fields uses joint normalization and adds a distinct divisive component, independent of the subtractive surround.

In the end it was decided that due to the large variance in results from different studies and the limitation to a single spatial filter a lower spatial constants should

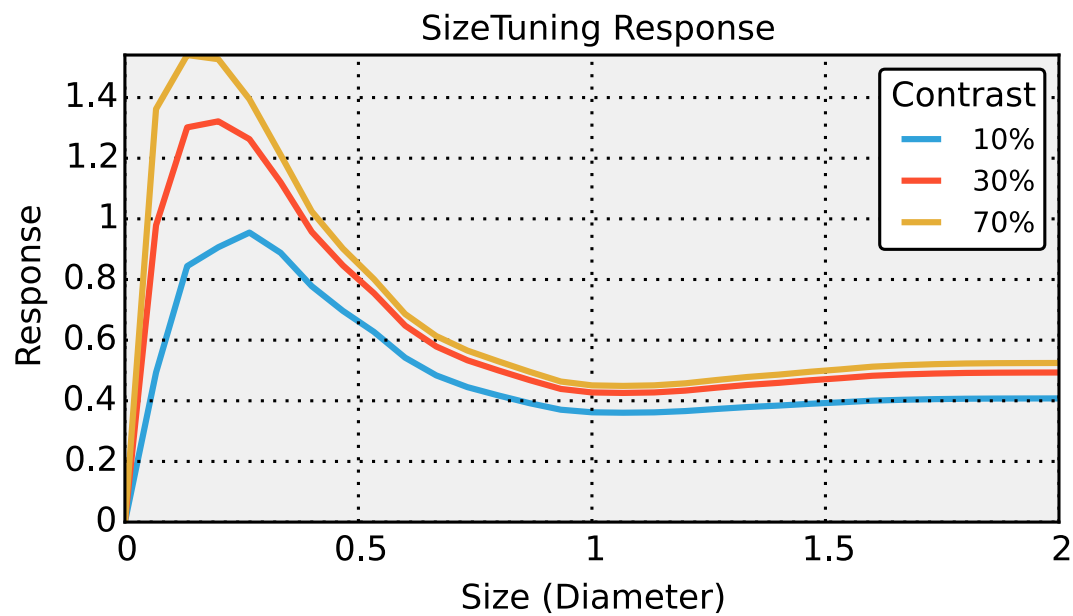


Figure 4.1

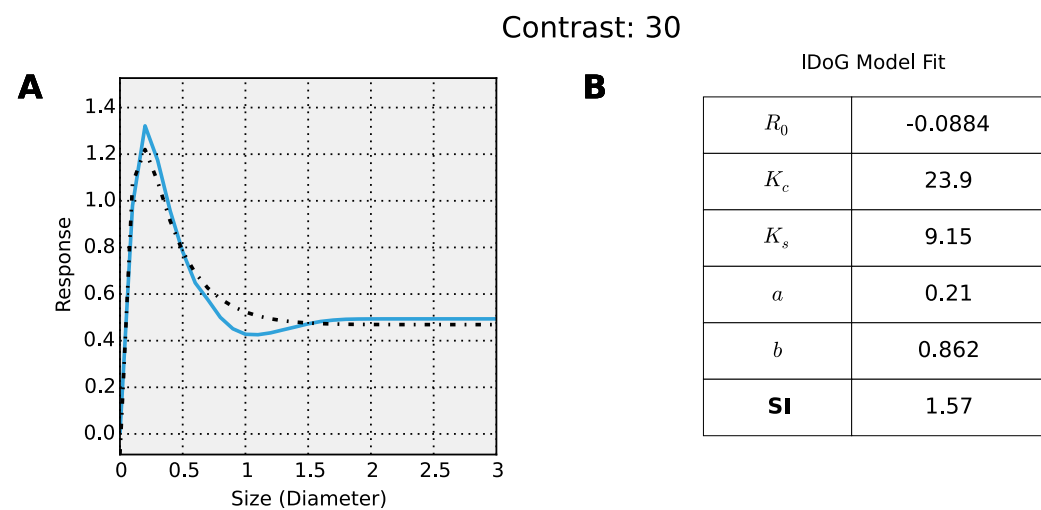


Figure 4.2: A) LGN area-summation curve (blue) fit using an integrated Difference-of-gaussian model (dotted). B) Parameters of the iDoG model fit.

Model parameter	Value
σ_c	0.1°
σ_s	0.15°
σ_{gc}	0.25°
radius_{c+s}	0.3°
radius_{gc}	0.5°
LGN _{aff} strength	14
LGN _{GC} strength	0.6

Table 4.2: Parameters for S-patially CAL-ibrated (SCAL) LGN model.

be chosen for the center-surround mechanism. This choice allowed a fairly broad range of spatial frequencies to be relayed to V1 to account for the lack of spatial filter diversity. Future models should aim to cover the full distribution of spatial frequency and size sensitivities. The final model parameters are summarized in 4.2 and visualized in Figure 4.3.

4.3 THE V1 MODEL

As we saw above in the LGN section the model described here is heavily based on the GCAL model (?)Stevens2013), however it does differ in one major respect, it employs divisive rather than subtractive inhibition.

Each V1 neuron in each model receives connections from three different connection types or ‘projections’ (p), i.e., the afferent projection from the ON/OFF sheets (both channels concatenated into one input vector; $p = A$), the recurrent lateral excitatory projection ($p = E$), and the recurrent lateral inhibitory projection ($p = I$) from other V1 neurons.

The contribution $C_{j,p}$ to the activation of unit j from each projection type ($p = A, E, I$) is calculated as:

$$C_{j,p}(t + \delta t) = \sum_{i \in F_{j,p}} \eta_{i,p}(t) \omega_{ij,p} \quad (4.7)$$

where $\eta_{i,p}$ is the activation of unit i taken from the set of neurons in V1 to which unit j is connected (its connection field F_j) and $\omega_{ij,p}$ is the connection weight from unit i in V1 to unit j in V1 for the projection p . Afferent activity ($p = A$) remains constant after the first update from the retina, but the other contributions change over 16 settling steps, depending on the activity in V1.

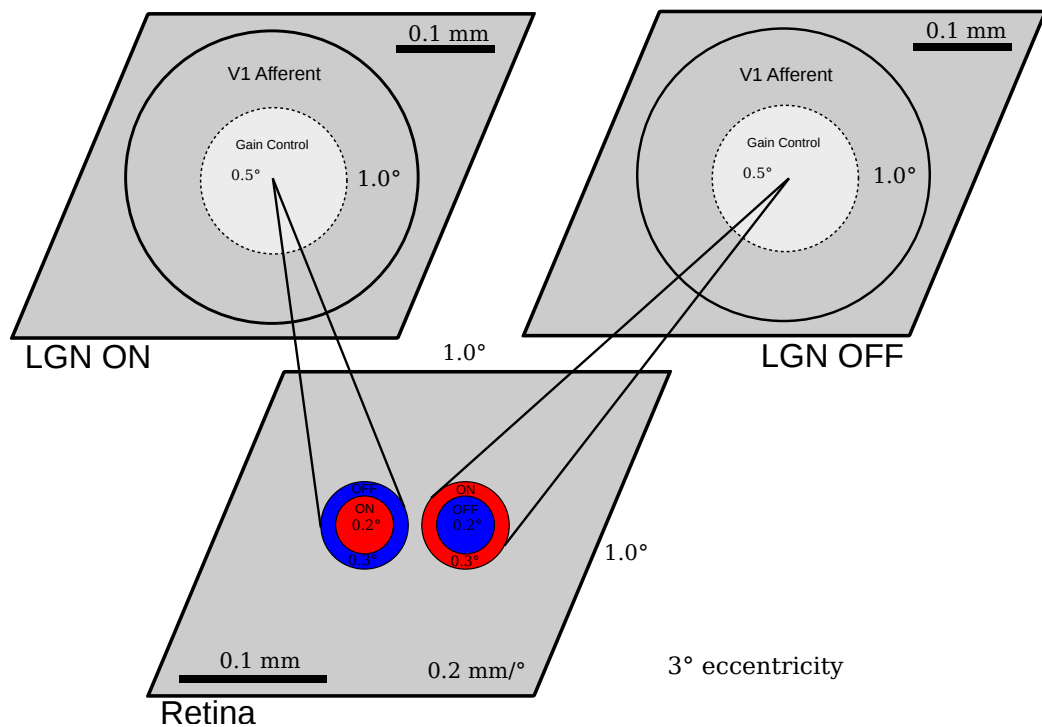


Figure 4.3: Diagram of the SCAL-LGN stage of the model showing the spatial scales of the various excitatory (red) and inhibitory (blue) connections. Saturated colors indicate the kernel radii, while lightly shaded regions indicate kernel cut-off extents.

The contributions from all three projections to V1 (afferent and lateral) described above are combined using equation 4.8 to calculate the activation of a neuron j in V1 at time t :

$$\eta_{j,V}(t) = f \left(\sum_p \gamma_p C_{jp}(t) \right) \quad (4.8)$$

The projection strength scaling factors γ are defined for each projection type set to provide a balance between excitation and inhibition, and between afferent and lateral influences, to provide robust formation of activity bubbles that allows smooth maps to form. The function f defines a variable threshold point (θ) dependent on the average activity of the unit as described in the next subsection, but in all cases the gain is fixed at unity.

Once all 16 settling steps are complete, the settled V1 activation pattern is deemed to be the V1 response to the presented pattern. At this point we use the V1 response to update the threshold point (θ) of V1 neurons (using the adaptation process described below) and to update the afferent and lateral inhibitory weights via Hebbian learning. V1 activity is then reset to zero and a new pattern is presented.

Adaptation

In order to set the threshold for activation, each neuron unit j in V1 calculates a smoothed exponential average of its settled activity patterns ($\bar{\eta}_j$):

$$\bar{\eta}_j(t) = (1 - \beta)\eta_j(t) + \beta\bar{\eta}_j(t-1) \quad (4.9)$$

The smoothing parameter ($\beta = 0.991$) determines the degree of smoothing in the calculation of the average. $\bar{\eta}_j$ is initialized to the target average V1 unit activity (μ), which for all simulations is $\bar{\eta}_{j,A}(0) = \mu = 0.024$. The threshold is updated using:

$$\theta(t) = \theta(t-1) + \lambda(\bar{\eta}_j(t) - \mu) \quad (4.10)$$

where $\lambda = 0.01$ is the homeostatic learning rate. The effect of this scaling mechanism is to bring the average activity of each V1 unit closer to the specified target. If the activity in a V1 unit moves away from the target during training, the threshold for activation is thus automatically raised or lowered in order to bring it closer to the target. Note that an alternative rule with only a single smoothing parameter (rather than β and λ) could be formulated, but the rule as presented here makes it simple for the modeler to set a desired target activity μ .

Learning

Initial connection field weights are isotropic 2D Gaussians for the lateral excitatory projection and uniformly random within a Gaussian envelope for afferent and lateral inhibitory projections. Specifically, for a neuron located at (0,0):

$$\omega_{ij} = \frac{1}{Z_p} u \exp\left(-\frac{x^2 + y^2}{2\sigma_p^2}\right) \quad (4.11)$$

where (x, y) is the sheet-coordinate location of the presynaptic neuron, $u = 1$ for the lateral excitatory projection ($p = E$) and u is a scalar value drawn from a uniform random distribution for the afferent and lateral inhibitory projections ($p = A, I$), σ_p determines the width of the Gaussian in sheet coordinates ($\sigma_A = 0.27, \sigma_E = 0.025, \sigma_I = 0.075$), and Z_p is a constant normalizing term that ensures that the total of all weights ω_{ij} to neuron j in projection p is 1.0. Weights for each projection are only defined within a specific maximum circular radius r_p ($r_A = 0.27, r_E = 0.1, r_I = 0.23$).

In the model, as images are presented to the photoreceptors, V1 afferent connection weights $\omega_{ij,A}$ from the ON/OFF sheets are adjusted once per iteration (after V1 settling is completed) using a simple Hebbian learning rule. This rule results in connections that reflect correlations between the pre-synaptic ON/OFF unit activities and the post-synaptic V1 response. Hebbian connection weight adjustment at each iteration is dependent on the pre-synaptic activity, the post-synaptic response, and the Hebbian learning rate:

$$\omega_{ij,p}(t) = \frac{\omega_{ij,p}(t-1) + \alpha \eta_j \eta_i}{\sum_k (\omega_{kj,p}(t-1) + \alpha \eta_j \eta_k)} \quad (4.12)$$

where for unit j , α is the Hebbian learning rate for the afferent connection field F_j . Unless it is constrained, Hebbian learning will lead to ever-increasing (and thus unstable) values of the weights (?). In all the models the weights are constrained using divisive post-synaptic weight normalization (equation 4.12), which is a simple and well understood mechanism. Afferent connection weights from ON and OFF units are normalized together in the model. We expect that a more biologically motivated homeostatic mechanism for normalization such as multiplicative synaptic scaling (???) or a sliding threshold for plasticity (?) would achieve similar results, but have not tested these.

The learning rates α are defined separately for the afferent, lateral excitatory and lateral inhibitory projections. The density-specific value used in the equation above is then calculated as $\alpha = \frac{\alpha_A}{\tau_A}$, where τ_A is the number of connections per connection field in the afferent projection.

Visual Area	Magnification Factor (mm/ deg)	Anisotropy Index
Retina ¹	0.223	-
LGN ²	0.324	1.0-2.0
V1 ³	2.54-3.545	1.0-3.0

Table 4.3: Magnification Factors and Anisotropy Index associated with different visual areas at 3° eccentricity estimated from areal and linear magnification factor equations. Footnotes: ¹ - Perry and Cowey (1985), ² - Connolly and Van Essen (1984), ³ - Van Essen et al. (1984)

4.4 SPATIALLY CALIBRATING V1 RECEPTIVE FIELDS

A neuron in primary visual cortex receives input from a variety of sources, including feedforward connections from the LGN, horizontal connections from within V1 and feedback connections from extrastriate cortex as seen in Figure ???. Achieving a consistent spatial tuning is therefore a complex problems relying on a large variety of measurements.

The first step towards a spatially calibrated model is to decide on the region of V1 that should be targeted. Most studies of V1 particularly in the surround modulation literature focuss on parafoveal regions between 2 – 5° in eccentricity. Therefore we have chosen a region at around 3° eccentricity. This already gives us a number of constraints, first of all gives us an approximate V1 magnification factor of 3 mm/deg as described by Van Essen et al. (1984) and shown in Table 4.3.

Secondly to give actual scale to our model we can measure the orientation map hypercolumn distance, which has been well established in the literature. Using estimates provided by the Wolf group the hypercolumn distance in macaque V1 has been estimated at roughly $710 \pm 50\mu\text{m}$. By combining this information with the magnification factor we can establish that we'd expect roughly 4.2 hypercolumns per visual degree and to keep things simple we will keep a 1:1 mapping between visual angle and sheet coordinates of the model. We will also define an acceptable range of hypercolumn cycles per degree to ensure later models do not diverge too far from the spatial tuning implemented here. Taking the confidence intervals for both the magnification factor and hypercolumn distance into account the acceptable range of hypercolumns per sheet coordinate is between 3.29 and 5.3.

4.4.1 Methods

The hypercolumn distance was calculated by taking the 2D Fourier transform of the orientation map, reducing it to one dimension and applying a least-squares fit of

Connection	Literature	Species	Layer	σ
LGN-V1 Afferents	Angelucci et al. (2002a)	macaque	4C α	0.8 – 1.6°
	Angelucci and Sainsbury (2006)	macaque	4A/4C β	0.91 ± 0.041°
V1 local excitation	Buzas et al. (2006)	cat	2-4 single cell	288 μ m
	Buzas et al. (2006)	cat	2-4 population	520 μ m
V1 basket cells	Buzás et al. (2001)	cat	2-6	0.7 – 1.9°
	Buzás et al. (2001)	cat	2-6	0.76 – 2.6mm
V1 long-range excitation	Angelucci et al. (2002b)	macaque	2/3	6 ± 0.7mm (3-9)
			4B/4C α	6.7 ± 0.7mm (4.7-10)
			population	2.47 ± 0.3°
	Buzas et al. (2006)	cat	2/3	6mm

Table 4.4: Anatomical estimates of the spatial profiles of V1 connectivity.

Measurement	Literature	Species	Layer	σ
V1 hsRF	Levitt and Lund (2002)	macaque	2-6	1.0 ± 0.2° (0.3 - 2.2)
V1 Excitatory DoG fit	Levitt and Lund (2002)	macaque	2-6	0.9°
	Sceniak and Hawken (2001)	cat	2-6	1.0°
	Cavanaugh et al. (2002b)	macaque	2-6	1.4°
	Solomon et al. (2002)	macaque	not stated	0.94°
V1 Inhibitory DoG fit	Levitt and Lund (2002)	macaque	2-6	1.9°
	Sceniak and Hawken (2001)	cat	2-6	2.2°
	Cavanaugh et al. (2002b)	macaque	2-6	2.7°
	Solomon et al. (2002)	macaque	not stated	2.97°

Table 4.5: Functional estimates of V1 receptive field size using Difference-of-Gaussian models.

a Gaussian curve with additional linear and quadratic terms (see Kaschube et al. (2010) for more details). A sample fit to an SCAL orientation map can be seen in Figure 4.4. The actual spatial calibration procedure then was an iterative process between this hypercolumn fit and ensuring that all the connectivity kernels matched the experimental results outlined in the tables outlining both anatomical results (4.4) and electrophysiological measurements (4.5).

In particular we confirmed the spatial tuning of the afferents, independently from the lateral connections. While electrophysiological results were again fit using the DoG model and compared against experimental results, the lateral connectivity was fit with a descriptive model of the patchy, excitatory connectivity found in layer 2/3 of the visual cortex and again compared against the experimentally observed values.

4.4.2 Feedforward

The first step in the fitting procedure was to repeat the protocols applied to the LGN, i.e. measuring area summation curves and fitting DoG models to the results. Using

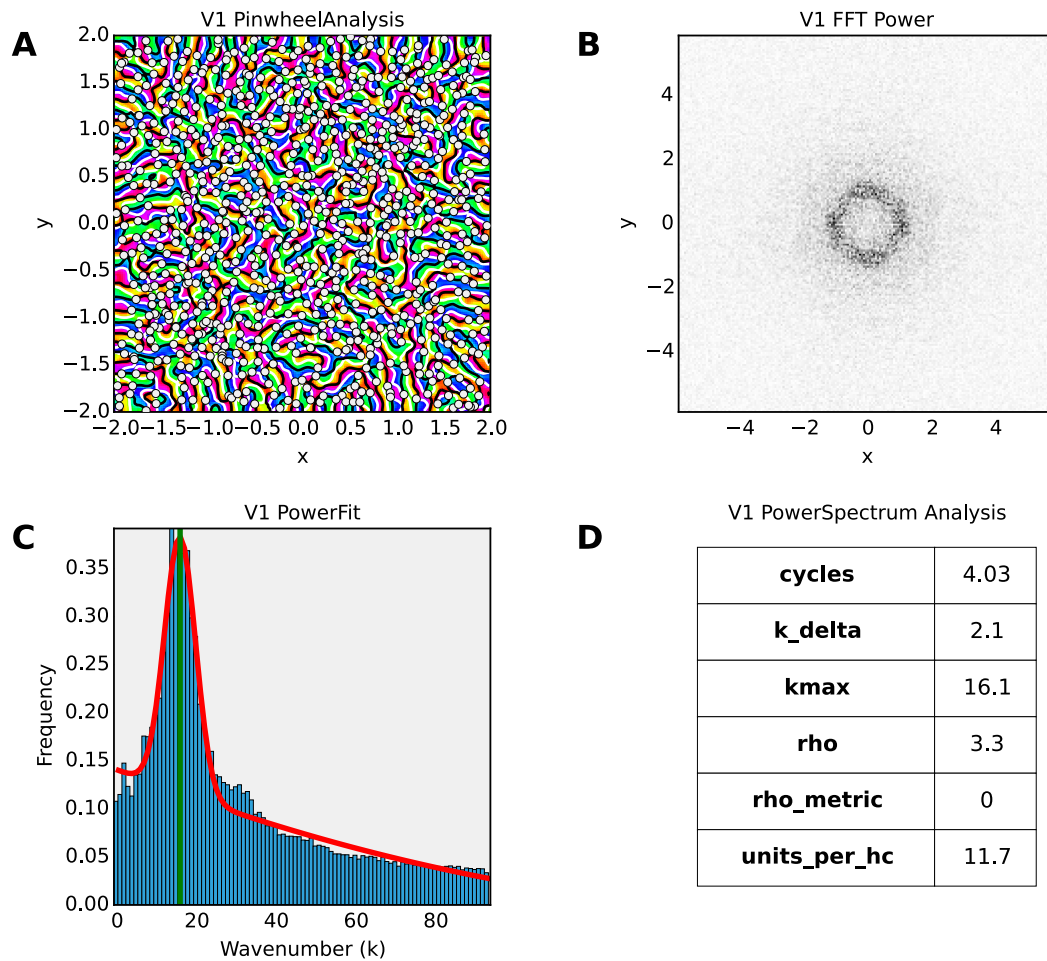


Figure 4.4: Hypercolumn and pinwheel density fitting procedure. A) Orientation map in V1 overlaid with real and imaginary contours and pinwheels at their intersections. B) 2D FFT of the orientation map showing a ring identifying the periodicity of the map. C) 1D histogram of the FFT along with Gaussian fit marking the best fit hypercolumn distance. D) Summary table showing various parameters of the fit, along with pinwheel density (ρ) which classifies the quality of the map.

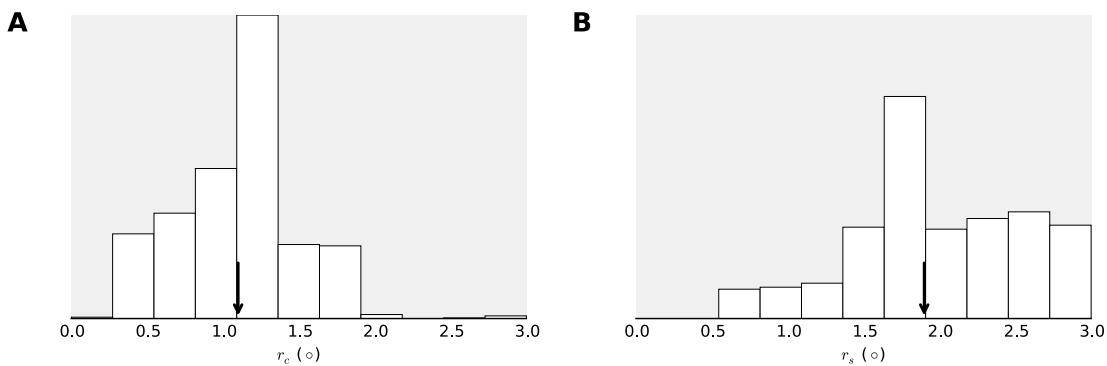


Figure 4.5: Distribution of excitatory (A) and inhibitory (B) Difference-of-Gaussian components fitted to area-summation curves measured in the SCAL V1 model. These results provide a close match to the results seen in Fig. 12 & 14 of [Sceniak and Hawken \(2001\)](#).

this approach we obtained a large number of size estimates for the excitatory and inhibitory kernels contributing to the V1 response.

4.4.3 *Intracortical connectivity*

The intracortical connectivity can be further divided into excitatory and inhibitory populations, we will outline the protocols for tuning each.

4.4.3.1 *Excitatory Connections*

The literature has had a much harder time of picking apart the contribution of intracortical and particularly the patchy lateral connectivity found in V1 so to confirm that these connections have developed as expected is to compare it to anatomical measurements. For this purpose we will be fitting a descriptive model, developed by [Buzas et al. \(2006\)](#) to the lateral connectivity data.

The model describes the patchy lateral connectivity found in layer 2/3 of V1 as a function of two distinct components. A short range isotropic Gaussian pattern and a long range pattern, defined as a von Mises function, which is combined with the orientation map. The model therefore assumes that lateral connectivity develops as a function of both the proximity in space but also along a particular feature dimension, in this case the orientation.

The vonMises function is defined as:

$$V(\phi, \kappa, \mu) = \frac{1}{2\pi I_0(\kappa)} e^{\kappa \cos 2(\phi - \mu)} \quad (4.13)$$

where ϕ is the difference in the orientation preference between the pre- and post-synaptic neuron, μ is the orientation preference of the post-synaptic neuron, κ is the

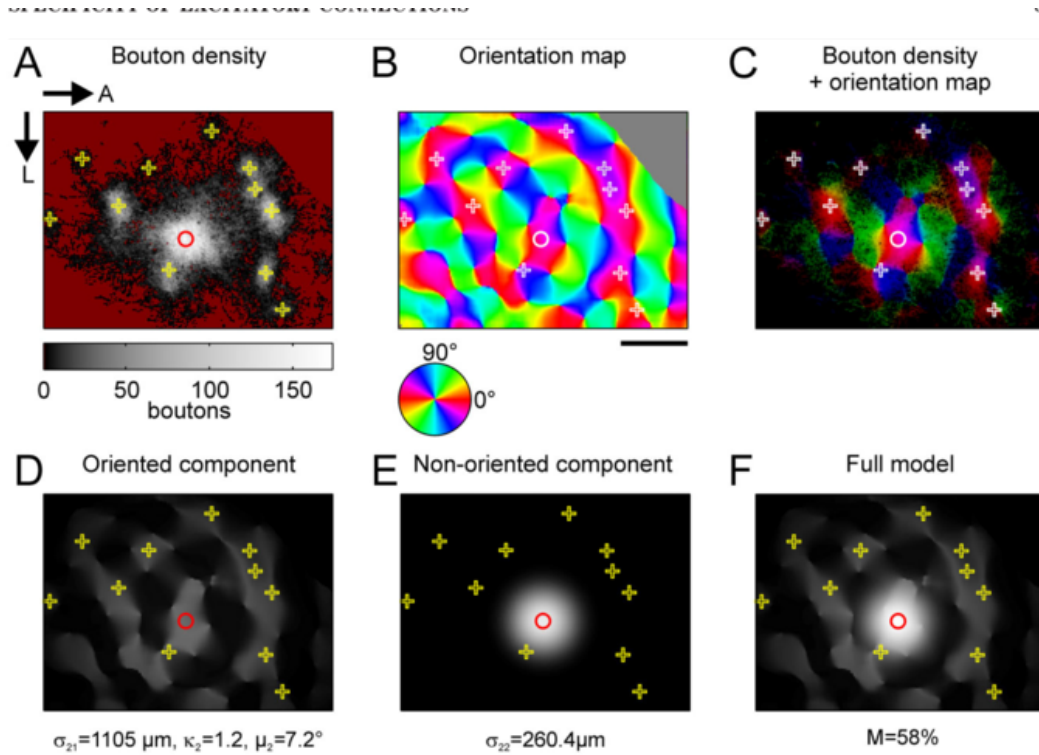


Figure 4.6: Lateral excitatory projection bouton density and orientation maps in layer 2/3 of cat V1 fit using a Gaussian and vonMises model, replicated from Buzas et al. (2006).

concentration parameter and $I_0(\kappa)$ is the modified Bessel function of the first kind of zero order.

The Gaussian component on the other hand is a simple 2D Gaussian function, where x and y are the cortical coordinates and σ the SD of the Gaussian:

$$G(x, y, \sigma) = \frac{1}{2\pi\sigma^2} e^{-\frac{x^2+y^2}{2\sigma^2}} \quad (4.14)$$

These two components can be combined into a single spatially weighted vonMises distribution in the orientation map by simple multiplying the components.

$$D_1(x, y, \phi) = s_1[G_{11}(x, y, \sigma_{11})V_1(\phi, \kappa_1, \mu_1)] \quad (4.15)$$

In order to accurately estimate the local isotropic kernel an additional Gaussian component is added, such that the full model is described by:

$$D_2(x, y, \phi) = s_1[G_{11}(x, y, \sigma_{11})V_1(\phi, \kappa_1, \mu_1) + G_{22}(x, y, \sigma_{22})] \quad (4.16)$$

The full model fitting procedure for an experimentally traced lateral connection field is shown in Figure 4.6. By applying this fitting procedure we can effectively estimate the spatial extents of both the local isotropic local kernel and the long-range

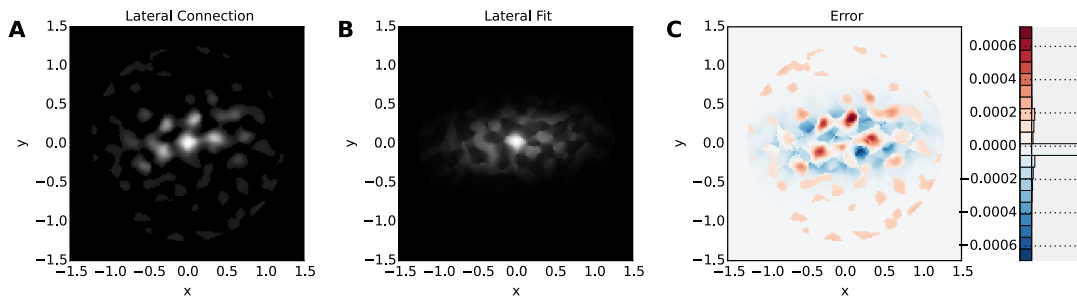


Figure 4.7: Distribution of spatial constant obtained by fitting the [Buzas et al. \(2006\)](#) vonMises+Gaussian model to long-range lateral excitatory connections developed as part of the SCAL model.

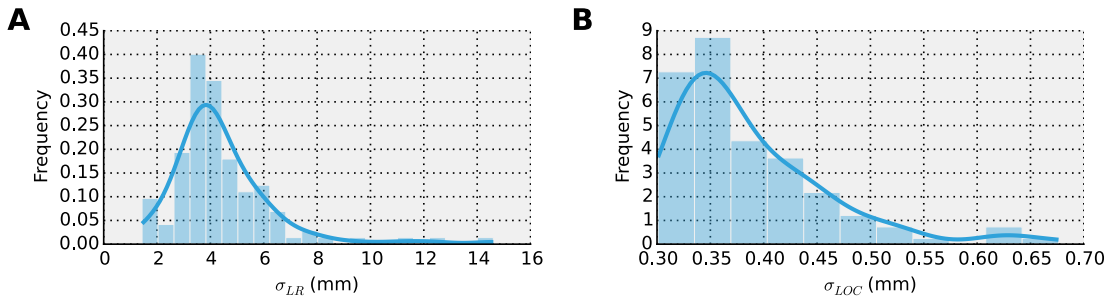


Figure 4.8: Distribution of spatial constant obtained by fitting the [Buzas et al. \(2006\)](#) vonMises+Gaussian model to long-range lateral excitatory connections developed as part of the SCAL model.

excitatory kernel. In Figure ?? demonstrates what one such fit looks like for the SCAL model, while the full distribution of local and long-range kernel values is shown in 4.8.

The distance of long-range connectivity varies even more considerably across species so using some anatomical estimates from macaque we will attempt to refine our estimates of the long-range oriented component. Anatomic data suggests that the spatial spread of lateral connections can be anywhere between 3-10 mm (on average 6-7 mm) in total length [Angelucci et al. \(2002b\)](#). Along its principal axis the visuotopic monosynaptic spread of V1 horizontal connections has a mean of $2.47^\circ \pm 0.3^\circ$. This falls well within the range of estimates for the lsRF as published in a number of studies [Sceniak et al. \(1999\)](#); [Sceniak and Hawken \(2001\)](#); [Shushruth et al. \(2009\)](#), which employed the iDoG protocol.

The results of our fitting procedure shown in Figure 4.8 show good correspondence with these experimental estimates with a mean long-range connectivity that has a spatial constant of around 5 mm but extends beyond that with our cut-off defined at 2.5° or 7.5mm. The local excitatory kernel also matches experimental estimates closely with a mean local excitatory kernel with a spatial constant of around 350 μ m, compared to the 280 μ m estimated in cat V1.

4.4.4 Inhibitory connectivity

The literature surrounding inhibitory connectivity is much more limited and no good estimates of cell-type specific spatial profiles particularly for the primate visual cortex exist. Therefore we have to extrapolate from existing data. In the literature review we explored the known properties of various cell classes and identified fast-spiking Parvalbumin-expressing interneurons as the most likely source of connectivity to drive development, particularly due to their broad tuning profile and high abundance in the thalamocortical recipient layers. Since the SCAL model does not have distinct populations of V1 we will consider the maximal extent of known basket cells as the maximal permitted extent of the inhibitory profile in the model. We will revisit the spatial profiles of inhibitory connections in the next chapter.

4.5 CONCLUSIONS

To be done:

- Add further plots describing the size and frequency tuning of SCAL V1.
- Provide further details on the lateral connectivity model fits and suggest extension based on selectivity.
- Optionally add analysis showing that RF nx/ny ratios closely follow Ringach results.
- Potentially add section that shows that the model can develop with realistic numbers of afferents (30) and that lateral connectivity can be hugely sparsified (over 90%) with little effect.

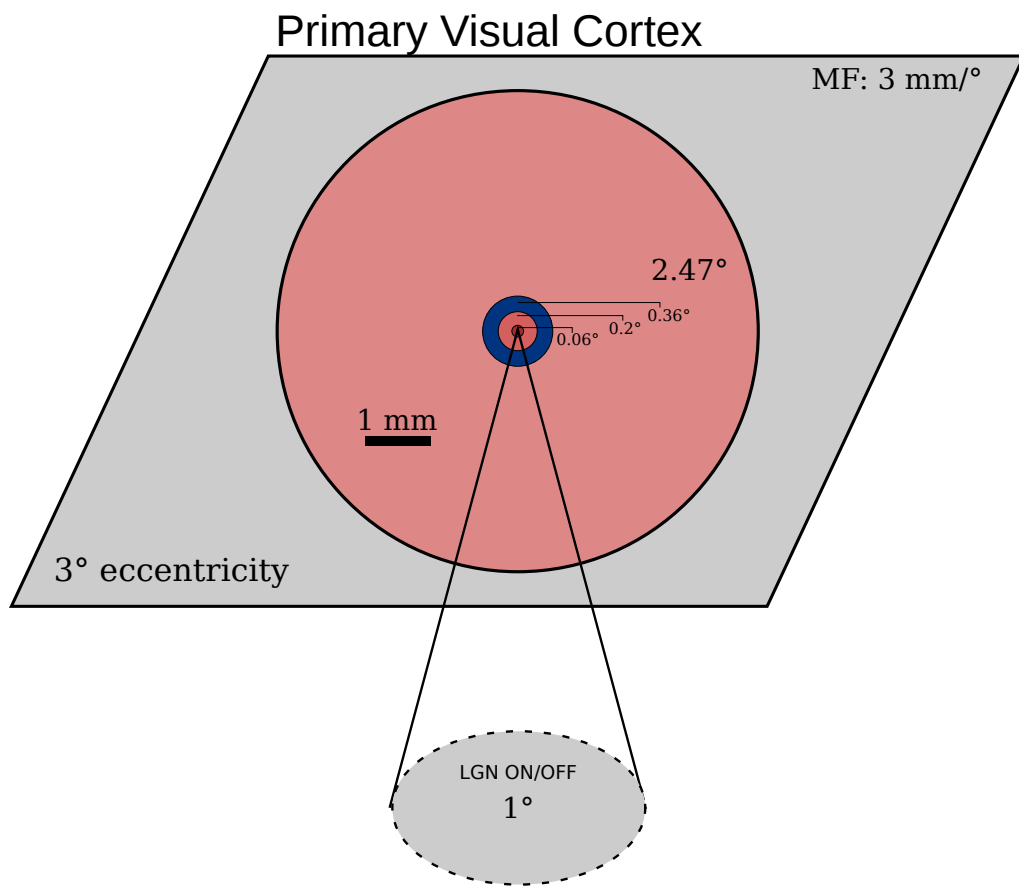


Figure 4.9: Diagram of the SCAL V1 stage of the model showing the spatial scales of the various excitatory (red) and inhibitory (blue) connections. Saturated colors indicate the kernel radii, while lightly shaded regions indicate kernel cut-off extents.

EXPLORING THE ROLE OF INHIBITION IN CORTICAL DEVELOPMENT

Surround suppression is one of the most well described phenomena in neural circuits, yet no definite conclusions on the sources of various forms of suppressions can be drawn so far. In the literature section of this thesis we described the known properties of various inhibitory cell classes and what roles they might perform. In particular we discovered that PV and SOM-expressing interneurons exhibit highly distinct response properties and layer-specific expression patterns. With recent techniques allowing targeting of specific populations there is now huge interest in understanding their role both in development and in mediating and gating the both contextual and attentional modulation phenomena.

In this chapter we will propose models that incorporate the distinct response properties of PV and SOM interneuron populations, allowing us to make concrete predictions about their role in developmental and behavioural phenomena. First we establish that the fast response and linear response of the PV-ir, fast-spiking interneuron population makes them ideally suited towards controlling feedforward activity, sparsifying activity and thereby driving map formation. While demonstrating robust and stable map formation even in the presence of strong lateral excitation, we show that the broad tuning properties of the PV population makes them badly suited to mediate context and feature specific modulation. By introducing a secondary inhibitory population modeled on the response properties of SOM+ neurons we extend the model to demonstrate how their weaker and facilitating inputs (Bartley et al., 2008; Beierlein et al., 2003; Bartley et al., 2008; Tan et al., 2008) lead to the development of highly tuned neurons, which respond only for high contrasts or large stimuli, thereby mediating a range of surround modulation phenomena.

5.1 THE ROLE OF INHIBITION IN DEVELOPMENT

Most developmental models of the primary visual cortex are based around the concept of so called Mexican hat connectivity. This is the idea that there is a local attractive force which pulls similar features together and a larger repulsive force, which pushes dissimilar features away. This is what enables the self-organization of feature maps, which itself can be explained in terms of dimensionality reduction, specifically

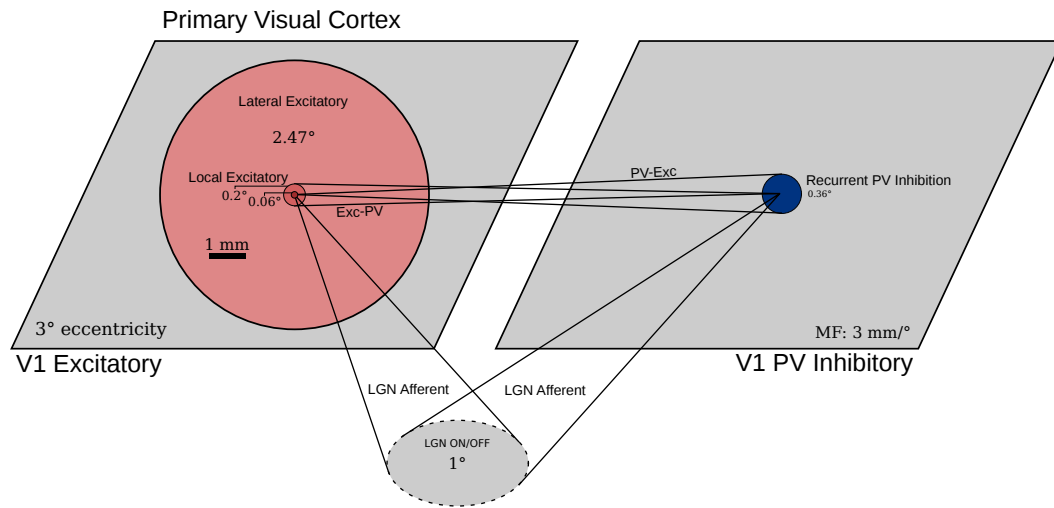


Figure 5.1: Diagram of the SEPI V1 stage of the model showing the spatial scales of the various excitatory (red) and inhibitory (blue) connections. Saturated colors indicate the kernel radii, while lightly shaded regions indicate kernel cut-off extents.

forming a discretized approximation of the principal surface of the input (?). In most of these models ([Miikkulainen and Bednar, 2005](#)) these interactions are modeled using point neurons which provide excitatory and inhibitory input. In the previous chapter we showed that an adapted version of the GCAL model ([Stevens et al., 2013](#)), which employs divisive inhibition can still demonstrate robust and stable map development. Here we will extend this

5.1.1 The SEPI Model

5.1.2 Results

5.2 THE ROLE OF INHIBITION IN SURROUND MODULATION

5.2.1 The LESPI model

$$\eta_{exc} = \frac{\eta_A + \eta_{LOC}}{1 + \eta_{PV}} * \eta_{SM} \quad (5.1)$$

where η_A is the LGN afferent activity, η_{LOC} the local excitatory contribution, η_P the PV inhibitory contribution and the surround modulation term η_{SM} is defined as:

$$\eta_{SM} = 1 + \eta_{LAT} - \eta_S \quad (5.2)$$

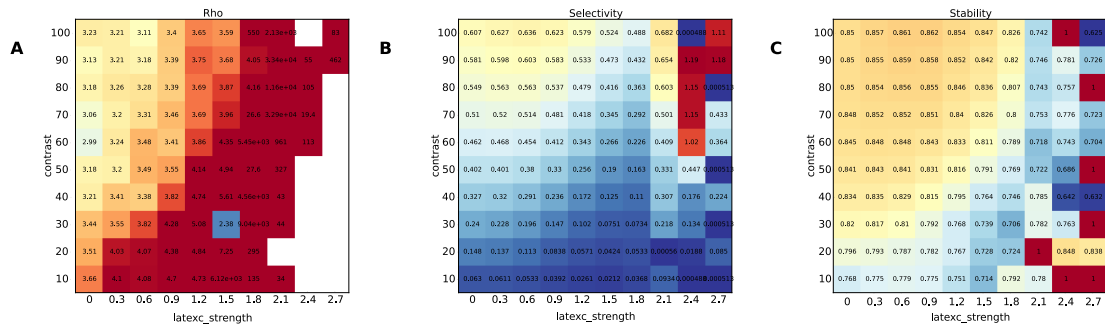


Figure 5.2: Parameter explorations of three separate metrics of orientation map development using the SCAL model. Varied parameters are the strength of long-range lateral excitation and the stimulus contrast. The three metrics are **A** the ρ pinwheel density metric, which characterizes the quality of the map, **B** the average selectivity over the time course of development and **C** the stability metric measuring how much the map changes throughout the course of development. The model shows good robustness to varying stimulus contrasts at low levels of lateral excitation but quickly deteriorates with increasing levels of excitation. White values indicate instabilities in the model causing the model to terminate.

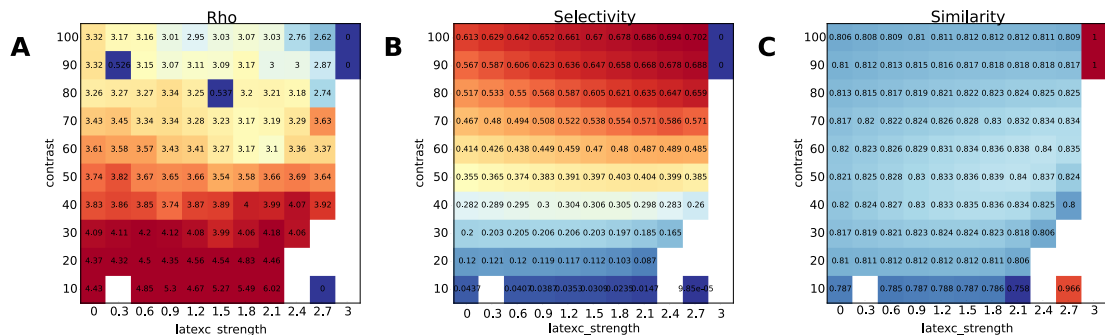


Figure 5.3: Parameter explorations of three separate metrics of orientation map development using the SEPI model. In comparison to the SCAL model the pinwheel metric is not as robust to changes in contrast, however the model is far more robust to strong lateral excitation and maintains almost uniform stability across almost all explored parameter values. Uncoupling of excitation and inhibition allows the model to handle changes in parameter strengths but in absence of a homeostatic mechanism may disrupt map formation at low contrasts.

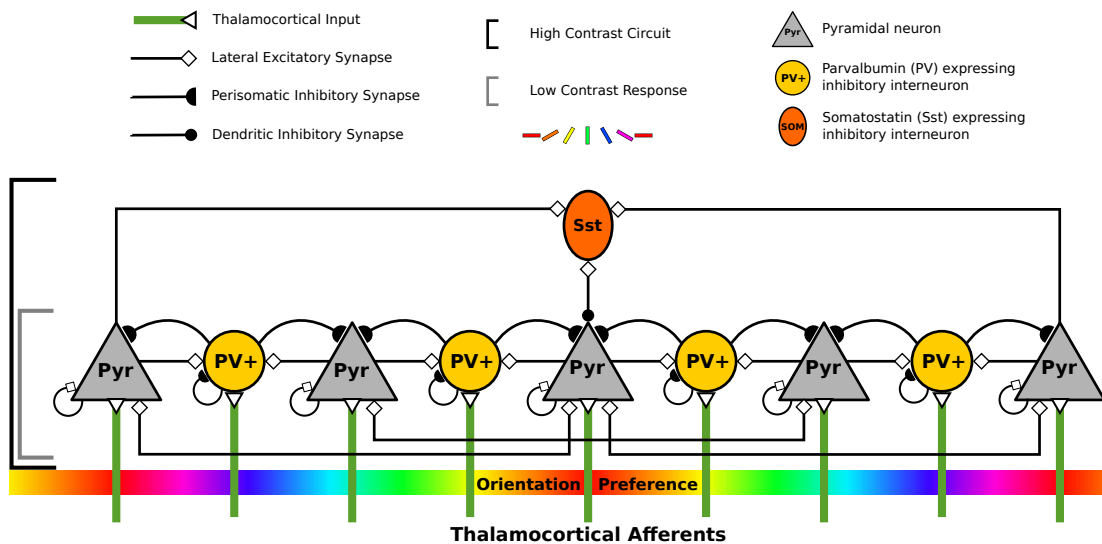


Figure 5.4: High-level circuit diagram of the LESPI model.

where η_{LAT} represents the long-range lateral excitatory contribution and η_S is the Sst inhibitory contribution. In the SEPI model the η_{SM} term simply reduces to 1, eliminating all long-range interactions. The surround modulatorion term provides gain when excitation exceeds inhibition and shunting inhibition when the reverse is true. As such, this term provides a convenient abstraction to model the modulatory influence of the dendritic integration of long-range inputs.

The effective excitatory gain may not be a bad approximation to the effect of long-range horizontal connections, which have been shown to be strongly voltage dependent (Hirsch and Gilbert, 1991). Since Sst neurons generally target distal dendrites they have generally been associated with subtractive inhibition, they do however also have a multiplicative component (Wilson et al., 2012). Additionally, their preference for targeting distal dendrites may allow them to effectively gate horizontal excitatory and feedback inputs (Ma et al., 2011; Gentet et al., 2012). Additionally theoretical studies indicate active dendritic spike backpropagation can lead to multiplicative increases in gain, while reduction in spike backpropagation can lead to divisive scaling of the firing rate (Mehaffey et al., 2005).

MODELLING THE EFFECTS OF VISUAL STATISTICS ON LONG-RANGE LATERAL CONNECTIVITY IN VISUAL CORTEX

One of the major problems in computational neuroscience is in understanding how the brain can robustly capture information about its environment to improve how new information is encoded and processed. One of the major benefits of the models developed in the previous chapter is that we can not only access synaptic weights that have developed through activity-dependent processes but due to the spatial calibration and sub-type specific connectivity we can extract the visual statistics embedded in them, compare them against existing experimental measurements.

In collaboration with Laurent Perrinet we developed analyses that allow characterizing the effect of natural image statistics on the development of long-range lateral excitatory connectivity in the model. ? analyse the edge co-occurrence statistics in a natural dataset of animals and a dataset of man made and natural images to demonstrate that they are sufficient to classify which class an image belonged to. Noting that humans are rapidly able to distinguish between animals and inanimate objects, they suggest that even early visual areas may make use of natural image statistics to categorize images rather than requiring the activity to propagate to higher visual cortices. This explanation would be more consistent with the rapid classification that has been observed in human psychophysical studies. In order to explore how the lateral connectivity could encode these statistics and make functional use of them, multiple analyses were developed to extract the statistics from the model.

The first step was to train the model on the different image datasets, which had already been analyzed for their co-occurrence statistics (see figure 6.1). The datasets fed to the model comprised the two datasets used as part of the paper and one additional image dataset recorded in ferret cages, which features great numbers of extended, high-contrast bars (shown in figure 6.2).

After training the model independently on each of the datasets the lateral connection fields were analyzed using a number of novel analyses. The first analysis that was performed was implemented by Jean-Luc Stevens and involved aligning the lateral connection field of each V1Exc neuron along the axis of preferred orientation and averaging them together. This analysis provides a way to quickly visually assess whether and how strongly lateral connection fields are biased along the axis of preferred orientation and is shown in figure ??.

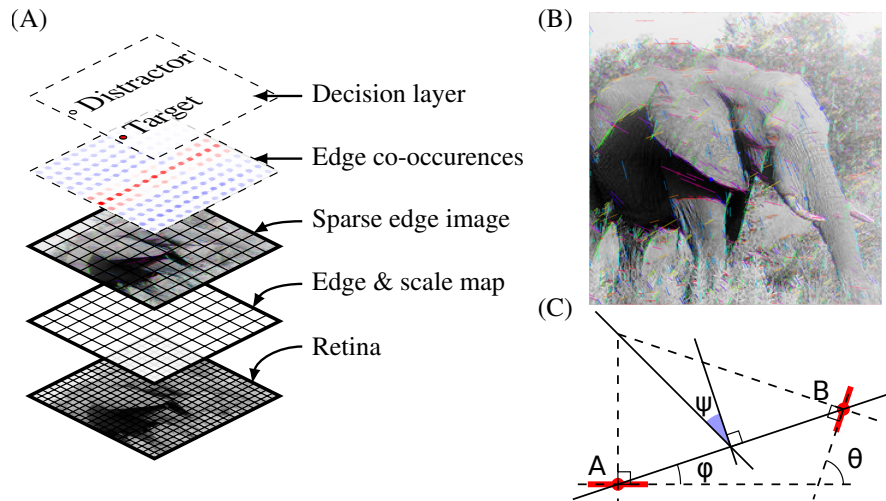


Figure 6.1: Diagrammatic representation of how a classifier is trained to distinguish between natural images and inanimate objects. A) The different layers used to train the classifier. The natural images are first fed through a model retina, all the edges are labeled with positions and scales. Using a greedy algorithm a set of edges accounting for the largest amount of luminance variance within the original image are selected. Using this set of edges the edge co-occurrence statistics were computed and finally the classifier was trained based on these statistics. B) The sparse set of labelled edges extracted from a single image. C) Diagram showing how the angular difference θ and azimuth angle ϕ and relative azimuth ψ are computed from two edges. Reproduced from ?.



Figure 6.2: The three image datasets used to train the model. From left to right 1) Artificial dataset 2) Animal dataset 3) Ferret cage dataset.

In addition a more detailed analysis, which took into account the position preference of each pre- and post-synaptic neuron was implemented. A circular histogram of weight strength was computed by calculating the azimuth, ϕ , between the pre- and post-synaptic neuron for each connection in all the lateral connection fields.

Finally the co-occurrence statistics encoded within the lateral connections were computed. This analysis was largely based around the ? code to compute the co-occurrence statistics from sets of sparse labelled edges. As before the azimuth was computed for all the connections, however additionally the difference in the pre- and post-synaptic orientation preference θ , angular location of the second edge relative to the reference edge ϕ and the distance d were calculated. Furthermore we define angle $\psi = \phi - \theta/2$, which reduces to $\psi = 0$ for co-circular edges. By binning and weighting each connection weight according to these properties a co-occurrence histogram was computed for various distances.

It was found that for the distances that are contained within one lateral field there was very little difference when binning the data separately, which matches the fact that the classifier employed by ? could extract little information from the distance. In order to reduce the local contribution the central weights within the same microcolumn were masked out. The resultant plots are shown in figure ???. Generally a good match is found between the co-occurrence statistics in the dataset and the statistics encoded in the long-range connections of the model. The difference is clearest when comparing the laboratory dataset to the natural dataset, likely because the statistics are so radically different between these datasets.

- First order orientation distribution
- Describe Buzas fitting process
- Describe decoding orientation and azimuth histograms from lateral connectivity
- Describe anisotropy results for different datasets
- Discuss further work including:
 - Better decoding of position preference
 - Include orientation selectivity in Buzas model

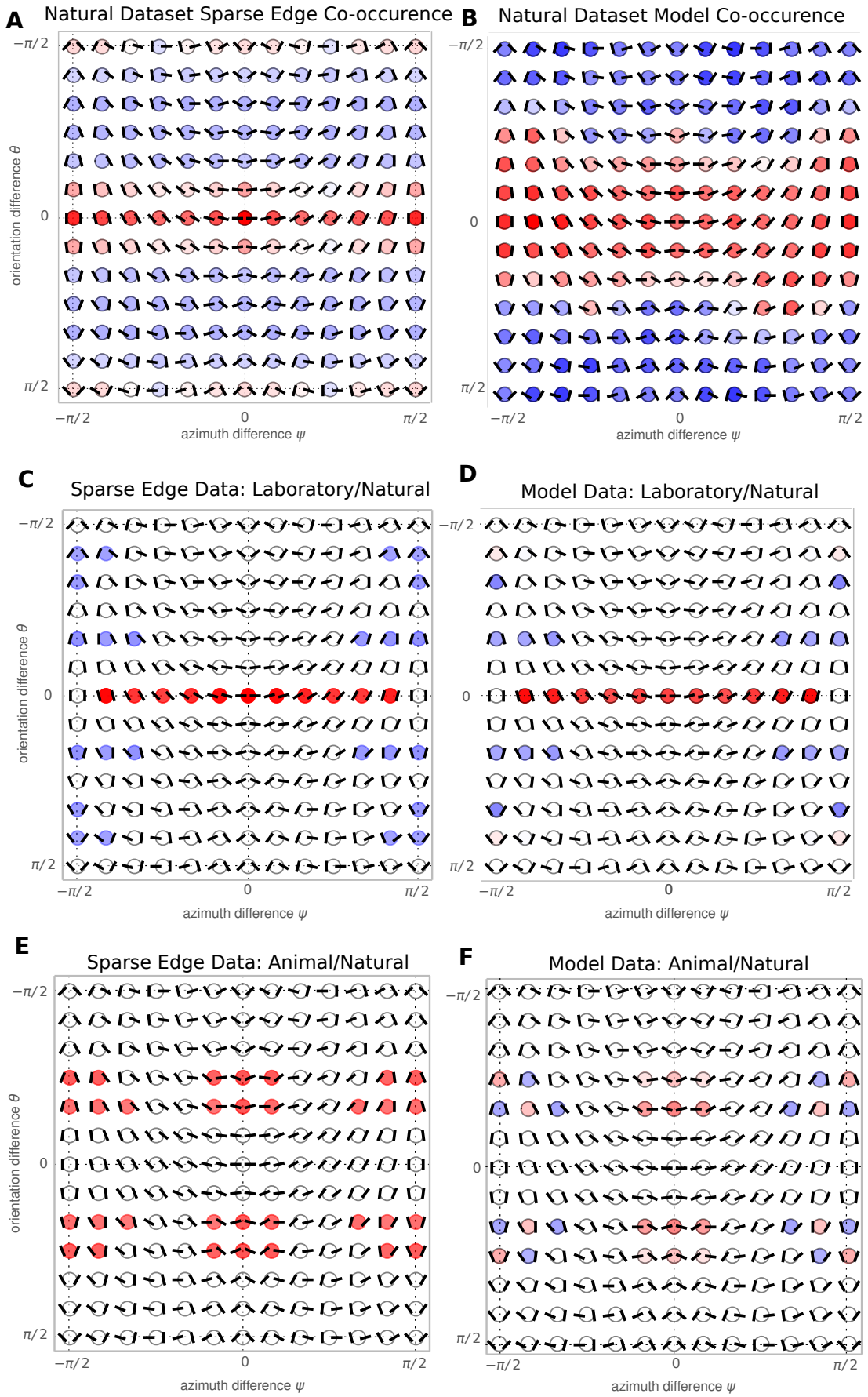


Figure 6.3: Co-occurrence histograms comparing the distribution of orientation and relative azimuth of edges extracted from two image datasets and the equivalent distribution extracted from the lateral connection patterns of the LESPI model, highlighting that the model was able to capture the most characteristic features of this dataset.

MODELING THE EFFECT OF VISUAL INPUT STATISTICS ON SURROUND MODULATION IN V₁

The previous chapter should have established that the lateral connectivity in the model encodes various second order statistics including the co-occurrence of relative azimuths and orientation found in a particular dataset. In this chapter we will discover how these differences affect the encoding of information and surround modulation.

The following analysis have been implemented and are ready to go:

- Various flanker protocols replicating [Kapadia et al. \(1995\)](#), [Mizobe et al. \(2001\)](#) and [Polat et al. \(1998\)](#)
- Decoding of activities based on feature maps.

These are the suggested next steps to complete this work:

- Decode activities in response to various levels of curvature to compute what information lateral connections are conveying to the central neuron.
- Using these protocols demonstrate not only that the model exhibits contrast dependent flanker facilitation and suppression but that it is dependent on the training dataset.

8

GENERAL DISCUSSION

8.0.1 *Simple and complex cells*

Outline the issues with modeling only simple cells and offer suggestions on extending the model to complex cells

8.0.2 *Inhibitory subtypes*

Summarize what we have learned about the role of PV in visual cortex and how it fits into current research on plasticity

Discuss role of Sst in gating feedback connectivity and suggest roles for ViP population.

8.0.3 *Neuromodulation of visuo-cortical information processing*

Detail plans on modeling modulatory influences on the developed circuitry.

LIST OF FIGURES

Figure 2.1	The early visual pathway in primates (at least superficially the same for most other mammals) from the retina to the primary visual cortex (V1) via the lateral geniculate nucleus (LGN) of the thalamus. The left panel shows the pathway, while the right panels highlight noteworthy sections including the structure of the retina, the LGN and V1 broken down into their different layers and showing different cell types. Reprinted from Solomon and Lennie (2007).	5
Figure 2.2	The centre-surround receptive field structure of some retinal ganglion cells and LGN neurons, illustrating how a contrast edge activates different portions of the field and thereby results in different activation patterns. From left to right one can see that as the light-dark edge moves into the ON surround field spontaneous activity is suppressed and as it moves further over the OFF center field is deactivated causing activity to sharply spike. Adapted from Bear et al. (2006).	6
Figure 2.3	A) Orientation preference map in a ferret generated by overlaying the activity maps for different orientations and artificially colouring each area according to the orientation preference laid out in the legend below. The image also highlights three recurrent features of orientation maps in white. The square highlights a saddle point, where a patch of cortex selective for a particular direction is almost bisected by a patch selective to another direction. The circle highlights a pinwheel arrangement, where different orientations preference patches are arranged in a circular shape. Finally the rectangular shape highlights a linear zone in which orientation preference change continuously. B) Magnifications of a linear zone and two pinwheel arrangements. Adapted from Bosking et al. (1997).	7
Figure 2.4	Gabor Patches at 0 degree and 90/180 degree orientations with clearly visible ON (white) and OFF (black) regions.	8

Figure 2.5	Development of orientation map in ferret visual cortex from postnatal day 31 to 42 revealed using chronic optical imaging of intrinsic signals. Adapted from (Chapman et al., 1996).	9
Figure 2.6	Schematic of simplest GCAL model for development of simple cells with surround modulation, retinotopic organization and orientation preference maps. It consists of a retinal sheet, two RGC/LGN for ON and OFF cell responses and one V1 sheet, connected with intra- and inter-areal projections. The sheets are drawn to scale, with larger sheets for the RGC/LGN and retinal layers to avoid edge effects. Projections are illustrated with blue (feedforward connections) and yellow (lateral connections) ovals with cones converging on their target, all drawn to scale to show their spatial extents. RGC/LGN sheets consist of units with hardwired Difference of Gaussian RFs with ON and OFF center-surround regions. LGN Afferent projections to V1 are initially unspecific but develop Gabor-like RF structures through Hebbian learning as they are observed experimentally.	12
Figure 2.7	The receptive field structure of V1 neurons showing the minimum receptive field (mRF), high contrast summation RF (hsRF) and low contrast summation RF (lsRF). Taken from Angelucci and Bressloff (2006).	18
Figure 2.8	Comparisons between electrophysiological characterisation of RF structure and the spatial structure of geniculocortical projections to V1 in (a) diagrammatic and (b) chart form. Both demonstrate that the mRF and hsRF are coextensive with the spatial extents of geniculocortical afferents to V1. Taken from Angelucci and Bressloff (2006).	20
Figure 2.9	3D plot of Mexican Hat connectivity.	26
Figure 2.10	Local microcircuit for long-range suppression through di- or poly-synaptic circuit in V1. Reproduced from Miikkulainen et al. (2005) as adapted from Weliky et al. (1995).	27

Figure 2.11 Summary schematic comparing relationship between long-range basket cell and excitatory connectivity with the underlying orientation preference structure. Upper legend represents different orientation domains in the cortical topographic map. Grey dotted lines indicate the orientation column within which soma of the simplified basket cell and excitatory neuron are found. The grey field with minus signs indicates the extent of inhibition provided by the basket cell connections considered in the current study. The grey region with plus signs indicates the excitatory field of a stereotypical pyramidal cell based on previous data by Bosking et al. (1997); Kisvárdy et al. (1997) and others. The height of the grey plus/minus regions indicates the number of axon terminals provided in that column. While basket cell terminals show local maxima every half hypercolumn distance, pyramidal cell terminals are maximal at every full hypercolumn distance. Reproduced from Buzás et al. (2001).

Figure 2.12	Inhibitory networks involving fast-spiking parvalbumin-immunoreactive neurons in thalamocortical, interlaminar and interareal cortical circuits. Feedforward excitatory thalamocortical inputs to pyramidal cells, spiny stellate neurons (▲) and fast spiking interneurons (●) in layers 2-4 (a). Inputs to interneurons are stronger (large arrowheads) than inputs to spiny cells. PV neurons provide strong (large rectangular endings) feedforward inhibition (b) to spiny cells. Feedback inhibition (c) results from PV neurons that are excited by the same spiny neurons that they inhibit. These reciprocally connected spiny neuron/PV neuron pairs share common inputs (e.g., cells in layer 4 from thalamus or cells in layer 2/3 from layer 4) creating recurrent excitatory (d) and inhibitory subnetworks (contained within blue shaded boxes). [Please insert intopreamble]Lateral[Please insert intopreamble] inhibition (e) of these subnetworks results from PV neurons that are driven by excitatory feedback connections (f) from outside the subnetworks (e.g., by layer 5 to layer 2/3 connections or feedback from higher cortical areas). Notice that [Please insert intopreamble]lateral[Please insert intopreamble] inhibition is weaker (small rectangular endings) than feedforward and feedback inhibition and impinges on multiple subnetworks. Reproduced from Burkhalter (2008)	33
Figure 2.13	Schematic illustration of the cortical circuit in layer 2/3 contributing to surround suppression. As a visual stimulus expands (larger stimuli are shown in lighter grey), recruitment of adjacent PCs increases Sst-ir excitation through horizontal axons (horizontal arrows). Reproduced from Adesnik et al. (2012) .	36
Figure 2.14	Distribution of GABAergic interneurons in S1 cortex by immunohistological marker. Reproduced from Rudy et al. (2011) .	37
Figure 2.15	Connectivity between somatostatin (Sst), parvalbumin (Pv), vasoactive intestinal peptide (Vip) expressing and pyramidal (Pyr) cell types. Adapted from Pfeffer et al. (2013) .	38
Figure 3.1	53
Figure 4.1	58
Figure 4.2	A) LGN area-summation curve (blue) fit using an integrated Difference-of-gaussian model (dotted). B) Parameters of the iDoG model fit.	58

Figure 4.3	Diagram of the SCAL-LGN stage of the model showing the spatial scales of the various excitatory (red) and inhibitory (blue) connections. Saturated colors indicate the kernel radii, while lightly shaded regions indicate kernel cut-off extents.	60
Figure 4.4	Hypercolumn and pinwheel density fitting procedure. A) Orientation map in V1 overlaid with real and imaginary contours and pinwheels at their intersections. B) 2D FFT of the orientation map showing a ring identifying the periodicity of the map. C) 1D histogram of the FFT along with Gaussian fit marking the best fit hypercolumn distance. D) Summary table showing various parameters of the fit, along with pinwheel density (ρ) which classifies the quality of the map.	65
Figure 4.5	Distribution of excitatory (A) and inhibitory (B) Difference-of-Gaussian components fitted to area-summation curves measured in the SCAL V1 model. These results provide a close match to the results seen in Fig. 12 & 14 of Sceniak and Hawken (2001).	66
Figure 4.6	Lateral excitatory projection bouton density and orientation maps in layer 2/3 of cat V1 fit using a Gaussian and vonMises model, replicated from Buzas et al. (2006).	67
Figure 4.7	Distribution of spatial constant obtained by fitting the Buzas et al. (2006) vonMises+Gaussian model to long-range lateral excitatory connections developed as part of the SCAL model.	68
Figure 4.8	Distribution of spatial constant obtained by fitting the Buzas et al. (2006) vonMises+Gaussian model to long-range lateral excitatory connections developed as part of the SCAL model.	68
Figure 4.9	Diagram of the SCAL V1 stage of the model showing the spatial scales of the various excitatory (red) and inhibitory (blue) connections. Saturated colors indicate the kernel radii, while lightly shaded regions indicate kernel cut-off extents.	70
Figure 5.1	Diagram of the SEPI V1 stage of the model showing the spatial scales of the various excitatory (red) and inhibitory (blue) connections. Saturated colors indicate the kernel radii, while lightly shaded regions indicate kernel cut-off extents.	72

Figure 5.2	Parameter explorations of three separate metrics of orientation map development using the SCAL model. Varied parameters are the strength of long-range lateral excitation and the stimulus contrast. The three metrics are A the ρ pinwheel density metric, which characterizes the quality of the map, B the average selectivity over the time course of development and C the stability metric measuring how much the map changes throughout the course of development. The model shows good robustness to varying stimulus contrasts at low levels of lateral excitation but quickly deteriorates with increasing levels of excitation. White values indicate instabilities in the model causing the model to terminate.	73
Figure 5.3	Parameter explorations of three separate metrics of orientation map development using the SEPI model. In comparison to the SCAL model the pinwheel metric is not as robust to changes in contrast, however the model is far more robust to strong lateral excitation and maintains almost uniform stability across almost all explored parameter values. Uncoupling of excitation and inhibition allows the model to handle changes in parameter strengths but in absence of a homeostatic mechanism may disrupt map formation at low contrasts.	73
Figure 6.3	Co-occurrence histograms comparing the distribution of orientation and relative azimuth of edges extracted from two image datasets and the equivalent distribution extracted from the lateral connection patterns of the LESPI model, highlighting that the model was able to capture the most characteristic features of this dataset.	78

BIBLIOGRAPHY

- Abbott, L. F., Varela, J. a., Sen, K., and Nelson, S. B. (1997). Synaptic depression and cortical gain control. *Science (New York, N.Y.)*, 275(5297):220–4. (Cited on page 28.)
- Adesnik, H., Bruns, W., Taniguchi, H., Huang, Z. J., and Scanziani, M. (2012). A neural circuit for spatial summation in visual cortex. *Nature*, 490(7419):226–31. (Cited on pages 35, 36, and 84.)
- Ahissar, M. and Hochstein, S. (2004). The reverse hierarchy theory of visual perceptual learning. *Trends in Cognitive Sciences*, 8(10):457–64. (Cited on page 23.)
- Albus, K. and Wahle, P. (1994). The Topography of Tangential Inhibitory Connections in the Postnatally Developing and Mature Striate Cortex of the Cat. *European Journal of Neuroscience*, 6:779–792. (Cited on page 32.)
- Angelucci, A. and Bressloff, P. C. (2006). Contribution of feedforward, lateral and feedback connections to the classical receptive field center and extra-classical receptive field surround of primate V1 neurons. *Progress in Brain Research*, 154(6):93–120. (Cited on pages 18, 19, 20, 23, 24, and 82.)
- Angelucci, A. and Bullier, J. (2003). Reaching beyond the classical receptive field of V1 neurons: horizontal or feedback axons? *Journal of Physiology*, 97(2-3):141–54. (Cited on page 23.)
- Angelucci, A., Levitt, J. B., and Lund, J. S. (2002a). Anatomical Origins of the Classical Receptive Field of Single Neurons in Macaque Visual Cortical Area V1. *Progress in Brain Research*, 136:373–88. (Cited on page 64.)
- Angelucci, A., Levitt, J. B., Walton, E. J. S., Hupe, J.-M., Bullier, J., and Lund, J. S. (2002b). Circuits for local and global signal integration in primary visual cortex. *The Journal of Neuroscience*, 22(19):8633–46. (Cited on pages 19, 20, 21, 22, 23, 24, 43, 64, and 68.)
- Angelucci, A. and Sainsbury, K. (2006). Contribution of Feedforward Thalamic Afferents and Corticogeniculate Feedback to the Spatial Summation Area of Macaque V1 and LGN. *The Journal of Comparative Neurology*, 498(April):330–351. (Cited on pages 17, 18, 19, 20, and 64.)
- Antolík, J. and Bednar, J. A. (2011). Development of maps of simple and complex cells in the primary visual cortex. *Frontiers in Computational Neuroscience*, 5(April):17. (Cited on page 10.)
- Atick, J. J. and Redlich, N. A. (1992). What does the Retina Know about Natural Scenes? *Neural Computation*, 4:196–210. (Cited on pages 25 and 42.)
- Bair, W., Cavanaugh, J. R., and Movshon, J. A. (2003). Time course and time-distance relationships for surround suppression in macaque V1 neurons. *The Journal of Neuroscience*, 23(20):7690–701. (Cited on page 22.)
- Bartley, A. F., Huang, Z. J., Huber, K. M., and Gibson, J. R. (2008). Differential activity-dependent, homeostatic plasticity of two neocortical inhibitory circuits. *Journal of*

- Neurophysiology*, 100(4):1983–94. (Cited on pages 32, 35, and 71.)
- Bear, M. F., Connors, B., and Paradiso, M. (2006). *Neuroscience: Exploring the Brain*. Lippincott Williams and Wilkins, 3rd revise edition. (Cited on pages 6 and 81.)
- Bednar, J. a. and Miikkulainen, R. (2003). Self-organization of spatiotemporal receptive fields and laterally connected direction and orientation maps. *Neurocomputing*, 52–54(02):473–480. (Cited on pages 9 and 10.)
- Beierlein, M., Gibson, J. R., and Connors, B. W. (2003). Two dynamically distinct inhibitory networks in layer 4 of the neocortex. *Journal of Neurophysiology*, 90(5):2987–3000. (Cited on pages 35 and 71.)
- Bezrukov, S. and Vodyanoy, I. (1997). Stochastic resonance in non-dynamical systems without response thresholds. *Nature*, 385:319–321. (Cited on page 28.)
- Binzegger, T., Douglas, R. J., and Martin, K. a. C. (2004). A quantitative map of the circuit of cat primary visual cortex. *The Journal of Neuroscience*, 24(39):8441–53. (Cited on page 30.)
- Blakemore, C., Carpenter, R., and Georgeson, M. (1970). Lateral inhibition between orientation detectors in the human visual system. *Nature*, (228):37–39. (Cited on page 25.)
- Blasdel, G. G. and Fitzpatrick, D. (1984). Physiological organization of layer 4 in macaque striate cortex. *The Journal of Neuroscience*, 4(3):880–895. (Cited on page 29.)
- Bonin, V., Mante, V., and Carandini, M. (2005). The suppressive field of neurons in lateral geniculate nucleus. *The Journal of Neuroscience*, 25(47):10844–56. (Cited on pages 13, 14, and 57.)
- Bosking, W. H., Zhang, Y., Schofield, B., and Fitzpatrick, D. (1997). Orientation selectivity and the arrangement of horizontal connections in tree shrew striate cortex. *The Journal of Neuroscience*, 17(6):2112–27. (Cited on pages 7, 10, 21, 31, 43, 81, and 83.)
- Bullier, J., Hupe, J.-M., James, A. C., and Girard, P. (2001). The role of feedback connections in shaping the responses of visual cortical neurons. *Progress in Brain research*, 134:193–204. (Cited on page 23.)
- Burkhalter, A. (2008). Many specialists for suppressing cortical excitation. *Frontiers in neuroscience*, 2(2):155–67. (Cited on pages 33 and 84.)
- Buzás, P., Eysel, U. T., Adorján, P., and Kisvárday, Z. F. (2001). Axonal topography of cortical basket cells in relation to orientation, direction, and ocular dominance maps. *The Journal of comparative neurology*, 437(3):259–85. (Cited on pages 30, 31, 64, and 83.)
- Buzas, P., Kovacs, K., Ferecskó, A. S., Budd, J. M., Eysel, U. T., and Kisvárday, Z. F. (2006). Model-Based Analysis of Excitatory Lateral Connections in the Visual Cortex. *The Journal of comparative neurology*, 881(May):861–881. (Cited on pages 64, 66, 67, 68, and 85.)
- Carandini, M., Heeger, D. J., and Senn, W. (2002). A synaptic explanation of suppression in visual cortex. *The Journal of neuroscience : the official journal of the Society for Neuroscience*, 22(22):10053–65. (Cited on pages 28 and 29.)
- Cavanaugh, J. R., Bair, W., and Movshon, J. A. (2002a). Nature and interaction of signals from the receptive field center and surround in macaque V1 neurons. *Journal of Neurophysiology*, 88(5):2530–46. (Cited on page 29.)

- Cavanaugh, J. R., Bair, W., and Movshon, J. A. (2002b). Selectivity and spatial distribution of signals from the receptive field surround in macaque V1 neurons. *Journal of Neurophysiology*, 88(5):2547–56. (Cited on page 64.)
- Chapman, B., Stryker, M. P., and Bonhoeffer, T. (1996). Development of orientation preference maps in ferret primary visual cortex. *The Journal of Neuroscience*, 16(20):6443–53. (Cited on pages 8, 9, and 82.)
- Connolly, M. and Van Essen, D. (1984). The representation of the visual field in parvocellular and magnocellular layers of the lateral geniculate nucleus in the macaque monkey. *The Journal of Comparative Neurology*, 226(4):544–64. (Cited on pages 19 and 63.)
- Cruikshank, S. J., Lewis, T. J., and Connors, B. W. (2007). Synaptic basis for intense thalamocortical activation of feedforward inhibitory cells in neocortex. *Nature Neuroscience*, 10(4):462–8. (Cited on page 31.)
- DeAngelis, G. and Robson, J. (1992). Organization of suppression in receptive fields of neurons in cat visual cortex. *Journal of Neurophysiology*, 68(1):144–163. (Cited on page 32.)
- Derrington, A. M. and Lennie, P. (1984). Spatial and temporal contrast sensitivities of neurones in lateral geniculate nucleus of macaque. *The Journal of Physiology*, 357:219–40. (Cited on pages 15 and 20.)
- Di Cristo, G., Wu, C., Chattopadhyaya, B., Ango, F., Knott, G., Welker, E., Svoboda, K., and Huang, Z. J. (2004). Subcellular domain-restricted GABAergic innervation in primary visual cortex in the absence of sensory and thalamic inputs. *Nature Neuroscience*, 7(11):1184–6. (Cited on page 34.)
- Dosher, A. B. and Lu, Z.-l. (2000). Noise Exclusion in Spatial Attention. *Psychological Science*, 11(2):139–146. (Cited on page 41.)
- Douglas, R. and Martin, K. (1991). A functional microcircuit for cat visual cortex. *The Journal of Physiology*, 440:735–769. (Cited on page 27.)
- Fagiolini, M., Fritschy, J.-M., Löw, K., Möhler, H., Rudolph, U., and Hensch, T. K. (2004). Specific GABA_A circuits for visual cortical plasticity. *Science (New York, N.Y.)*, 303(5664):1681–3. (Cited on page 38.)
- Fagiolini, M. and Hensch, T. K. (2000). Inhibitory threshold for critical-period activation in primary visual cortex. *Nature*, 404(6774):183–6. (Cited on page 38.)
- Fanselow, E., Richardson, K. A., and Connors, B. W. (2008). Selective, state-dependent activation of somatostatin-expressing inhibitory interneurons in mouse neocortex. *Journal of Neurophysiology*, 100:2640–2652. (Cited on page 35.)
- Felleman, D. J. and Van Essen, D. C. (1991). Distributed hierarchical processing in the primate cerebral cortex. *Cerebral Cortex*, 1(1):1–47. (Cited on page 23.)
- Firth, S. I., Wang, C.-T., and Feller, M. B. (2005). Retinal waves: mechanisms and function in visual system development. *Cell Calcium*, 37(5):425–32. (Cited on page 9.)
- Fregnac, Y. and Imbert, M. (1978). Early development of visual cortical cells in normal and dark-reared kittens: relationship between orientation selectivity and ocular dominance. *The Journal of physiology*, 278:27–44. (Cited on page 37.)
- Freund, T. F. and Katona, I. (2007). Perisomatic inhibition. *Neuron*, 56(1):33–42. (Cited on page 30.)

- Fu, Y., Tucciarone, J. M., Espinosa, J. S., Sheng, N., Darcy, D. P., Nicoll, R. a., Huang, Z. J., and Stryker, M. P. (2014). A cortical circuit for gain control by behavioral state. *Cell*, 156:1139–1152. (Cited on page 36.)
- Gabernet, L., Jadhav, S. P., Feldman, D. E., Carandini, M., and Scanziani, M. (2005). Somatosensory integration controlled by dynamic thalamocortical feed-forward inhibition. *Neuron*, 48(2):315–27. (Cited on page 31.)
- Geisler, W. S., Perry, J. S., Super, B. J., and Gallogly, D. P. (2001). Edge co-occurrence in natural images predicts contour grouping performance. *Vision research*, 41(6):711–24. (Cited on page 42.)
- Gentet, L. J., Kremer, Y., Taniguchi, H., Huang, Z. J., Staiger, J. F., and Petersen, C. C. H. (2012). Unique functional properties of somatostatin-expressing GABAergic neurons in mouse barrel cortex. *Nature Neuroscience*, 15(4):607–12. (Cited on pages 35 and 74.)
- Gilbert, C. and Wiesel, T. (1983). Clustered intrinsic connections in cat visual cortex. *The Journal of Neuroscience*, 3(5):1116. (Cited on page 9.)
- Gilbert, C. and Wiesel, T. (1990). The influence of contextual stimuli on the orientation selectivity of cells in primary visual cortex of the cat. *Vision research*, 30(II). (Cited on page 27.)
- Gonchar, Y., Wang, Q., and Burkhalter, A. (2007). Multiple distinct subtypes of GABAergic neurons in mouse visual cortex identified by triple immunostaining. *Frontiers in neuroanatomy*, 1(March):3. (Cited on page 34.)
- Grinvald, A., Lieke, E. E., Frostig, R. D., and Hildesheim, R. (1994). Cortical point-spread function and long-range lateral interactions revealed by real-time optical imaging of macaque monkey primary visual cortex. *The Journal of Neuroscience*, 14(5):2545–68. (Cited on page 26.)
- Hawken, M. J., Shapley, R. M., and Grosof, D. H. (2009). Temporal-frequency selectivity in monkey visual cortex. *Visual Neuroscience*, 13(03):477. (Cited on page 29.)
- Hensch, T. K. and Stryker, M. P. (2004). Columnar architecture sculpted by GABA circuits in developing cat visual cortex. *Science (New York, N.Y.)*, 303(5664):1678–81. (Cited on page 38.)
- Higley, M. (2014). Localized GABAergic inhibition of dendritic Ca²⁺ signalling. *Nature Reviews Neuroscience*, (August). (Cited on page 36.)
- Hirsch, J. a. and Gilbert, C. D. (1991). Synaptic physiology of horizontal connections in the cat's visual cortex. *The Journal of Neuroscience*, 11(6):1800–9. (Cited on pages 22, 26, 27, and 74.)
- Hirsch, J. a., Martinez, L. M., Pillai, C., Alonso, J.-M., Wang, Q., and Sommer, F. T. (2003). Functionally distinct inhibitory neurons at the first stage of visual cortical processing. *Nature Neuroscience*, 6(12):1300–8. (Cited on pages 29 and 32.)
- Hofer, S. B., Ko, H., Pichler, B., Vogelstein, J., Ros, H., Zeng, H., Lein, E., Lesica, N. a., and Mrsic-Flogel, T. D. (2011). Differential connectivity and response dynamics of excitatory and inhibitory neurons in visual cortex. *Nature Neuroscience*, 14(8):1045–52. (Cited on page 32.)
- Hogan, D., Terwilleger, E., and Berman, N. (1992). Development of subpopulations of GABAergic neurons in cat visual cortical areas. *NeuroReport*, 3:1069–1072. (Cited on page 30.)

- Hubel, D. and Wiesel, T. N. (1961). Integrative Action in the Cat's Lateral Geniculate Body. *Journal of Physiology*, 155:385–398. (Cited on page 14.)
- Hunt, J. J., Bosking, W. H., and Goodhill, G. J. (2011). Statistical structure of lateral connections in the primary visual cortex. *Neural systems & circuits*, 1(1):3. (Cited on page 43.)
- Hupé, J.-M., James, A., Payne, B., Lomber, S., Girard, P., and Bullier, J. (1998). Cortical feedback improves discrimination between figure and background by V₁, V₂ and V₃ neurons. *Nature*, 394(6695):784–787. (Cited on page 23.)
- Huxlin, K. and Pasternak, T. (2001). Long-term neurochemical changes after visual cortical lesions in the adult cat. *Journal of Comparative Neurology*, 429:221–241. (Cited on page 30.)
- Ichida, J. M., Schwabe, L., Bressloff, P. C., and Angelucci, A. (2007). Response facilitation from the "suppressive" receptive field surround of macaque V₁ neurons. *Journal of Neurophysiology*, 98(4):2168–81. (Cited on pages 23 and 24.)
- Jin, J., Wang, Y., Swadlow, H. a., and Alonso, J. M. (2011). Population receptive fields of ON and OFF thalamic inputs to an orientation column in visual cortex. *Nature Neuroscience*, 14(2):232–238. (Cited on page 9.)
- Kapadia, M. K., Ito, M., Gilbert, C. D., and Westheimer, G. (1995). Improvement in visual sensitivity by changes in local context: parallel studies in human observers and in V₁ of alert monkeys. *Neuron*, 15(4):843–56. (Cited on page 79.)
- Kapadia, M. K., Westheimer, G., and Gilbert, C. D. (1999). Dynamics of spatial summation in primary visual cortex of alert monkeys. *Proceedings of the National Academy of Sciences of the United States of America*, 96(21):12073–8. (Cited on page 43.)
- Kaschube, M., Schnabel, M., Löwel, S., Coppola, D., White, L., and Wolf, F. (2010). Universality in the evolution of orientation columns in the visual cortex. *Science*, 330(6007):1113–1116. (Cited on page 64.)
- Katz, L. C., Weliky, M., and Crowley, J. C. (2000). Activity and the Development of the Visual Cortex: New Perspectives. In *The New Cognitive Neurosciences*, chapter 13, pages 199–221. MIT Press, Cambridge, MA. (Cited on page 9.)
- Kepecs, A. and Fishell, G. (2014). Interneuron cell types are fit to function. *Nature*, 505(7483):318–26. (Cited on page 36.)
- Kisvárday, Z., Ferecskó, A., and Kovács, K. (2002). One axon-multiple functions: specificity of lateral inhibitory connections by large basket cells. *Journal of Neurocytology*, 264(2002):255–264. (Cited on pages 30 and 32.)
- Kisvárday, Z. F., Tóth, E., Rausch, M., and Eysel, U. T. (1997). Orientation-specific relationship between populations of excitatory and inhibitory lateral connections in the visual cortex of the cat. *Cerebral Cortex*, 7(7):605–18. (Cited on pages 27, 31, 32, and 83.)
- Klausberger, T., Roberts, J. D. B., and Somogyi, P. (2002). Cell type- and input-specific differences in the number and subtypes of synaptic GABA(A) receptors in the hippocampus. *The Journal of neuroscience : the official journal of the Society for Neuroscience*, 22(7):2513–21. (Cited on page 38.)
- Kuhlman, S. J., Olivas, N. D., Tring, E., Ikrar, T., Xu, X., and Trachtenberg, J. T. (2013). A disinhibitory microcircuit initiates critical-period plasticity in the visual cortex. *Nature*, pages 1–7. (Cited on page 39.)

- Law, J. S., Antolik, J., and Bednar, J. A. (2011). Mechanisms for stable and robust development of orientation maps and receptive fields. (Cited on page 10.)
- Lee, S., Kruglikov, I., Huang, Z. J., Fishell, G., and Rudy, B. (2013). A disinhibitory circuit mediates motor integration in the somatosensory cortex. *Nature neuroscience*, 16(11):1662–70. (Cited on page 36.)
- Letzkus, J. J., Wolff, S. B. E., Meyer, E. M. M., Tovote, P., Courtin, J., Herry, C., and Lüthi, A. (2011). A disinhibitory microcircuit for associative fear learning in the auditory cortex. *Nature*, 480(7377):331–5. (Cited on page 39.)
- Levitt, J. B. and Lund, J. S. (1997). Contrast dependence of contextual effects in primate visual cortex. *Nature*, 387:73–76. (Cited on page 29.)
- Levitt, J. B. and Lund, J. S. (2002). The spatial extent over which neurons in macaque striate cortex pool visual signals. *Visual Neuroscience*, 19(4):439–52. (Cited on pages 20, 21, and 64.)
- Levitt, J. B., Schumer, R. a., Sherman, S. M., Spear, P. D., and Movshon, J. a. (2001). Visual response properties of neurons in the LGN of normally reared and visually deprived macaque monkeys. *Journal of Neurophysiology*, 85(5):2111–29. (Cited on pages 15 and 57.)
- Li, L.-Y., Xiong, X. R., Ibrahim, L. a., Yuan, W., Tao, H. W., and Zhang, L. I. (2014). Differential Receptive Field Properties of Parvalbumin and Somatostatin Inhibitory Neurons in Mouse Auditory Cortex. *Cerebral Cortex*, 14:2–3. (Cited on page 34.)
- Li, Z. (2002). A saliency map in primary visual cortex. *Trends in Cognitive Sciences*, 6(1):9–16. (Cited on page 41.)
- Liu, Y.-J., Ehrengruber, M., Negwer, M., Shao, H.-J., Cetin, A., and Lyon, D. (2013). Tracing Inputs to Inhibitory or Excitatory Neurons of Mouse and Cat Visual Cortex with a Targeted Rabies Virus. *Current Biology*, pages 1–10. (Cited on page 37.)
- Lund, J. and Yoshioka, T. (1991). Local circuit neurons of macaque monkey striate cortex: III. Neurons of laminae 4B, 4A, and 3B. *Journal of Comparative Neurology*, 311:234–258. (Cited on page 30.)
- Lund, J. S. (1987). Local circuit neurons of macaque monkey striate cortex: IV. Neurons of laminae 4C and 5A. *The Journal of comparative neurology*, 257:60–92. (Cited on page 30.)
- Ma, W.-p., Liu, B.-h., Li, Y.-t., Huang, Z. J., Zhang, L. I., and Tao, H. W. (2011). Visual Representations by Cortical Somatostatin Inhibitory Neurons - Selective but with Weak and Delayed Responses. *Journal of Neuroscience*, 30(43):14371–14379. (Cited on pages 32, 34, and 74.)
- Markram, H., Toledo-Rodriguez, M., Wang, Y., Gupta, A., Silberberg, G., and Wu, C. (2004). Interneurons of the neocortical inhibitory system. *Nature Reviews Neuroscience*, 5(10):793–807. (Cited on pages 27 and 30.)
- Martin, K., Somogyi, P., and Whitteridge, D. (1983). Physiological and morphological properties of identified basket cells in the cat's visual cortex. *Experimental Brain Research*, 50:193–200. (Cited on page 30.)
- McGuire, B. a., Gilbert, C. D., Rivlin, P. K., and Wiesel, T. N. (1991). Targets of horizontal connections in macaque primary visual cortex. *The Journal of comparative neurology*, 305(3):370–92. (Cited on page 27.)

- McMains, S. a. and Somers, D. C. (2004). Multiple spotlights of attentional selection in human visual cortex. *Neuron*, 42(4):677–86. (Cited on page 41.)
- Mehaffey, W. H., Doiron, B., Maler, L., and Turner, R. W. (2005). Deterministic multiplicative gain control with active dendrites. *The Journal of neuroscience : the official journal of the Society for Neuroscience*, 25(43):9968–77. (Cited on page 74.)
- Miikkulainen, R. and Bednar, J. A. (2005). Development of Maps and Connections. In *Computational Maps in the Visual Cortex*, chapter 5, pages 85–132. Springer, Berlin. (Cited on page 72.)
- Miikkulainen, R., Bednar, J. A., Choe, Y., and Sirosh, J. (2005). Computational Maps in the Visual Cortex. *Graefes Archive for Clinical and Experimental Ophthalmology*, 245(4):616–616. (Cited on pages 27, 39, and 82.)
- Miller, K., Keller, J., and Stryker, M. (1989). Ocular dominance column development: Analysis and simulation. *Science*, 245(4918):605–615. (Cited on page 25.)
- Mizobe, K., Polat, U., Pettet, M. W., and Kasamatsu, T. (2001). Facilitation and suppression of single striate-cell activity by spatially discrete pattern stimuli presented beyond the receptive field. *Visual Neuroscience*, 18(3):377–91. (Cited on pages 21 and 79.)
- Nienborg, H., Hasenstaub, a., Nauhaus, I., Taniguchi, H., Huang, Z. J., and Callaway, E. M. (2013). Contrast Dependence and Differential Contributions from Somatostatin- and Parvalbumin-Expressing Neurons to Spatial Integration in Mouse V1. *Journal of Neuroscience*, 33(27):11145–11154. (Cited on page 32.)
- Nowak, L. G., Sanchez-Vives, M. V., and McCormick, D. a. (2008). Lack of orientation and direction selectivity in a subgroup of fast-spiking inhibitory interneurons: cellular and synaptic mechanisms and comparison with other electrophysiological cell types. *Cerebral Cortex*, 18(5):1058–78. (Cited on page 32.)
- Obermayer, K., Ritter, H., and Schulten, K. (1990). A principle for the formation of the spatial structure of cortical feature maps. *Proceedings of the National Academy of Sciences of the United States of America*, 87(21):8345–9. (Cited on page 21.)
- Ohki, K., Chung, S., Ch'ng, Y. H., Kara, P., and Reid, R. C. (2005). Functional imaging with cellular resolution reveals precise micro-architecture in visual cortex. *Nature*, 433(7026):597–603. (Cited on page 9.)
- Olshausen, B. a. and Field, D. J. (1996). Emergence of simple-cell receptive field properties by learning a sparse code for natural images. (Cited on page 42.)
- Perry, V. H. and Cowey, A. (1985). The ganglion cell and cone distributions in the monkey's retina: Implications for central magnification factors. *Vision Research*, 25(12):1795–1810. (Cited on page 63.)
- Pfeffer, C. K., Xue, M., He, M., Huang, Z. J., and Scanziani, M. (2013). Inhibition of inhibition in visual cortex: the logic of connections between molecularly distinct interneurons. *Nature Neuroscience*, (June):1–12. (Cited on pages 37, 38, and 84.)
- Polat, U., Mizobe, K., Pettet, M. W., Kasamatsu, T., and Norcia, A. M. (1998). Colinear stimuli regulate visual responses depending on cell's contrast threshold. *Nature*, 391(February):580–584. (Cited on page 79.)
- Poort, J., Raudies, F., Wannig, A., Lamme, V. a. F., Neumann, H., and Roelfsema, P. R. (2012). The role of attention in figure-ground segregation in areas v1 and v4 of the visual cortex. *Neuron*, 75(1):143–56. (Cited on page 41.)

- Ramsden, B. M., Hung, C. P., and Roe, a. W. (2001). Real and illusory contour processing in area V1 of the primate: a cortical balancing act. *Cerebral Cortex*, 11(7):648–65. (Cited on page 41.)
- Ringach, D. L. (2007). On the origin of the functional architecture of the cortex. *PLoS One*, 2(2):e251. (Cited on page 9.)
- Rodieck, R. W. (1965). Quantitative Analysis of Cat Retinal Ganglion Cell Response to Visual Stimuli. *Vision Research*, 5:583–601. (Cited on page 14.)
- Rodieck, R. W. and Stone, J. (1965a). Analysis of Receptive Fields of Cat Retinal Ganglion Cells. *Journal of Physiology*, 28(5):833–849. (Cited on page 14.)
- Rodieck, R. W. and Stone, J. (1965b). Response of Cat Retinal Ganglion Cells to Moving Visual Patterns. *Journal of Neurophysiology*, 28:819–832. (Cited on page 14.)
- Ruderman, D. L. (1997). Origins of scaling in natural images. *Vision research*, 37(23):3385–98. (Cited on page 42.)
- Rudolph, U., Crestani, F., Benke, D., Brünig, I., Benson, J. a., Fritschy, J. M., Martin, J. R., Bluethmann, H., and Möhler, H. (1999). Benzodiazepine actions mediated by specific gamma-aminobutyric acid(A) receptor subtypes. *Nature*, 401(6755):796–800. (Cited on page 38.)
- Rudy, B., Fishell, G., Lee, S., and Hjerling-Leffler, J. (2011). Three groups of interneurons account for nearly 100% of neocortical GABAergic neurons. *Developmental Neurobiology*, 71:45–61. (Cited on pages 36, 37, and 84.)
- Runyan, C. a., Schummers, J., Van Wart, A., Kuhlman, S. J., Wilson, N. R., Huang, Z. J., and Sur, M. (2010). Response features of parvalbumin-expressing interneurons suggest precise roles for subtypes of inhibition in visual cortex. *Neuron*, 67(5):847–57. (Cited on page 32.)
- Ruthazer, E. S. and Stryker, M. P. (1996). The role of activity in the development of long-range horizontal connections in area 17 of the ferret. *The Journal of Neuroscience*, 16(22):7253–69. (Cited on page 10.)
- Sceniak, M. and Hawken, M. (2001). Visual Spatial Characterization of Macaque V1 Neurons. *Journal of Neurophysiology*, 85:1873–1887. (Cited on pages 21, 22, 26, 64, 66, 68, and 85.)
- Sceniak, M., Ringach, D., and Hawken, M. (1999). Contrast's effect on spatial summation by macaque V1 neurons. *Nature*, 2(8):733–739. (Cited on pages 16, 21, 22, 43, and 68.)
- Sceniak, M. P., Chatterjee, S., and Callaway, E. M. (2006). Visual spatial summation in macaque geniculocortical afferents. *Journal of Neurophysiology*, 96(6):3474–84. (Cited on pages 16, 17, 22, 56, and 57.)
- Schmidt, K. E., Goebel, R., Löwel, S., and Singer, W. (1997). The Perceptual Grouping Criterion of Collinearity Is Reflected by Anisotropies of Connections in the Primary Visual Cortex. *European Journal of Neuroscience*, 9(December 1996):1083–1089. (Cited on page 43.)
- Schwabe, L., Obermayer, K., Angelucci, A., and Bressloff, P. C. (2006). The role of feedback in shaping the extra-classical receptive field of cortical neurons: a recurrent network model. *The Journal of Neuroscience*, 26(36):9117–29. (Cited on pages 23 and 28.)

- Schwartz, O. and Simoncelli, E. P. (2001). Natural signal statistics and sensory gain control. *Nature neuroscience*, 4:819–825. (Cited on page 42.)
- Shatz, B. C. J., Strykert, M. P., Shatz, C., and Stryker, M. (1978). Ocular dominance in layer IV of the cat's visual cortex and the effects of monocular deprivation. *Journal of Physiology*, 281(1):267–283. (Cited on page 37.)
- Sherman, S. M. and Guillory, R. W. (2002). The role of the thalamus in the flow of information to the cortex. *Philosophical transactions of the Royal Society of London. Series B, Biological sciences*, 357(1428):1695–708. (Cited on page 14.)
- Shmuel, A., Korman, M., Sterkin, A., Harel, M., Ullman, S., Malach, R., and Grinvald, A. (2005). Retinotopic axis specificity and selective clustering of feedback projections from V2 to V1 in the owl monkey. *The Journal of Neuroscience*, 25(8):2117–31. (Cited on page 24.)
- Shushruth, S., Ichida, J. M., Levitt, J. B., and Angelucci, A. (2009). Comparison of spatial summation properties of neurons in macaque V1 and V2. *Journal of Neurophysiology*, 102(4):2069–83. (Cited on pages 22 and 68.)
- Sigman, M., Cecchi, G. a., Gilbert, C. D., and Magnasco, M. O. (2001). On a common circle: natural scenes and Gestalt rules. *Proceedings of the National Academy of Sciences of the United States of America*, 98(4):1935–40. (Cited on page 42.)
- Silberberg, G. and Markram, H. (2007). Disynaptic inhibition between neocortical pyramidal cells mediated by Martinotti cells. *Neuron*, 53(5):735–46. (Cited on page 34.)
- Sillito, A. (1979). Inhibitory mechanisms influencing complex cell orientation selectivity and their modification at high resting discharge levels. *The Journal of physiology*, 289:33–53. (Cited on page 27.)
- Sillito, A. M., Cudeiro, J., and Jones, H. E. (2006). Always returning: feedback and sensory processing in visual cortex and thalamus. *Trends in Neurosciences*, 29(6):307–16. (Cited on page 14.)
- Simoncelli, E. and Olshausen, B. (2001). Natural image statistics and neural representation. *Annual Review of Neuroscience*, 24:1193–216. (Cited on page 42.)
- Sincich, L. C. and Blasdel, G. G. (2001). Oriented axon projections in primary visual cortex of the monkey. *The Journal of Neuroscience*, 21(12):4416–26. (Cited on page 43.)
- Solomon, S. G. and Lennie, P. (2007). The machinery of colour vision. *Nature Reviews Neuroscience*, 8(4):276–86. (Cited on pages 5 and 81.)
- Solomon, S. G., White, A. J. R., and Martin, P. R. (2002). Extraclassical receptive field properties of parvocellular, magnocellular, and koniocellular cells in the primate lateral geniculate nucleus. *The Journal of Neuroscience*, 22(1):338–49. (Cited on page 64.)
- Somers, D. C., Todorov, E. V., Siapas, a. G., Toth, L. J., Kim, D. S., and Sur, M. (1998). A local circuit approach to understanding integration of long-range inputs in primary visual cortex. *Cerebral Cortex*, 8(3):204–17. (Cited on pages 28 and 32.)
- Somogyi, P., Kisvárday, Z. F., Martin, K. a., and Whitteridge, D. (1983). Synaptic connections of morphologically identified and physiologically characterized large basket cells in the striate cortex of cat. *Neuroscience*, 10(2):261–94. (Cited on page 30.)
- Spear, P. D., Moore, R. J., Kim, C. B., Xue, J. T., and Tumosa, N. (1994). Effects of aging on the primate visual system: spatial and temporal processing by lateral genicu-

- late neurons in young adult and old rhesus monkeys. *Journal of Neurophysiology*, 72(1):402–20. (Cited on pages 15 and 57.)
- Srinivasan, M., Laughlin, S., and Dubs, A. (1982). Predictive coding: a fresh view of inhibition in the retina. *Proceedings of the Royal Society of London*, 216(1205):427–459. (Cited on page 42.)
- Stemmler, M., Usher, M., and Niebur, E. (1995). Lateral Interactions in Primary Visual Cortex: A Model Bridging Physiology and Psychophysics. *Science*, 269(5232):1877–1880. (Cited on page 28.)
- Stevens, J. L. (2011). *A temporal model of neural activity and VSD response in the primary visual cortex*. PhD thesis, The University of Edinburgh. (Cited on page 10.)
- Stevens, J.-l. R., Law, J. S., Antolik, J., and Bednar, J. A. (2013). Mechanisms for stable, robust, and adaptive development of orientation maps in the primary visual cortex. *Journal of Neuroscience*, 33(40):15747–15766. (Cited on pages 9, 54, 55, and 72.)
- Sur, M., Pallas, S. L., and Roe, A. W. (1990). Cross-modal plasticity in cortical development: Differentiation and specification of sensory neocortex. *Trends in Neurosciences*, 13(6):227–233. (Cited on page 11.)
- Swadlow, H. a. (2003). Fast-spike interneurons and feedforward inhibition in awake sensory neocortex. *Cerebral Cortex*, 13(1):25–32. (Cited on page 31.)
- Tan, Z., Hu, H., Huang, Z. J., and Agmon, a. (2008). Robust but delayed thalamocortical activation of dendritic-targeting inhibitory interneurons. *Proceedings of the National Academy of Sciences*, 105(6):2187–2192. (Cited on pages 35 and 71.)
- Thomson, A. and Deuchars, J. (1994). Temporal and spatial properties of local circuits in neocortex. *Trends in neurosciences*, 2:119–126. (Cited on page 28.)
- Thomson, A., West, D., and Deuchars, J. (1995). Properties of single axon excitatory postsynaptic potentials elicited in spiny interneurons by action potentials in pyramidal neurons in slices of rat neocortex. *Neuroscience*, 69(3):727–738. (Cited on page 28.)
- Treue, S. (2003). Visual attention: the where, what, how and why of saliency. *Current Opinion in Neurobiology*, 13(4):428–432. (Cited on page 23.)
- Troyer, T. W., Krukowski, A. E., Priebe, N. J., and Miller, K. D. (1998). Contrast-Invariant Orientation Tuning in Cat Visual Cortex: Thalamocortical Input Tuning and Correlation-Based Intracortical Connectivity. *Journal of Neuroscience*, 18(15):5908–5927. (Cited on page 32.)
- Tsodyks, M. V. and Markram, H. (1997). The neural code between neocortical pyramidal neurons depends. *Proceedings of the National Academy of Sciences*, 94:719–723. (Cited on page 28.)
- Van Brederode, J. F., Mulligan, K. a., and Hendrickson, a. E. (1990). Calcium-binding proteins as markers for subpopulations of GABAergic neurons in monkey striate cortex. *The Journal of comparative neurology*, 298(1):1–22. (Cited on page 30.)
- Van Essen, D. C., Newsome, W. T., and Maunsell, J. H. (1984). The visual field representation in striate cortex of the macaque monkey: asymmetries, anisotropies, and individual variability. *Vision Research*, 24(5):429–48. (Cited on pages 19 and 63.)
- von der Malsburg, C. (1973). Self-organization of orientation sensitive cells in the striate cortex. *Kybernetik*, 14(2):85–100. (Cited on pages 21 and 25.)

- Webb, B. S., Dhruv, N. T., Solomon, S. G., Tailby, C., and Lennie, P. (2005). Early and late mechanisms of surround suppression in striate cortex of macaque. *The Journal of neuroscience : the official journal of the Society for Neuroscience*, 25(50):11666–75. (Cited on page 29.)
- Weliky, M., Kandler, K., Fitzpatrick, D., and Katz, L. C. (1995). Patterns of excitation and inhibition evoked by horizontal connections in visual cortex share a common relationship to orientation columns. *Neuron*, 15(3):541–52. (Cited on pages 26, 27, and 82.)
- Wickersham, I. R., Lyon, D. C., Barnard, R. J. O., Mori, T., Conzelmann, K.-k., Young, J. a. T., Callaway, E. M., Manuscript, A., and Neurons, G. T. (2007). Monosynaptic Restriction of Transsynaptic Tracing from Single, Genetically Targeted Neurons. *Neuron*, 53(5):639–647. (Cited on page 36.)
- Wilson, N. R., Runyan, C. a., Wang, F. L., and Sur, M. (2012). Division and subtraction by distinct cortical inhibitory networks in vivo. *Nature*, 488(7411):343–8. (Cited on pages 30, 34, and 74.)
- Xing, D., Shapley, R. M., Hawken, M. J., and Ringach, D. L. (2005). Effect of Stimulus Size on the Dynamics of Orientation Selectivity in Macaque V1. *Journal of Neurophysiology*, 94:799–812. (Cited on page 29.)
- Xu, H., Jeong, H.-Y., Tremblay, R., and Rudy, B. (2013). Neocortical somatostatin-expressing GABAergic interneurons disinhibit the thalamorecipient layer 4. *Neuron*, 77(1):155–67. (Cited on pages 34 and 36.)
- Xu, X. and Callaway, E. M. (2009). Laminar specificity of functional input to distinct types of inhibitory cortical neurons. *The Journal of neuroscience : the official journal of the Society for Neuroscience*, 29(1):70–85. (Cited on page 34.)
- Xu, X., Roby, K. D., and Callaway, E. M. (2010). Immunochemical characterization of inhibitory mouse cortical neurons: three chemically distinct classes of inhibitory cells. *The Journal of comparative neurology*, 518(3):389–404. (Cited on pages 34 and 37.)

COLOPHON

Final Version as of January 15, 2016 (classicthesis version 4.0).